ERDC/GSL TR-05-16

Geotechnical and Structures Laboratory

US Army Corps
of Engineers®
Engineer Research and
Development Center

Laboratory Characterization of Fine Aggregate Cementitious Material

Erin M. Williams, Stephen A. Akers, and Paul A. Reed

July 2005

ERDC/GSL TR-05-16
July 2005

Laboratory Characterization of Fine Aggregate Cementitious Material

Erin M. Williams, Stephen A. Akers, and Paul A. Reed

Geotechnical and Structures Laboratory
U.S. Army Engineer Research and Development Center
3909 Halls Ferry Road
Vicksburg, MS 39180-6199

Final report

Prepared for U.S. Army Corps of Engineers
Washington, DC 20314-1000

Under Military Engineering Basic Research Work Package, Work Unit No. AT22-AR-002
"Strain Rate Effects in Simulating Impulsive Loading Events"

ABSTRACT: Personnel of the Geotechnical and Structures Laboratory, U.S. Army Engineer Research and Development Center, conducted a laboratory investigation to characterize the strength and constitutive property behavior of a fine aggregate cemented material (FACM). The FACM was designed to have a 34-MPa (5,000-psi) unconfined strength and to contain no coarse aggregate. Forty-three mechanical property tests—two hydrostatic compression tests (HC), four unconfined compression tests (UC), 16 triaxial compression tests (TXC), two uniaxial strain tests (UX), four uniaxial strain load/biaxial strain unloading tests (UX/BX), three uniaxial strain load/constant volume tests (UX/CV), three uniaxial strain load/constant strain path tests (UX/SP), five direct pull tests (DP), one conventional triaxial extension test (CTE), and three reduced triaxial extension tests (RTE)—were successfully completed. In addition to the mechanical property tests, nondestructive pulse-velocity measurements were performed on each specimen. The TXC tests exhibited a continuous increase in principal stress difference with increasing confining stress. A recommended compression failure surface was developed from the TXC and UC test results. Test data from the RTE, CTE, and DP tests were used to develop a recommended extension failure surface for FACM. Results from the stress paths of the strain path tests and the recommended compression failure surface exhibited good agreement.

Contents

List of Figures

Preface

This laboratory mechanical property investigation of a fine aggregate cementitious material (FACM) was conducted by personnel of the U.S. Army Engineer Research and Development Center (ERDC) at the Waterways Experiment Station (WES) for the Military Engineering Basic Research Work Package, Work Unit No. AT22-AR-002, "Strain Rate Effects in Simulating Impulsive Loading Events." This study was conducted from March to August 2003 by personnel of the Impact and Explosion Effects Branch (IEEB), Engineering Systems and Materials Division (ESMD), Geotechnical and Structures Laboratory (GSL), ERDC, under the general direction of Mr. Henry S. McDevitt, Chief, IEEB, Dr. Albert J. Bush, Chief, ESMD, and Dr. David W. Pittman, Director, GSL.

The Principal Investigator for this project was Dr. Stephen A. Akers, IEEB. Material property data were processed by Ms. Erin M. Williams, IEEB, co-investigator for this project. The laboratory characterization tests were performed by Mr. Paul A. Reed, IEEB, under the technical direction of Dr. Akers. Instrumentation support was provided by Mr. A. Leroy Peeples, Instrumentation Systems Development Division, ERDC Information Technology Laboratory. The FACM material was designed and developed by Mr. Brian H. Green and associates of the Concrete and Materials Branch, GSL. This report was written by Ms. Williams, under the direction of Dr. Akers.

At the time of publication of this report, Dr. James R. Houston was Director of ERDC, and COL James R Rowan, EN, was Commander and Executive Director.

1 Introduction

Background

Personnel of the Geotechnical and Structures Laboratory (GSL), U.S. Army Engineer Research and Development Center, conducted a laboratory investigation to characterize the strength and constitutive property behavior of a fine aggregate cementitious material under the Military Engineering Basic Research Work Package, Work Unit No. AT22-AR-002, "Strain Rate Effects in Simulating Impulsive Loading Events." In this document, this material designed and developed by Brian Green and associates of the Concrete and Materials Branch, GSL, will be identified as fine aggregate cementitious material (FACM). The design requirements for FACM were 34 MPa (5000 psi) unconfined strength and no coarse aggregate. GSL personnel conducted a total of 45 mechanical property tests of which 43 were successfully completed. The 43 successfully completed tests consisted of two hydrostatic compression tests, four unconfined compression tests, 16 triaxial compression tests, two uniaxial strain tests, four uniaxial strain load/biaxial strain unloading tests, three uniaxial strain load/constant volume tests, three uniaxial strain load/constant strain path tests, five direct pull tests, one conventional triaxial extension test, and three reduced triaxial extension tests. In addition to the mechanical property tests, nondestructive pulse-velocity measurements were performed on each specimen.

Purpose and Scope

The primary purpose of this report is to document the results from the laboratory mechanical property tests conducted on the FACM specimens. In addition, results from the nondestructive pulse-velocity measurements are documented. The physical and composition properties, test procedures, and test results are documented in Chapter 2. Comparative plots and analyses of the experimental results are presented in Chapter 3. A summary is provided in Chapter 4.

2 Laboratory Tests

Material Description

Brian Green and associates of the Concrete and Materials Branch, GSL, designed and developed FACM under the requirements of no coarse aggregate and an unconfined strength of 34 MPa (5000 psi). Table 1 displays the mix design for FACM. During the placement of FACM for projectile penetration targets, representative samples of FACM were taken from each batch for laboratory mechanical property tests. The test specimens used in this investigation were cored from these samples. Typically, each section of core was of sufficient length to obtain two approximately 0.102 m (4 in.) long test specimens. Additional details are documented in the Specimen Preparation section of this chapter.

Composition Property Tests

Prior to performing the mechanical property tests, the height, diameter, and mass for each test specimen were determined. These measurements were used to compute the specimen's "as-tested" wet or bulk density. Results from these calculations are provided in Table 2. Measurements of posttest water content[1] were conducted in accordance with procedures given in American Society for Testing and Materials (ASTM) D 2216 (ASTM 2002e). Based on the appropriate values of posttest water content, wet density, and an assumed grain density of 2.60 Mg/m^3, values of dry density, porosity, degree of saturation, and volumes of air, water, and solids were calculated (Table 2). Also listed in the table are maximum, minimum, and mean values and the standard deviation about the mean for each quantity. The FACM specimens had a mean wet density of 2.099 Mg/m^3 and a mean water content of 5.67 percent and a mean dry density of 1.987 Mg/m^3.

Ultrasonic Pulse-Velocity Determinations

Prior to performing a mechanical property test, ultrasonic pulse-velocity measurements were collected on each test specimen. This involved measuring the transit distance and time for each P (compressional) or S (shear) pulse to propa-

[1] Water content is defined as the mass of water (removed during drying in a standard oven) divided by the mass of dry solids.

gate through a given specimen. The velocity was then computed by dividing the transit distance by the transit time. A matching pair of 1 Hz piezoelectric transducers were used to transmit and receive the ultrasonic P waves. A pair of 2.25 MHz piezoelectric transducers were used to transmit and receive the ultrasonic S waves. The transit time was measured with a 100 MHz digital oscilloscope and the transit distance was measured with a digital micrometer. All of these wave-velocity determinations were made under atmospheric conditions, i.e.; no prestress of any kind was applied to the specimens. The tests were conducted in accordance with procedures given in ASTM C 597 (ASTM 2002c).

One compressional-wave (P-wave) and one shear-wave (S-wave) velocity were determined axially through each specimen. Radial P- and S-wave velocities were determined for each specimen in the following manner. Six radial P-wave velocities were determined, two transverse to each other at elevations of 1/4, 1/2, and 3/4 the specimen height. Two radial S-wave velocities were measured; both of these determinations were made at the mid-height of the specimen transverse to each other. The P- and S-wave velocities determined for the test specimens are provided in Table 2; the radial-wave velocities listed in Table 2 are the average values.

Mechanical Property Tests

Forty-three mechanical property tests were successfully performed on the FACM specimens to characterize the strength and constitutive properties of the material. All of the mechanical property tests were conducted quasi-statically with axial strain rates on the order of 10^{-4} to 10^{-5} per second and times to peak load on the order of 5 to 30 min. Mechanical property data were obtained under several different stress and strain paths. Undrained bulk compressibility data were obtained during the hydrostatic loading phase of the triaxial compression (TXC) tests and from several hydrostatic compression (HC) tests. Shear and failure data were obtained from unconsolidated-undrained TXC tests, conventional triaxial extension (CTE) tests, reduced triaxial extension (RTE) tests, and from the direct pull (DP) tests. One-dimensional compressibility data were obtained from undrained uniaxial strain (UX) tests with lateral stress measurements (or K_o tests). Three different types of undrained strain-path tests were conducted during the test program. All of the strain-path tests were initially loaded under uniaxial strain boundary conditions to some prescribed level of stress or strain. At the end of the UX loading, constant axial to radial strain ratios (ARSR) of 0, -1.33, and -2.0 were applied. The ARSR = 0 path is a constant axial strain unloading path and produces a forced state of volumetric expansion; these tests will be referred to as UX/BX tests. The UX/SP tests have an ARSR = -1.33, which simply produces a path that has a constant strain ratio when loading. The ARSR = -2.0 path is a constant volume strain loading path and these paths will be referred to as UX/CV tests. The terms undrained and unconsolidated signify that no pore fluid (liquid or gas) was allowed to escape or drain from the membrane-enclosed specimens during the shear and hydrostatic phases of the test, respectively. The completed test matrix, presented in Table 3, lists the types of tests conducted, the number of tests, the nominal peak radial stress applied to specimens prior to

shear loading or during the HC, UX, or strain-path loading, the test numbers for each group, and the tests numbers of the specimens that had cyclic loading.

Specimen preparation

The mechanical-property test specimens were cut from cores of FACM that were obtained using a diamond-bit core barrel and following the procedures provided in ASTM C 42 (ASTM 2002b). The ends of all the test specimens were cut to the correct length, and ground flat, parallel to each other, and perpendicular to the sides of the core in accordance with procedures in ASTM D 4543 (ASTM 2002f). Prior to testing, the prepared specimens were measured for height and diameter, their mass was determined, and ultrasonic measurements were made. This information was used to calculate the composition properties and wave velocities of the specimens. The prepared test specimens had a nominal height of 110 mm and a diameter of 50 mm.

Prior to testing, each specimen was placed between hardened steel top and base caps. With the exception of the unconfined compression (UC) and the direct pull (DP) test specimens, two 0.6-mm-thick membranes were placed around the specimen, and the exterior of the outside membrane was coated with a liquid synthetic rubber to inhibit deterioration caused by the confining-pressure fluid (Figure 1). The confining fluid was a mixture of kerosene and hydraulic oil. Finally, the specimen, along with its top cap and base cap assembly, was placed on the instrumentation stand of the test apparatus, and the instrumentation setup was initiated.

Test devices

Four different sets of test devices were used in this test program. The axial load for all of the UC tests was provided by a 3.3-MN (750-thousand pound) loading machine. The application of load was manually controlled with this test device. No pressure vessel was required for the UC tests, only a base and instrumentation (load cell and axial and radial deformeters) were necessary.

Direct pull tests are performed by using the direct pull apparatus in which end caps are attached to unconfined specimens with a high-modulus high-strength epoxy (Sikadur 31 Hi-Mod Gel). A manual hydraulic pump is used to pressurize the direct pull chamber. When the direct pull chamber is pressurized, a piston rises producing tensile loading on the test specimen. Measurements for the tensile loading of the specimen are recorded by a 280 kN load cell.

To perform a RTE or CTE test, a static high-pressure triaxial test device (HPTX) was used (Figure 2). Axial and radial pressures are manually controlled: the test device has a maximum pressure range of 100 MPa. The pumping equipment that is used during the operation of this device limits the peak pressure that can be achieved to 70 MPa. When the triaxial extension top cap is used with the HPTX device, independent control of the axial and radial stresses is permitted. The specimen top cap is bolted to the extension loading piston and the surface on

top of the piston is pressurized. During a RTE test, the confining pressure (or radial stress) is kept constant while the axial stress is reduced. When performing a CTE test, the axial stress is constant and the confining pressure is increased (Akers, Reed, and Ehrgott 1986).

All of the remaining tests were conducted in a 600-MPa-capacity pressure vessel, and the axial load was provided by an 8.9-MN (2-million-pound) loading machine. With these later test devices, the application of load, pressure, and axial displacement were regulated by a servo-controlled data acquisition system. This servo-controlled system allows the user to program rates of load, pressure, and axial displacement in order to achieve the desired stress or strain path. Confining pressure was measured external to the pressure vessel by a pressure transducer mounted in the confining fluid line. A load cell mounted in the base of the specimen pedestal was used to measure the applied axial loads inside the pressure vessel (Figure 1).

Outputs from the various instrumentation sensors were electronically amplified and filtered, and the conditioned signals recorded by computer-controlled 16-bit analog-to-digital converters. The data acquisition systems were programmed to sample the data channels every 1 to 5 seconds, convert the measured voltages to engineering units, and store the data for further posttest processing.

Test instrumentation

The vertical (axial) deflection measurement system in all the test areas except the DP test area consisted of two linear variable differential transformers (LVDTs) mounted vertically on the instrumentation stands and positioned 180 degrees apart. They were oriented to measure the displacement between the top and base caps, thus providing a measure of the axial deformations of the specimen. For the confined tests, a linear potentiometer was mounted external to the pressure vessel so as to measure the displacement of the piston through which axial loads are applied. This provided a backup to the vertical LVDTs in case they exceeded their calibrated range. The axial strains from the DP tests were measured by strain gauges attached to the test specimens.

Two different radial deflection measurement systems were used in this test program. Both deformeters measure the radial displacement of two footings that are glued to the sides of the test specimen (Figures 1 and 3). These two small steel footings are mounted 180 deg apart at the specimen's mid-height. The footing faces have been machined to match the curvature of the test specimen. A threaded post extends from the outside of each footing and protrudes through the membrane. The footings must be mounted to the specimen prior to placement of the membrane. When the membranes are in place, steel caps are screwed onto the threaded posts to seal the membrane to the footing. The lateral deformeter ring is attached to these steel caps with set screws (Figure 3).

One lateral deformeter consists of an LVDT mounted on a hinged ring; the LVDT measures the expansion or contraction of the ring. This lateral deformeter is used over smaller ranges of radial deformation when the greatest measurement

accuracy is required. This lateral deformeter was used for all of the HC, UC, UX, and strain-path tests and for the TXC tests at confining pressures less than 50 MPa. This design is similar to the radial-deformeter design provided by Bishop and Henkel (1962). When the specimen expands (or contracts), the hinged-deformeter ring opens (or closes) causing a change in the electrical output of the horizontally mounted LVDT.

The second lateral deformeter referred to as the "spring arm" lateral deformeter and shown in Figure 3, was used for all of the TXC tests at confining pressures of 50 MPa and above. It consists of two strain-gauged spring-steel arms mounted on a double-hinged ring; the strain-gauged arms deflect as the ring expands or contracts. This lateral deformeter is used when the greatest radial deformation range is required, and therefore, it is less accurate than the LVDT deformeter. With this deformeter, when the specimen expands or contracts, the rigid deformeter ring flexes about its hinge causing a change in the electrical output of the strain-gauged spring-arm. Radial measurements were not performed during the DP tests.

Test descriptions

The UC and TXC tests were performed in accordance with ASTM C 39 and ASTM C 801, respectively (ASTM 2002a,d). A TXC test is conducted in two phases. During the first phase, the hydrostatic compression phase, the cylindrical test specimen is subjected to an increase in hydrostatic pressure while measurements of the specimen's height and diameter changes are made. The data are typically plotted as pressure versus volumetric strain, the slope of which, assuming elastic behavior, is termed the bulk modulus, *K*. The second phase of the TXC test, the shear phase, is conducted after the desired confining pressure has been applied during the HC phase. While holding the desired confining pressure constant, axial load is increased, and measurements of the changes in the specimen's height and diameter are made. The axial (compressive) load is increased until the specimen fails. The shear data are generally plotted as curves of principal stress difference versus axial strain, the slope of which represents Young's modulus, *E*. The maximum principal stress difference that a given specimen can support, or the principal stress difference at 15 percent axial strain during shear loading, is defined as the peak strength.

Note that the UC test is a TXC test in which no confining pressure is applied. The maximum principal stress difference observed during a UC test is defined as the unconfined compressive strength of the material.

Extension data was obtained for FACM by performing a CTE test, five DP tests, and three RTE tests. The DP tests have no confining pressure during the tests unlike the CTE and RTE tests. To conduct the DP tests, end caps are attached with epoxy to the specimen. The end caps are screwed into the direct pull apparatus and the specimen is pulled apart axially when pressure is applied to the piston. Strain gauges are attached to the specimen to measure the axial strain until the specimen fails. The RTE tests are conducted with the HPTX device and the TXE top cap (Figure 2). To begin the RTE test, the specimen is

loaded hydrostatically to a desired confining pressure. After the hydrostatic loading has been applied and while the radial stress is held constant, the axial stress is reduced until the specimen fails. Throughout the RTE test, the specimen's height and diameter changes are recorded. CTE tests are performed the same as RTE tests except the radial stress is increased while the axial stress is held constant (Akers, Reed, and Ehrgott 1986). Extension shear data for a material is generally plotted as curves of principal stress difference versus axial strain and as curves of principal stress difference versus mean normal stress.

A uniaxial strain (UX) test is conducted by applying axial load and confining pressure simultaneously so that as the cylindrical specimen compresses, its diameter remains unchanged; i.e.; zero radial strain boundary conditions are maintained. The data are generally plotted as curves of axial stress versus axial strain, the slope of which is the constrained modulus M. The data are also generally plotted as principal stress difference versus mean normal stress, the slope of which is twice the shear modulus G divided by the bulk modulus K ; i.e.; 2G/K, or, in terms of Poisson's ratio ν, $3(1-2\nu)/(1+\nu)$.

The strain-path tests in this test program were conducted in two phases. Initially, the specimens were subjected to a uniaxial-strain loading up to a desired level of mean normal, radial, or axial stress. At the end of the UX loading, constant axial to radial strain ratios of 0, -1.33, or -2.0 were applied; these tests were identified earlier as UX/BX, UX/SP, and UX/CV tests, respectively. In order to conduct these tests, the software controlling the servo-controls had to correct the measured inputs for system compressibility and for the nonlinear calibrations of specific transducers.

Definition of stresses and strains

During the mechanical property tests, measurements are typically made of the axial and radial deformations of the specimen as confining pressure and/or axial load is applied or removed. These measurements along with the pretest measurements of the initial height and diameter of the specimen are used to convert the measured test data to true stresses and engineering strains.[1]

Axial strain, ϵ_a, is computed by dividing the measured axial deformation, Δh (change in height), by the original height h_o; i.e., $\epsilon_a = \Delta h/h_o$. Similarly, radial strain, ϵ_r, is computed by dividing the measured radial deformation, Δd (change in diameter), by the original diameter d_o; i.e., $\epsilon_r = \Delta d/d_o$. For this report, the volumetric strain is assumed to be the sum of the axial strain and twice the radial strain, $\epsilon_v = \epsilon_a + 2\epsilon_r$.

The principal stress difference q is calculated by dividing the axial load by the cross-sectional area of the specimen A which is equal to the original cross-sectional area A_o multiplied by $(1 - \epsilon_r)^2$. In equation form:

[1] Compressive stresses and strains are assumed to be positive.

$$q = (\sigma_a - \sigma_r) = \frac{Axial\ \ Load}{A_o(1-\varepsilon_r)^2} \quad (1)$$

where σ_a is the axial stress and σ_r is the radial stress. The axial stress is related to the confining pressure and the principal stress difference by:

$$\sigma_a = q + \sigma_r \quad (2)$$

The mean normal stress, p, is the average of the applied principal stresses. In cylindrical geometry,

$$p = \frac{(\sigma_a + 2\sigma_r)}{3} \quad (3)$$

Results

Results from all of the mechanical property tests except those from the direct pull tests are presented in Plates 1-38. One data plate is presented for each test with reliable results. Results from the HC tests are presented on the plates in four plots: (a) mean normal stress versus volumetric strain, (b) mean normal stress versus axial strain, (c) axial versus radial strain, and (d) mean normal stress versus radial strain. Each plate for the UC, TXC, UX, strain-paths, CTE, and RTE tests displays four plots: (a) principal stress difference versus mean normal stress, (b) principal stress difference versus axial strain, (c) volumetric strain versus mean normal stress, and (d) volumetric strain versus axial strain.

Table 1
FACM Mix Design

Materials	Mass per cubic meter batch, kg	Liters
Portland Cement Type I/II	474	
Fine aggregate: Masonry sand	1445	
Water	275	
Water Reducing Admixture: B 200 N		1.54

Table 2
Physical and Composition Properties of Fine Aggregate Cementitious Material Test Specimens[1]

Test Number	Type of Test	Plate Number	Wet Density Mg/m^3	Posttest Water Content %	Dry Density Mg/m^3	Porosity %	Degree of Saturation %	Volume of Air %	Volume of Water %	Volume of Solids %	Axial P Wave Velocity km/s	Radial P Wave Velocity km/s	Axial S Wave Velocity km/s	Radial S Wave Velocity km/s
01	HC	1	2.140	6.50	2.009	22.73	57.45	9.67	13.06	77.27	4.093	4.073	2.564	2.562
02	HC	2	2.106	6.31	1.981	23.81	52.51	11.31	12.50	76.19	4.117	3.990	2.572	2.546
03	TXC/5	7	2.088	6.31	1.964	24.44	50.71	12.05	12.40	75.56	4.062	4.030	2.485	2.559
04	TXC/5	8	2.154	6.64	2.020	22.31	60.11	8.90	13.41	77.69	4.165	4.063	2.568	2.571
05	TXC/10	9	2.107	6.69	1.975	24.06	54.91	10.85	13.21	75.94	4.146	4.051	2.568	2.532
06	TXC/10	10	2.097	6.50	1.969	24.26	52.75	11.46	12.80	75.74	4.136	4.058	2.580	2.580
07	TXC/20	11	2.156	6.98	2.015	22.49	62.53	8.43	14.07	77.51	4.211	4.099	2.615	2.576
08	TXC/20	12	2.114	6.58	1.984	23.70	55.08	10.65	13.05	76.30	4.189	4.073	2.568	2.544
09	TXC/50	13	2.122	6.60	1.990	23.45	56.02	10.31	13.14	76.55	4.176	4.074	2.546	2.583
10	TXC/50	14	2.116	6.51	1.987	23.59	54.84	10.65	12.93	76.41	4.221	4.095	2.604	2.553
11	TXC/100	15	2.105	6.58	1.975	24.04	54.06	11.04	13.00	75.96	4.180	4.061	2.551	2.568
12	TXC/100	16	2.123	6.33	1.997	23.21	54.46	10.57	12.64	76.79	4.160	4.059	2.562	2.571
14	TXC/200	17	2.109	5.89	1.991	23.41	50.10	11.68	11.73	76.59	4.142	4.106	2.574	2.584
15	TXC/200	18	2.129	5.82	2.012	22.63	51.74	10.92	11.71	77.37	4.168	4.087	2.588	2.589
16	TXC/300	19	2.093	5.77	1.979	23.88	47.83	12.46	11.42	76.12	4.173	4.091	2.563	2.574
17	TXC/300	20	2.089	5.71	1.976	23.99	47.03	12.71	11.28	76.01	4.167	4.076	2.575	2.562
18	TXC/400	21	2.116	5.67	2.002	22.99	49.37	11.64	11.35	77.01	4.203	4.080	2.598	2.581
19	TXC/400	22	2.111	5.67	1.998	23.17	48.89	11.84	11.33	76.83	4.166	4.070	2.566	2.577
20	UX	27	2.103	5.62	1.991	23.43	47.75	12.24	11.19	76.57	4.139	4.056	2.568	2.566
21	UX	28	2.092	5.79	1.977	23.96	47.78	12.51	11.45	76.04	4.134	4.042	2.528	2.554
22	UX/BX	29	2.117	5.85	2.000	23.06	50.74	11.36	11.70	76.94	4.144	4.077	2.562	2.580
23	UX/BX	30	2.066	5.75	1.954	24.86	45.19	13.63	11.23	75.14	4.088	4.019	2.526	2.551
24	UX/BX	31	2.083	5.81	1.969	24.27	47.12	12.84	11.44	75.73	4.117	4.019	2.580	2.562
25	UX/BX	32	2.074	5.94	1.957	24.71	47.05	13.08	11.63	75.29	4.045	3.991	2.528	2.525

(Continued)

Table 2 (Concluded)[1]

Test Number	Type of Test	Plate Number	Wet Density Mg/m^3	Posttest Water Content %	Dry Density Mg/m^3	Porosity %	Degree of Saturation %	Volume of Air %	Volume of Water %	Volume of Solids %	Axial P Wave Velocity km/s	Radial P Wave Velocity km/s	Axial S Wave Velocity km/s	Radial S Wave Velocity km/s
26	UX/SP	33	2.096	5.84	1.980	23.84	48.51	12.27	11.56	76.16	4.103	3.992	2.557	2.535
27	UX/CV	34	2.102	5.60	1.991	23.43	47.58	12.28	11.15	76.57	4.155	4.056	2.545	2.581
29	UX/CV	35	2.075	5.17	1.973	24.11	42.32	13.90	10.20	75.89	4.125	3.998	2.557	2.538
30	UX/CV	36	2.076	5.24	1.972	24.15	42.80	13.81	10.33	75.85	4.063	3.981	2.505	2.533
31	UX/SP	37	2.092	5.42	1.985	23.67	45.45	12.91	10.76	76.33	4.133	3.999	2.579	2.538
32	UX/SP	38	2.115	5.28	2.009	22.73	46.68	12.12	10.61	77.27	4.799	4.055	2.599	2.554
33	RTE/65	23	2.076	5.29	1.972	24.15	43.19	13.72	10.43	75.85	4.111	4.000	2.539	2.547
34	RTE/65	24	2.079	5.27	1.975	24.03	43.32	13.62	10.41	75.97	4.093	4.006	2.553	2.555
35	RTE/50	25	2.087	5.12	1.985	23.64	43.00	13.47	10.17	76.36	4.123	4.068	2.573	2.571
36	CTE/10	26	2.067	5.12	1.966	24.38	41.28	14.32	10.07	75.62	4.141	4.014	2.559	2.563
37	UC	3	2.065	5.06	1.966	24.39	40.78	14.44	9.95	75.61	4.105	3.964	2.573	2.527
38	UC	4	2.059	5.01	1.961	24.59	39.95	14.77	9.82	75.41	4.030	4.010	2.546	2.517
39	UC	5	2.111	5.10	2.009	22.73	45.07	12.49	10.25	77.27	4.110	4.034	2.590	2.552
40	UC	6	2.087	5.23	1.984	23.70	43.77	13.33	10.37	76.30	4.110	3.997	2.563	2.550
41	DP/5		2.096	4.45	2.007	22.82	39.14	13.89	8.93	77.18	4.173	4.040	2.591	2.591
42	DP/4		2.079	4.44	1.991	23.44	37.70	14.60	8.84	76.56	4.157	4.049	2.533	2.521
43	DP/4		2.091	4.46	2.002	23.02	38.78	14.09	8.93	76.98	4.191	4.087	2.586	2.581
44	DP/4		2.101	4.48	2.011	22.65	39.79	13.64	9.01	77.35	3.965	3.939	2.504	2.499
45	DP/5		2.107	4.58	2.015	22.52	40.98	13.29	9.23	77.48	3.989	3.897	2.479	2.510
N			43	43	43	43	43	43	43	43	43	43	43	43
Mean			2.099	5.67	1.987	23.59	47.82	12.32	11.27	76.41	4.145	4.038	2.560	2.556
Stdv			0.022	0.686	0.017	0.670	6.046	1.528	1.366	0.670	0.116	0.046	0.030	0.023
Max			2.156	6.98	2.020	24.86	62.53	14.77	14.07	77.69	4.799	4.106	2.615	2.591
Min			2.059	4.44	1.954	22.31	37.70	8.43	8.84	75.14	3.965	3.897	2.479	2.499

[1] Calculations based on the assumed specific gravity of 2.6 Mg/m^3

Table 3
Completed FACM Test Matrix

Type of Test	No. of Tests	Test Nos.	Cycles in Test Nos.	Nominal Peak Radial Stress, MPa
Hydrostatic Compression	2	1, 2	2	500
Triaxial Compression	4	37, 38, 39, 40		0
	2	3, 4		5
	2	5, 6	6	10
	2	7, 8	8	20
	2	9, 10	10	50
	2	11, 12	12	100
	2	14, 15	14	200
	2	16, 17		300
	2	18, 19	19	400
UX Strain	2	20, 21	21	500
UX/BX	2	22, 23		200
	2	24, 25		100
UX/CV	1	30		65
	2	27, 29		100
UX/SP	3	26, 31, 32		100/50
DP	5	41, 42, 43, 44, 45		0
RTE	1	35		50
	2	33, 34		65
CTE	1	36		10
Total No. Tests:	43			

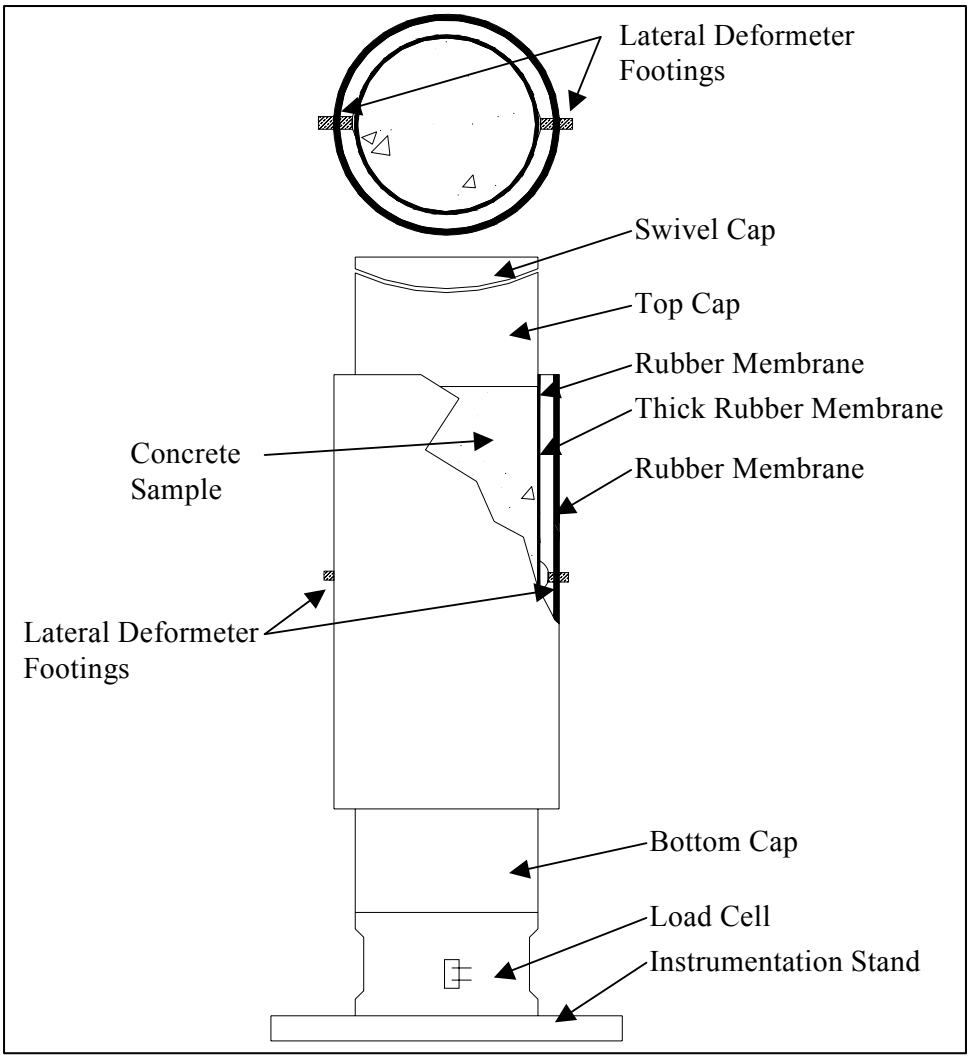

Figure 1. Typical test specimen setup

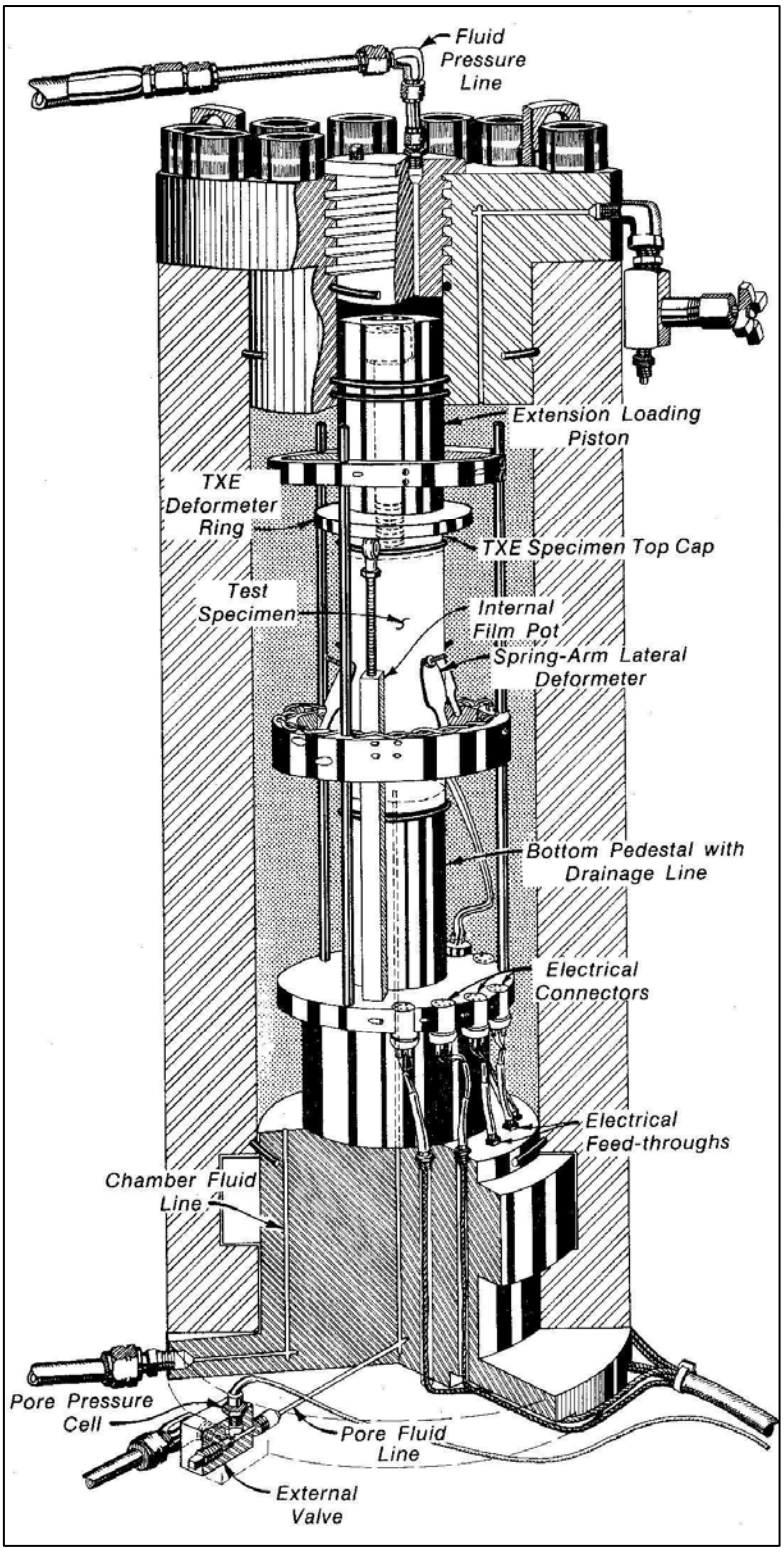

Figure 2. HPTX test device with TXE top cap

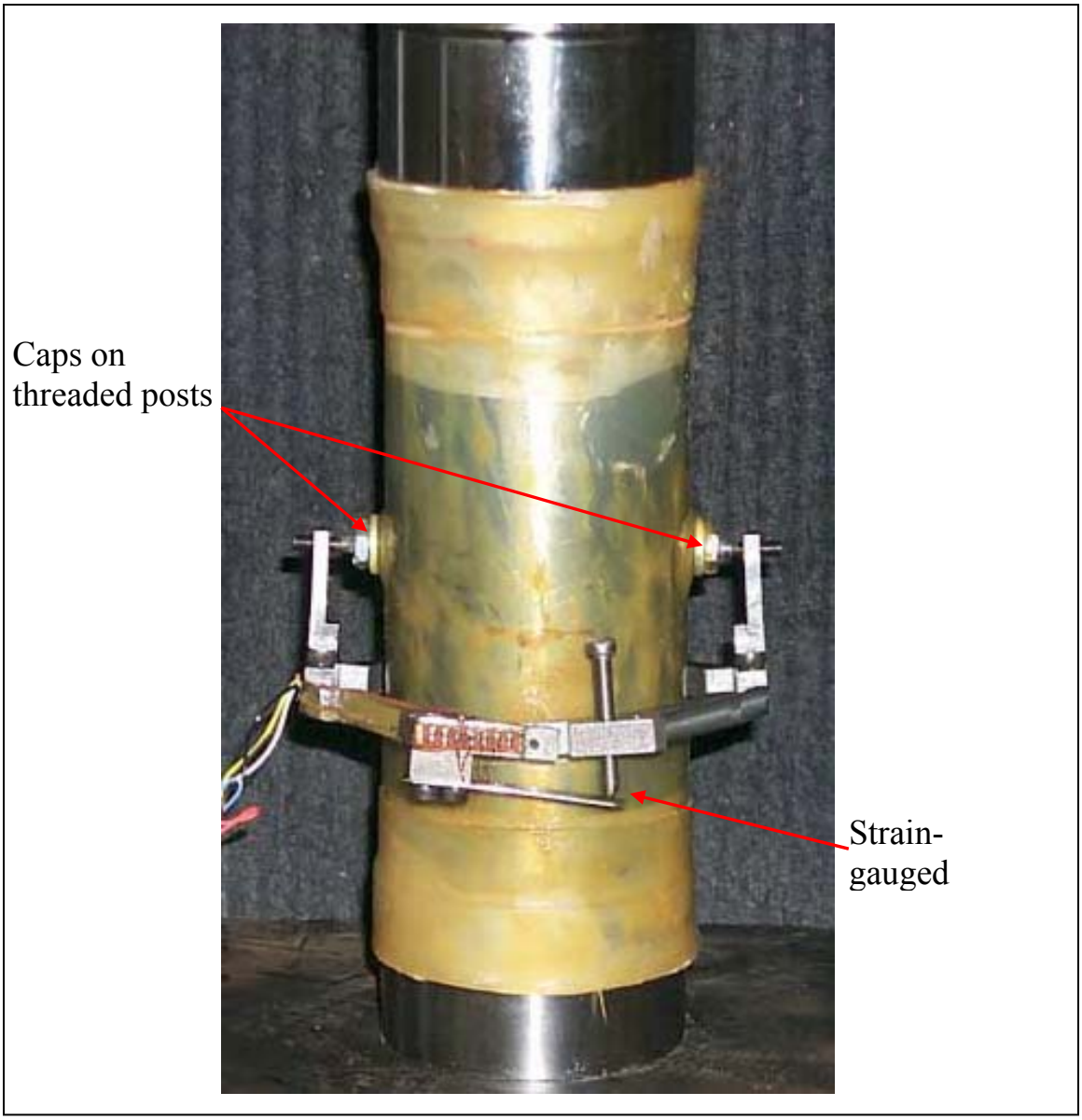

Figure 3. Spring-arm lateral deformeter mounted on test specimen

3 Analysis of Test Results

An analysis of the results from laboratory tests conducted on the FACM is presented in this chapter. The purpose of the investigation was to characterize the strength and constitutive property behavior of the material. As described in Chapter 2, a total of 45 mechanical property tests were conducted in this investigation; of the 45 tests, 43 tests were successfully completed. The analysis in this chapter is based on the results from the following numbers and types of tests: two hydrostatic compression tests, four unconfined compression tests, 16 triaxial compression tests, two uniaxial strain tests, four uniaxial strain load/biaxial strain unloading tests, three uniaxial strain load/constant volume tests, three uniaxial strain load/constant strain path tests, five direct pull tests, one conventional triaxial extension test, and three reduced triaxial extension tests.

Hydrostatic Compression Test Results

Undrained bulk compressibility data were obtained from two HC tests. The pressure-volume curves from the two HC tests are plotted in Figure 4. Unload-reload cycles were applied to one of the HC test specimens in order to get elastic moduli at intermediate levels of volume strain. These tests exhibited a minimal amount of scatter. This is attributed to the small differences in the dry densities of the specimens; the dry densities were 2.009 and 1.981 Mg/m^3. During both HC tests, the pressure was intentionally held constant for a period of time prior to the unloading cycles (Figure 4). During each hold in pressure, the volumetric strains continued to increase, indicating that FACM is susceptible to creep. Figure 5 presents the pressure-time histories for the HC tests. The pressure on specimen 01 was held constant at 508 MPa for 435 seconds, during which time the volume strain increased 0.27 percent. At the peak of the first cycle for specimen 02, the pressure was held at 254 MPa for 207 seconds, during which time a volume strain increase of 0.52 percent was measured. At the end of the second cycle, the pressure was held constant at 509 MPa for 304 seconds and a volume strain increase of 0.30 percent was measured.

Pressure-volume data obtained during the hydrostatic loading phase of the TXC tests are shown in Figure 6. Pressure-volume data from all of the TXC tests conducted between confining pressures of 100 – 400 MPa and the curves from Figure 4 are plotted in Figure 7. Figure 7 displays the good quality of the data when the results from the HC and TXC tests are compared. Additionally, there is no significant scatter in the pressure-volume data, although the initial modulus

from test 17 is less than the initial modulus depicted by the other tests. The results plotted in Figure 7 indicate that FACM begins to exhibit inelastic strains at a pressure (mean normal stress) level of approximately 27.6 MPa and at a corresponding volume strain of approximately 0.38 percent. For pressures and volume strains greater than 27.6 MPa and 0.38 percent, the pressure-volume response and the initial bulk modulus begin to soften appreciably. Based on these data, the initial elastic bulk modulus for FACM is approximately 10.1 GPa.

Triaxial Compression Test Results

Shear and failure data were successfully obtained from 4 unconfined compression tests and 16 unconsolidated-undrained TXC tests. Recall from Chapter 2 that the second phase of the TXC test, the shear phase, is conducted after the desired confining pressure has been applied during the HC phase. One should also recognize that the UC tests are a special type of TXC test without the application of confining pressure. Results from the UC tests are plotted in Figures 8 and 9, and results from the TXC tests are plotted in Figures 10 through 25. In these latter figures, the axial and volumetric strains at the beginning of the shear phase were set to zero; i.e., only the strains during shear are plotted.

Stress-strain data from the four UC tests are plotted in Figures 8 and 9; the data are plotted as principal stress difference versus axial strain during shear and as principal stress difference versus volumetric strain during shear. Deformeters as opposed to strain gauges were used to measure the axial and radial strains of the UC test specimens. During the UC tests, no attempt was made to capture the entire post-peak (or softening) stress-strain behavior of this material. The mean unconfined strength of the FACM was 46 MPa (6708 psi).

Figures 10 through 25 present the results from the TXC tests conducted at nominal confining pressures of 5, 10, 20, 50, 100, 200, 300, and 400 MPa. The TXC results are plotted as principal stress difference versus axial strain during shear and as principal stress difference versus volumetric strain during shear. The results are very good considering the inherent variability of the initial wet and dry densities and water contents of the specimens, the wet densities of the specimens ranged from 2.156 to 2.059 Mg/m^3, the dry densities ranged from 2.020 to 1.954 Mg/m^3, and the water contents ranged from 6.98 to 5.01 percent.

A few comments should be made concerning the results from specific tests. In the stress-strain curves of test 10 (Figure 16), test 11 (Figure 18), and test 14 (Figure 20) there are discernable drops and subsequent increases in principal stress difference at axial strains above 7.5 percent (at approximately 9, 8, and 8 percent axial strain in tests 10, 11, and 14, respectively). These were produced when the servo-controlled system was changed from a constant load rate to a constant displacement rate. Specimens during tests 18 and 19 (Figures 24 and 25) reached full saturation during the shear loading. When full saturation was achieved, the stress-strain curves exhibited no further increase in principal stress difference.

A few comments should also be made concerning the unloading results in general. The final unloading stress-strain responses at axial strains approaching 15 percent are less reliable than the unloadings at axial strains less than 11 percent. The reliable range of the vertical deformeters is exceeded at axial strains of approximately 11 percent. An external deformeter with less resolution is used to measure axial displacement for axial strains greater than 11 percent. The potential for this material to creep also caused problems when unloading the specimens. During the initial unloading, the creep strains are greater in magnitude than the recovered "elastic" strains. This behavior results in a net increase in axial strain (for example) during the initial unloading, rather than an expected decrease in axial strain.

For comparison purposes, typical stress-strain curves from TXC tests conducted at confining pressures less than 50 MPa are plotted in Figure 26 and several tests at the confining pressures greater than 50 MPa are plotted in Figure 27. Stress-strain data from selected TXC tests conducted at confining pressures between 5 and 400 MPa are plotted in Figures 28 and 29 as principal stress difference versus axial strain during shear and as principal stress difference versus volumetric strain during shear. One should note that the initial moduli of the TXC stress-strain curves (Figures 26 through 28) are a function of the material's initial volume changes during shear, which in turn are a function of the specimens' position on the material's pressure-volume curve at the start of shear. As confining pressure increases, the initial loading moduli of the material soften as the stress state moves into the crush regime of the pressure-volume curve, and then stiffen again as the material approaches void closure, i.e., the point at which all of the specimen's air-porosity is crushed out. At confining pressures of 5, 10, and 20 MPa, the specimens' initial volume changes are basically within the elastic regime of the pressure-volume curve[1] and the stress-strain curves exhibit stiff initial moduli. The TXC tests conducted at a confining pressure of 50 MPa had a softer response (lower moduli) during the initial shear loading than the tests at 5, 10, and 20 MPa. The tests conducted at a confining pressure of 100 MPa depicted the softest initial moduli in stress difference-axial strain space (Figure 28). The test specimen at 100 MPa also depicted the softest response in stress difference-volume strain space (see Figure 29). The TXC tests conducted at 200 and 400 MPa exhibited increasingly stiffer initial moduli and they were all stiffer than the test at 100 MPa. The subsequent increase in initial moduli with increasing confining pressure during shear is directly related to the increasing stiffness in the pressure-volume response of the concrete. The principal stress difference-volume strain curves for tests performed at 5 and 10 MPa (Figure 30) exhibit minimal compressive volume strains unlike the other TXC tests because, at confining pressures of 5 and 10 MPa, the material is still in the elastic region. Figure 31 includes plots from the non-cyclic TXC tests between 100 and 400 MPa. This figure displays the material tendency of FACM to saturate; i.e. the value for the peak principal stress difference for TXC with confining pressures of 200, 300, and 400 MPa.

[1] Recall that inelastic volume strains during hydrostatic loading stated at pressures above 27.6 MPa.

The TXC stress-strain results illustrate both the brittle and ductile nature of this material. At confining pressures of 20 MPa and below, the material behaves in a brittle manner; i.e., the material strain softens, and the majority of the post-peak stress or strain data is unreliable. All of these test specimens developed either through-going fractures or strain localizations. At confining pressures of 100 MPa and above, the material behaves in a ductile manner; i.e., the stress-strain curves exhibit strain hardening. Between 50 and 100 MPa, there is the brittle-to-ductile transition, where the material flows at a constant value of principal stress difference.

The failure data from all of the shear tests, UC and TXC tests, are plotted in Figure 32 as principal stress difference versus mean normal stress; one stress path at each confining stress is also plotted. In Figure 33, a recommended failure surface is plotted with the failure points. The quality of the failure data is very good in that very little scatter is exhibited. The unconfined compressive strength of FACM is 46.25 MPa; this failure point plots at a mean normal stress of 15.6 MPa in Figure 33. It is important to note that the failure points exhibit a continuous increase in principal stress difference with increasing values of mean normal stress. The rate of increase is reduced after reaching a mean normal stress of approximately 300 MPa. The response data from the 400 MPa TXC tests indicate that, at a mean normal stress of approximately 517 MPa, FACM has reached almost complete void closure, i.e. constant principal stress difference. Concrete materials will continue to gain strength with increasing pressure until all of the air porosity in the concrete has been crushed out; i.e., when void closure is reached. It is important to recognize that void closure can be attained during the shear loading phase of the TXC tests as well as under hydrostatic loading conditions. At levels of mean normal stress above void closure, the failure surface will have a minimal slope.

Results from TXC tests with confining pressures ranging from 5 to 400 MPa are plotted in Figure 34 as radial strain during shear versus axial strain during shear. A contour of zero volumetric strain during shear is also plotted on this figure. When the instantaneous slope of a curve is shallower than the contour of zero volumetric strain, the specimen is in a state of volume compression; when steeper, the specimen is in a state of dilation or volume expansion. Data points plotting below the contour signify that a test specimen has dilated and the current volume of the specimen is greater than the volume at the start of shear.

Although it is difficult to prove with the TXC data, this material is subject to significant shear-induced volumetric strains. This means that a significant portion of the volume changes observed in Figure 34 are due to shear and not changes in pressure. In an attempt to show this behavior, the pressure-volume data from two TXC tests are compared in Figure 35 to the pressure-volume data from the HC tests. The data from the TXC tests were plotted until the specimens began to dilate; i.e., only the compressive volumetric strains during the HC and shear phases were plotted. It is clear from this figure that, at a given pressure, all of the pressure-volume curves from the TXC tests exhibit larger volumetric strains than the HC tests. This increase in volume strain is due to compressive shear-induced volume changes. Shear-induced volume strains are addressed again in a later section of this chapter.

Conventional and Reduced Triaxial Extension Test Results

Extension shear and failure data were successfully obtained from five direct pull tests, one conventional triaxial extension test, and three reduced triaxial extension tests. The DP tests are a special type of RTE test without the application of confining pressure. Results from the DP tests are plotted in Figure 36, and results from the CTE test and the RTE tests are plotted in Figures 37 through 38. The stress-strain data from the CTE test and the RTE tests are plotted in Figure 37 and the stress-paths in Figure 38. The stress-strain data in Figure 37 displays the CTE test and the RTE test results conducted at confining pressures of 10, 50 and 65 MPa. All of the specimens fractured. The CTE and RTE test data in Figure 37 displays variations in the curves caused by the different paths, the different confining pressures, and the manual operation of the device used to perform these tests. The stress path for the CTE test at a confining pressure of 10 MPa exhibits similar failure data as the RTE tests run at a confining pressure of 65 MPa. The confining pressure for test 35 was increased to cause the specimen to fail after approaching zero axial stress. Figure 39 displays data from selected TXC tests; the results from the CTE test, the DP tests, and the RTE tests; and the recommended compression and extension failure surfaces for FACM. The figure shows that the area under the extension failure surface is less than the area under the compression failure surface. FACM can withstand more deviatoric stress in compression than extension before failure occurs, which is typical behavior for concrete materials.

Uniaxial Strain Test Results

One-dimensional compressibility data were obtained from undrained uniaxial strain (UX) tests with lateral stress measurements. Two UX tests were successfully conducted during the test program. Data from the two tests are plotted in Figures 40 through 43; the stress-strain data from the UX tests are plotted in Figure 40, the stress-paths in Figure 41, the pressure-volume data in Figure 42, and the stress paths with the failure surface data in Figure 43. The results indicate that during these tests, both specimens reached a fully saturated state, i.e., the volume strains achieved during the tests were greater than the air porosity of the specimens. Evidence for this conclusion can be observed in the decreasing moduli in the stress-paths of the tests, i.e., there is a noticeable softening observed in the stress paths at a principal stress difference of approximately 340 MPa.

From the initial UX stress-strain loading data, a constrained modulus of 21.3 GPa was calculated. UX data may also be plotted as principal stress difference versus principal strain difference; the slope of an elastic material in this space is 2G. A shear modulus of 8.4 GPa was calculated from the UX loading data. These two values may be used to calculate any of the other elastic constants; e.g., the elastic bulk modulus is 10.1 GPa, the Young's modulus is 19.7 GPa, and Poisson's ratio is 0.17. Note that the above value of bulk modulus is identical to the value obtained from HC tests.

The pressure-volume responses from a HC and a UX test are compared in Figure 44. The pressure-volume responses are very similar and the initial loading moduli are identical. However, the pressure-volume response of test 21 has a lower mean normal stress after the initial loading of the specimen. The dry densities of the test specimens were different, 2.009 and 1.981 Mg/m^3 for the HC test specimens and 1.991 and 1.977 Mg/m^3 for the UX test specimens. Unfortunately, this data cannot be used to support the argument for shear-induced volume change of this material because the plots in Figure 42 show similar pressure-volume responses.

Strain Path Test Results

Three types of strain-path tests were conducted in this test program: UX/BX tests, i.e., tests with a uniaxial strain loading followed by constant axial strain unloading; UX/CV tests, i.e., tests with a uniaxial strain loading followed by constant volume strain loading; and UX/SP tests, i.e., tests with a uniaxial strain loading followed by constant strain ratio loading. Data was obtained from four UX/BX tests that were loaded to two peak nominal axial stresses during the initial UX phase. Data from the tests are plotted in Figures 45 through 49. The stress-strain data from the UX/BX tests are plotted in Figure 45, the stress-paths in Figure 46, the pressure-volume data in Figure 47, the strain-path data in Figure 48, and the stress paths with the failure surface data in Figure 49.

The small variation in the stress-strain response of test number 22 compared to the other three test specimens is due to the differences in the initial properties. Specimen number 22 had the highest wet density (2.117 Mg/m^3) and highest dry density (2.000 Mg/m^3) of the four UX/BX test specimens. The stress-strain curves plotted in Figure 45 illustrate that the specimens in each test were allowed to creep under zero-radial-strain boundary conditions prior to initiating the BX unloading. The stress paths plotted in Figure 46 are typical of most concretes. At the end of the UX loading and the beginning of the BX unload, there was some stress relaxation during the system change. More stress relaxation occurred for tests 22 and 23 because the system change time for the starts of BX unload was shorter than for tests 24 and 25. During the time of the system change from a loading to an unloading path, the material was allowed to creep. After the drop in principal stress difference, the stress paths start to approach a limiting surface. At this limiting surface (in many cases, the material's failure surface), the stress paths exhibit much larger decreases in principal stress difference resulting in the stress paths following the limiting surface. The pressure-volume data presented in Figure 47 illustrates the large amount of volume recovery that occurs during the BX unloading. Most of the specimens recover more than one-half of their peak compressive volume strain. Recall that the BX unloadings acquire shear data under a forced state of volumetric expansion. Figure 49 shows good agreement between the BX unloading and the failure surface from the TXC tests. Test 24 does not follow the failure surface as closely as the other UX/BX tests because the specimen experiences more volumetric expansion. The UX/BX stress paths are sensitive to the volumetric expansion of the material during the BX unloading and the mean normal stress levels during the initial UX loading effects. The results from the UX/BX tests validate the TXC failure surface.

Data were obtained from three UX/CV tests that were loaded to three different peak axial stresses during the initial UX phase. Data from the tests are plotted in Figures 50 through 54. The stress-strain data from the UX/CV tests are plotted in Figure 50, the stress-paths in Figure 51, the pressure-volume data in Figure 52, the strain path data in Figure 53, and the stress paths with the failure surface data in Figure 54. The stress paths plotted in Figure 51 are typical of stress paths obtained from similar porous materials. At the beginning of the constant-volume loading, the stress paths exhibit increasing values of principal stress difference and decreasing values of mean normal stress. After reaching a limiting surface, the stress paths move up and along that surface with increasing values of both principal stress difference and mean normal stress. As in the UX/BX tests, that limiting surface is usually the material's failure surface (Figure 54).

Data from the UX/SP tests are plotted in Figures 55 through 59; the stress-strain data are plotted in Figure 55, the stress-paths in Figure 56, the pressure-volume data in Figure 57, the strain path data in Figure 58, and the stress paths with the failure surface in Figure 59. Data were obtained from two UX/SP tests that were loaded to approximately the same peak nominal axial stresses during the initial UX phase. The peak nominal axial stress for the UX part of test 26 was 250 MPa while specimens 31 and 32 were loaded to 150 MPa. The slight differences in the plots for the UX/SP tests 31 and 32 results from the difference of the dry densities of the specimens (1.985 Mg/m^3 and 2.009 Mg/m^3). The plotted stress paths (Figure 56) demonstrate increasing values of principal stress difference and decreasing values of mean normal stress after the strain-ratio loading initiates. After the limiting surface is reached, the principal stress difference and the mean normal stress are both increasing. Test 26 was stopped when the specimen leaked, which was near the limiting surface. The plot in Figure 59 confirms that the limiting surface for the UX/SP tests is similar to the material's failure surface.

Comparison plots of selected UX, UX/BX, UX/CV, and UX/SP test results are plotted in Figures 60 through 64, the stress-strain data are plotted in Figure 60, the stress-paths are plotted in Figure 61, the pressure-volume data are plotted in Figure 62, the strain paths are plotted in Figure 63, and the stress-paths with the failure surface are plotted in Figure 64. Various peak nominal axial stresses were used to load the different tests during the initial UX phase. The small variations in all of the test results are due to the variability of the initial properties of the specimens. The dry densities ranged from a low of 1.954 Mg/m^3 to a high of 2.009 Mg/m^3. Figure 64 illustrates that the UX portion of the stress paths lie well below the failure surface at levels of mean normal stress above 40 MPa and below 400 MPa.

A benefit of conducting tests under certain types of strain paths is that it allows one to define a section of failure surface from one test. In Figure 64, test results for each of the different strain path tests and the TXC failure surface are overlaid to illustrate the merger of the data in the vicinity of a failure surface. The UX/BX, UX/CV, and UX/SP stress paths exhibits very good agreement with the failure surface. This figure clearly shows that the stress paths from the UX/BX, the UX/CV, and the UX/SP tests are either moving along the failure surface or have contacted the failure surface.

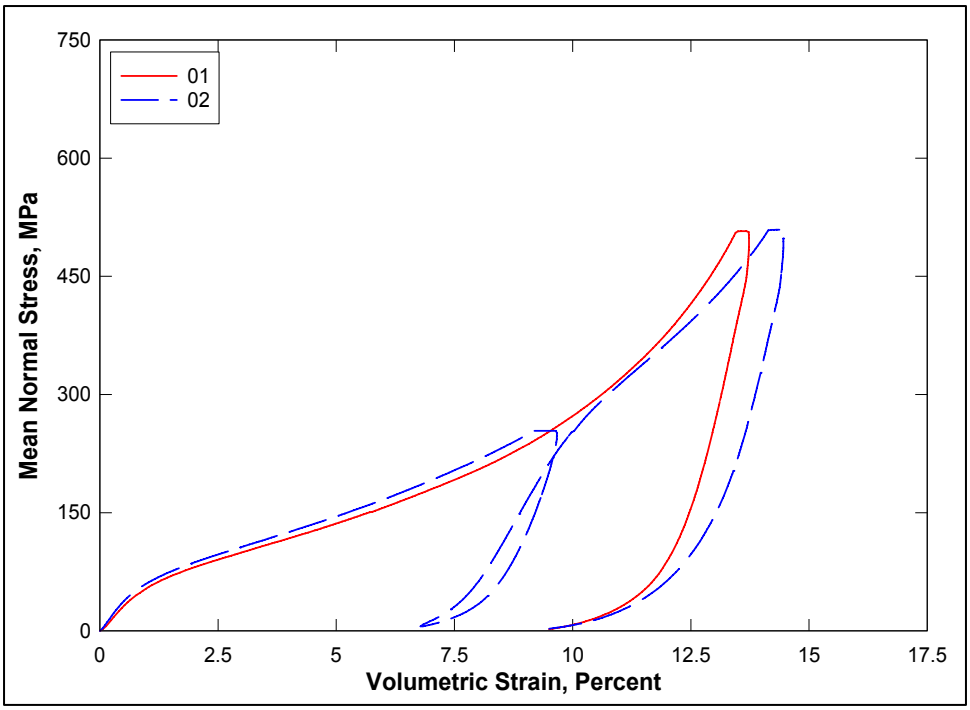

Figure 4. Pressure-volume responses from the HC tests

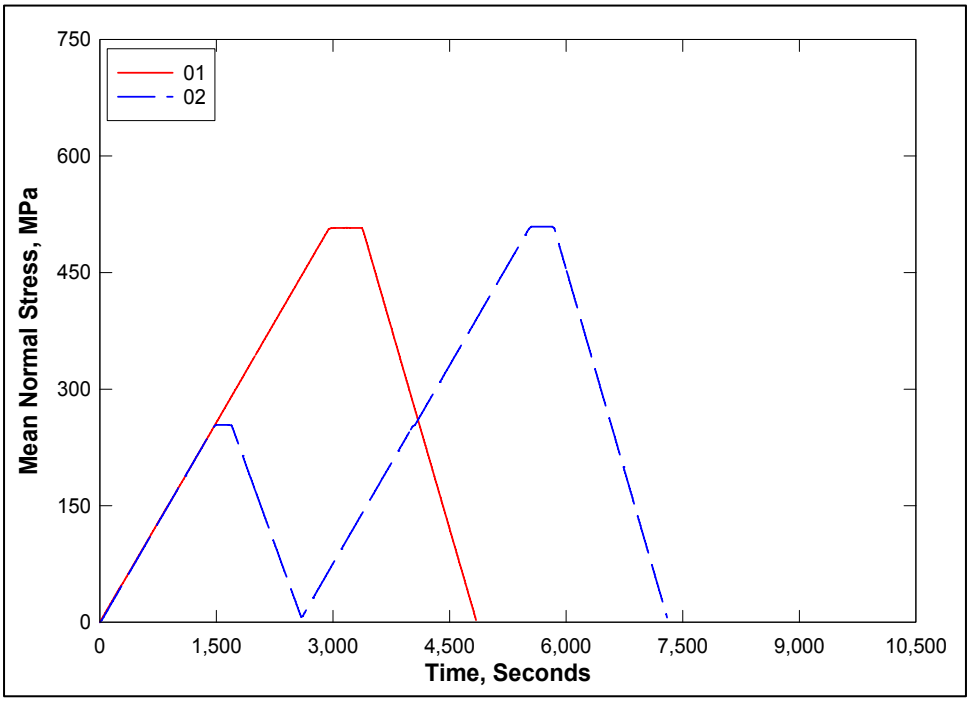

Figure 5. Pressure-time histories from the HC tests

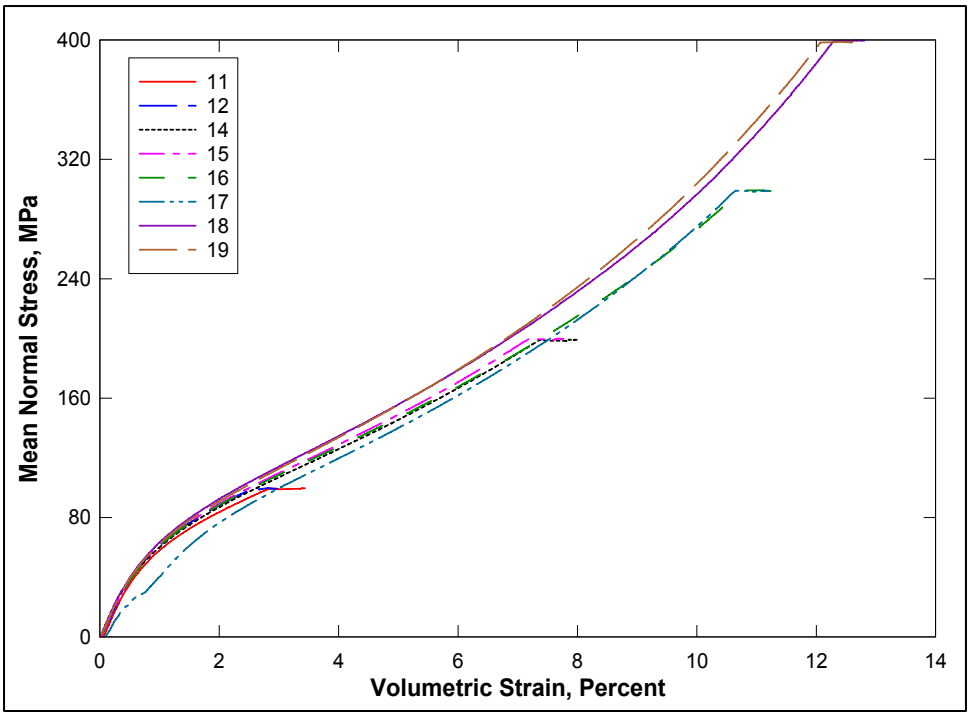

Figure 6. Pressure-volume responses from selected TXC tests

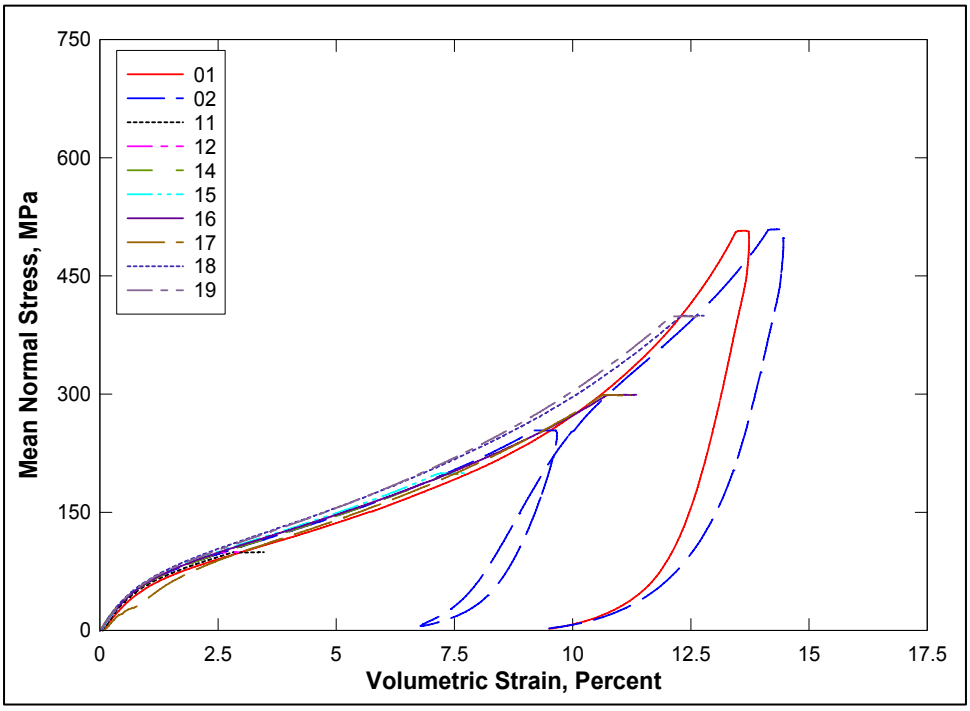

Figure 7. Pressure-volume responses from HC and selected TXC tests

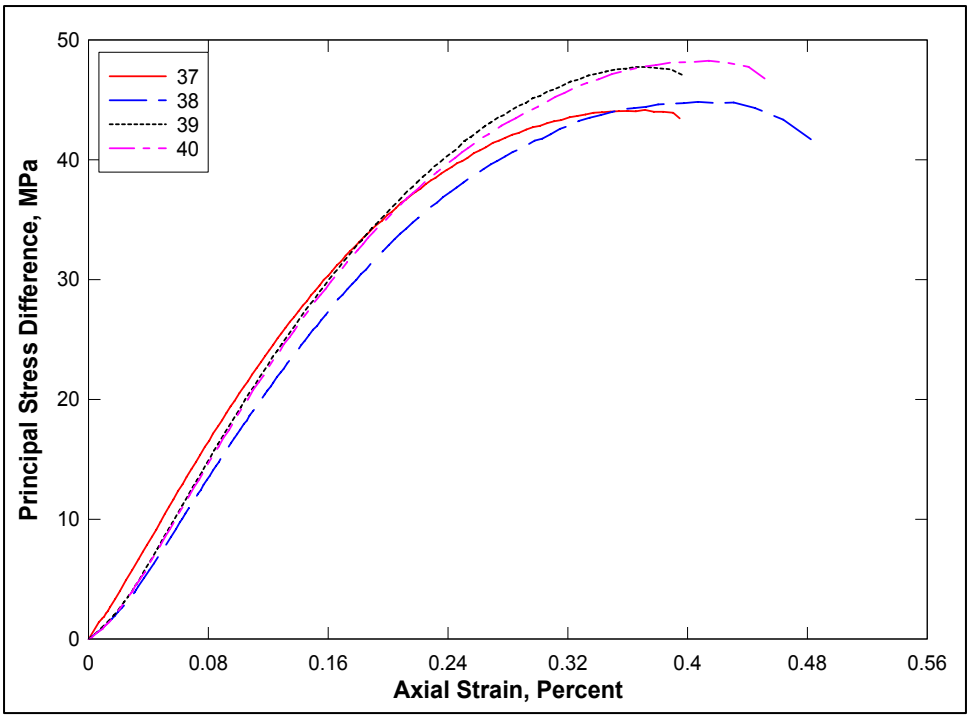

Figure 8. Stress-strain curves from UC tests

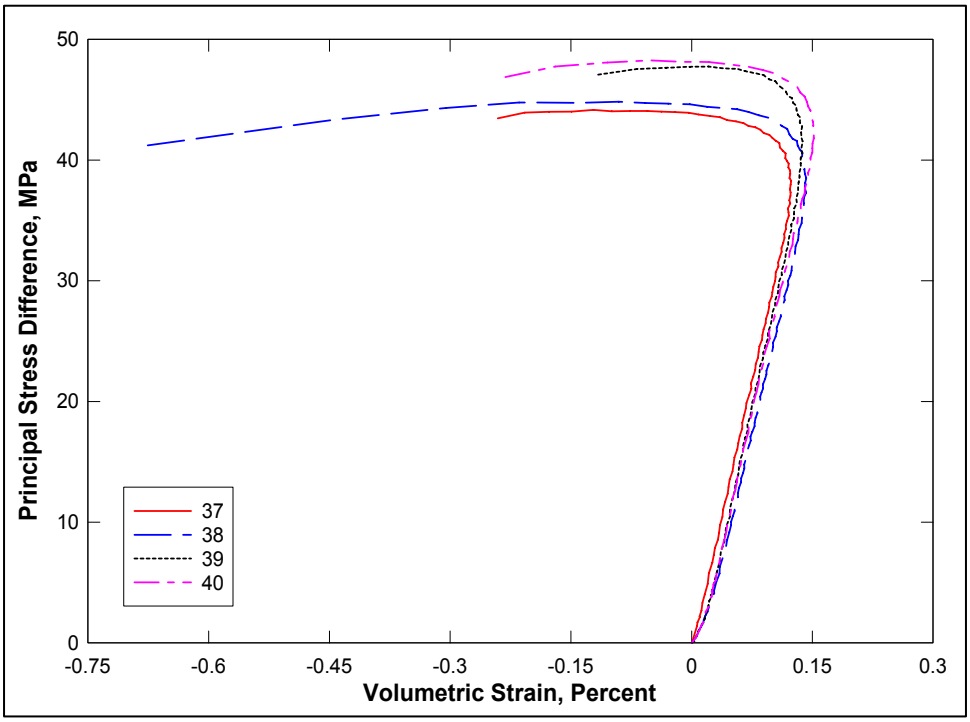

Figure 9. Stress difference-volume strain during shear from UC tests

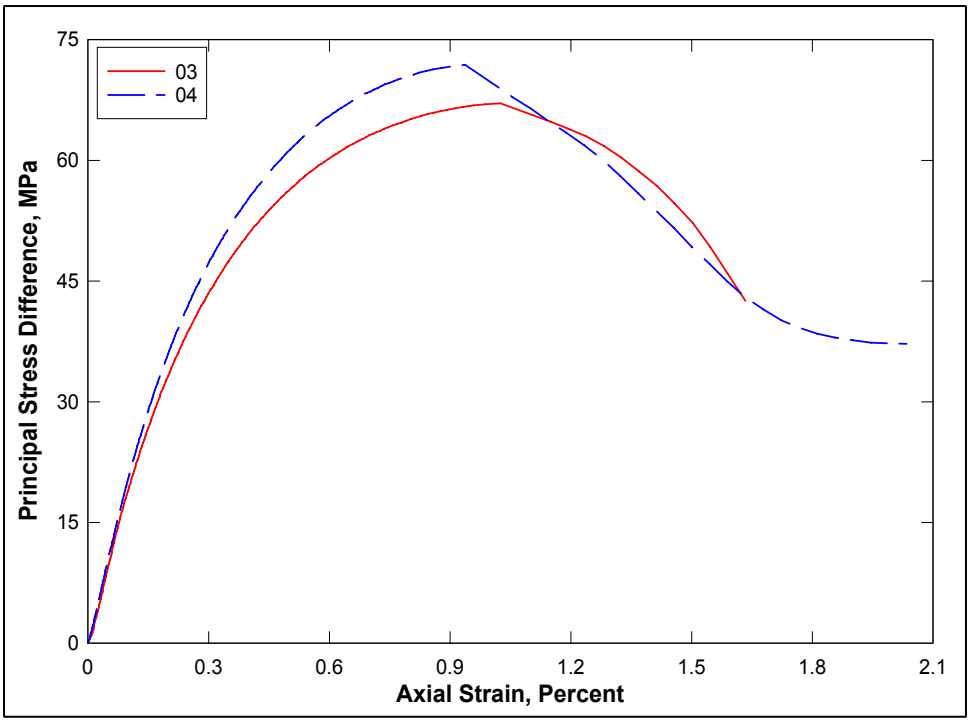

Figure 10. Stress-strain curves from TXC tests at a confining pressure of 5 MPa

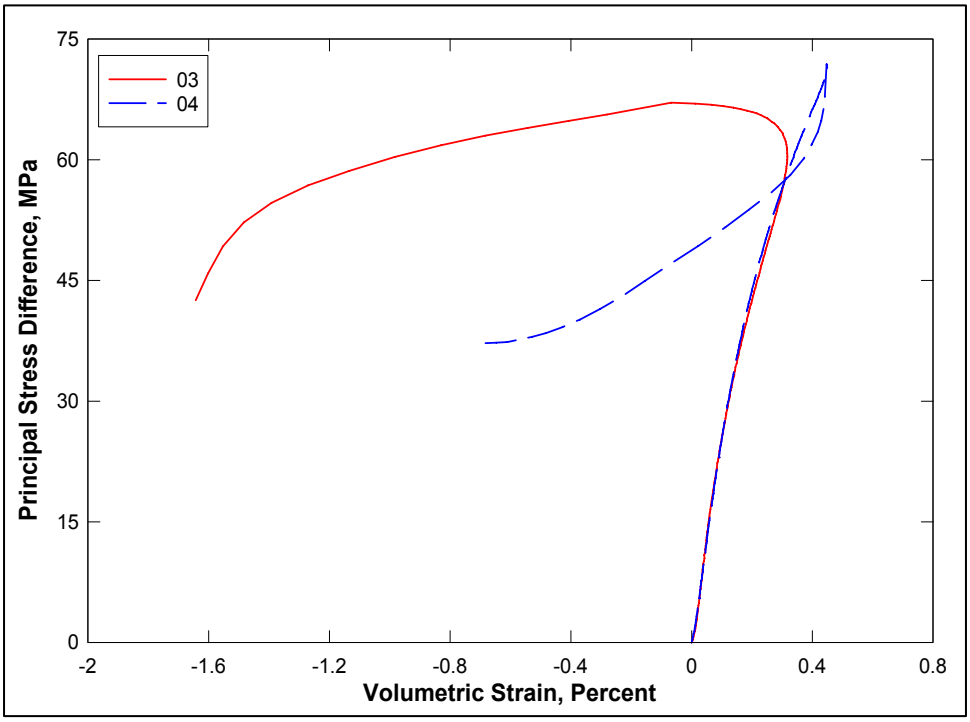

Figure 11. Stress difference-volume strain during shear from TXC tests at a confining pressure of 5 MPa

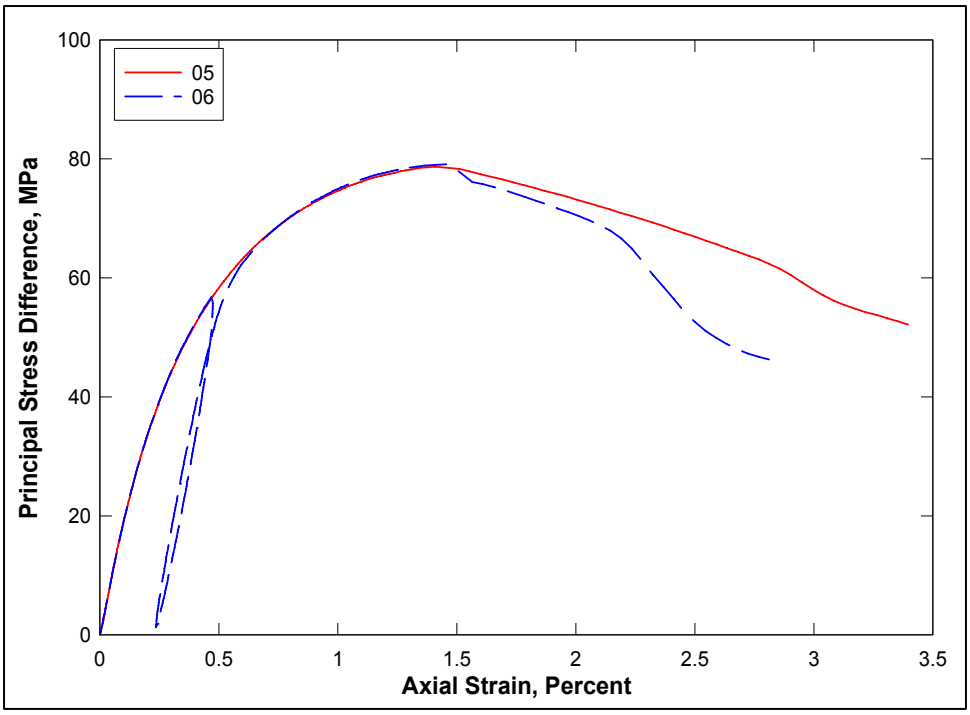

Figure 12. Stress-strain curves from TXC tests at a confining pressure of 10 MPa

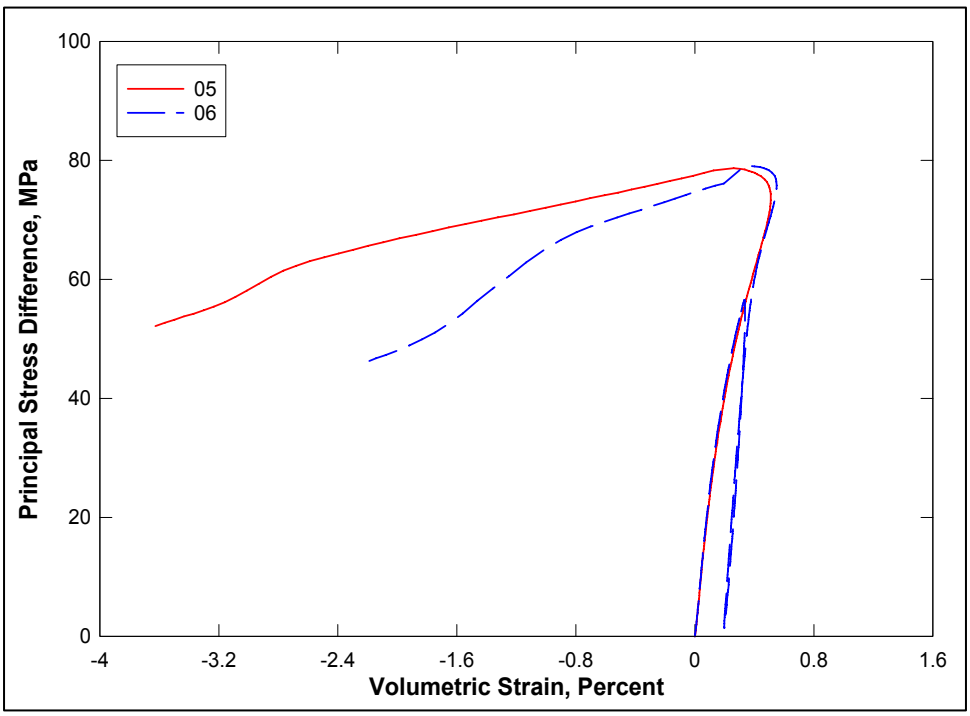

Figure 13. Stress difference-volume strain during shear from TXC tests at a confining pressure of 10 MPa

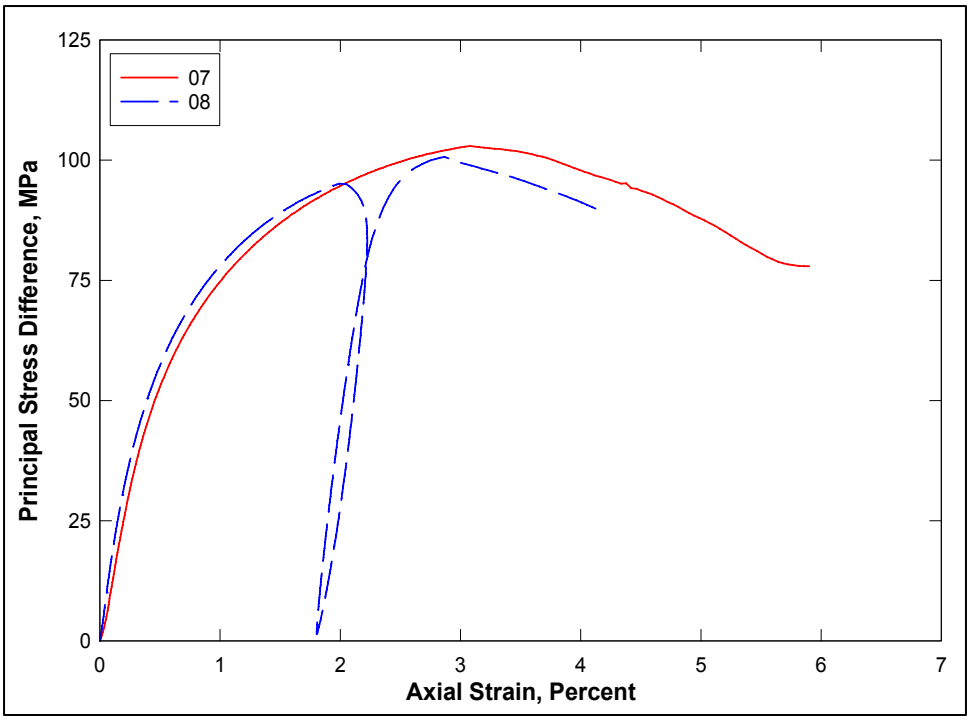

Figure 14. Stress-strain curves from TXC tests at a confining pressure of 20 MPa

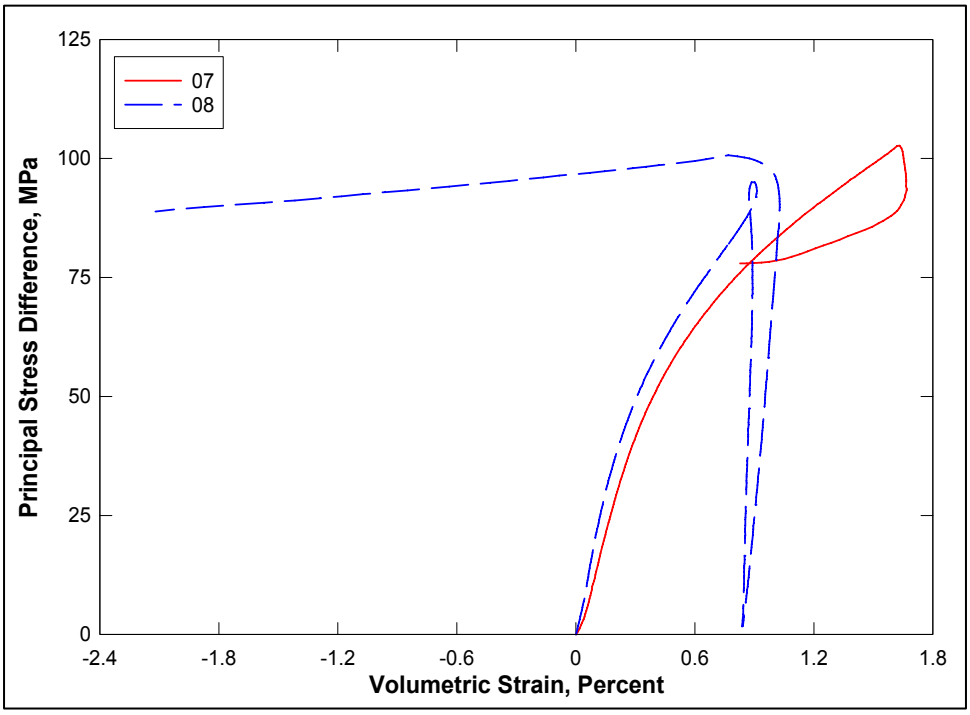

Figure 15. Stress difference-volume strain during shear from TXC tests at a confining pressure of 20 MPa

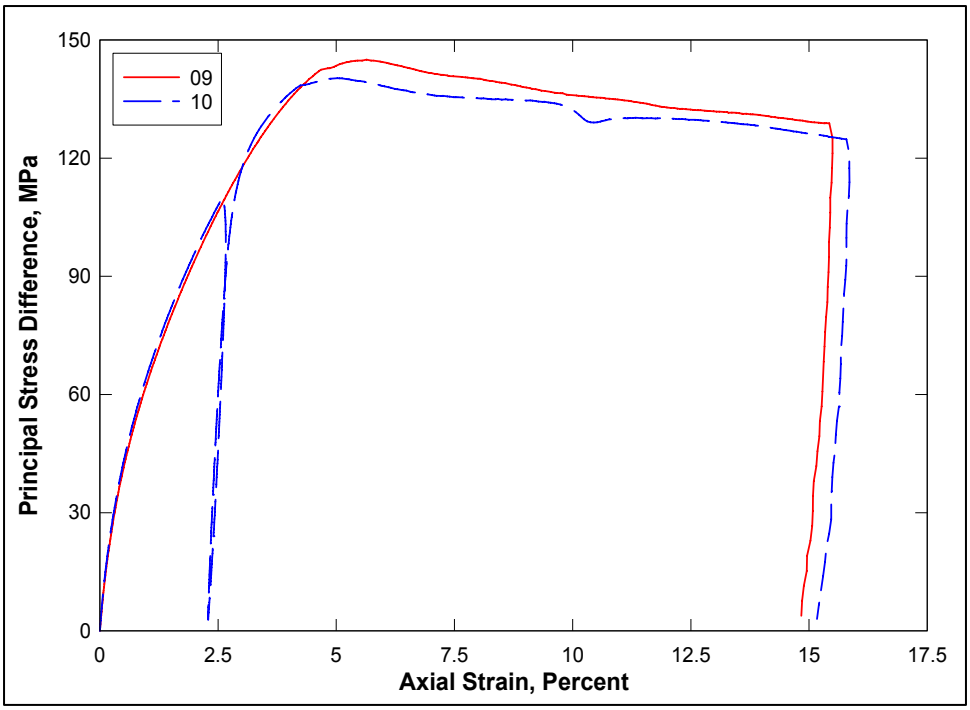

Figure 16. Stress-strain curves from TXC tests at a confining pressure of 50 MPa

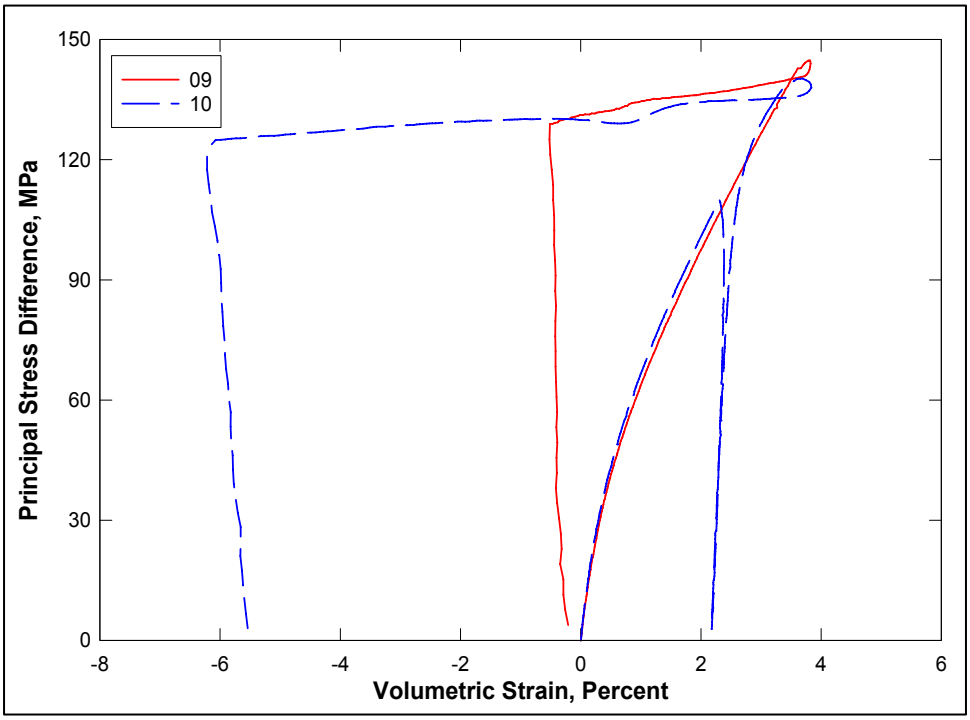

Figure 17. Stress difference-volume strain during shear from TXC tests at a confining pressure of 50 MPa

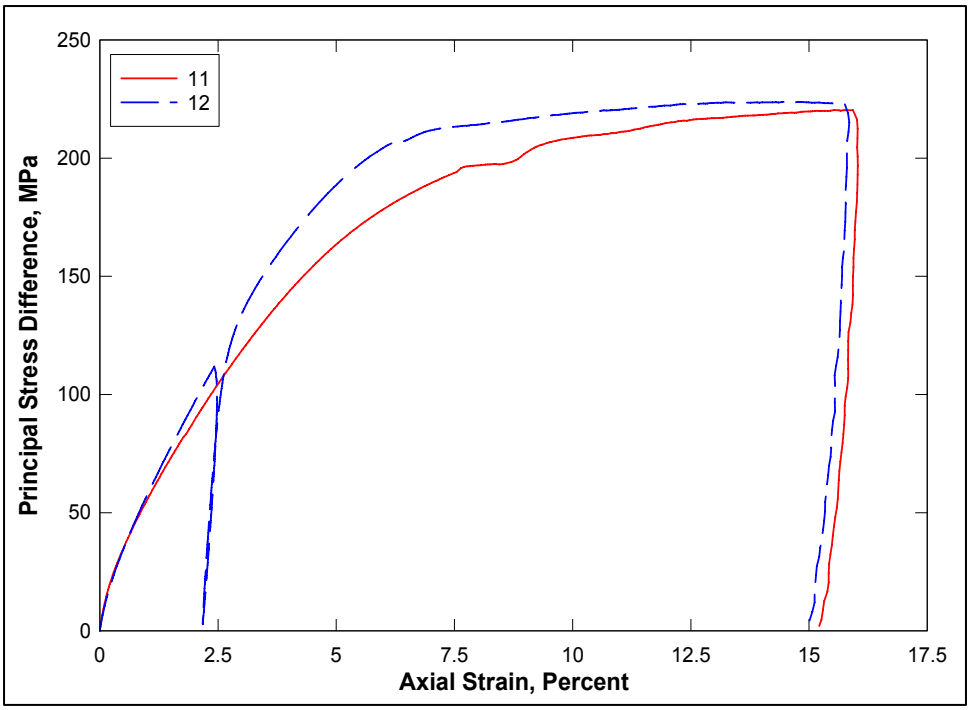

Figure 18. Stress-strain curves from TXC tests at a confining pressure of 100 MPa

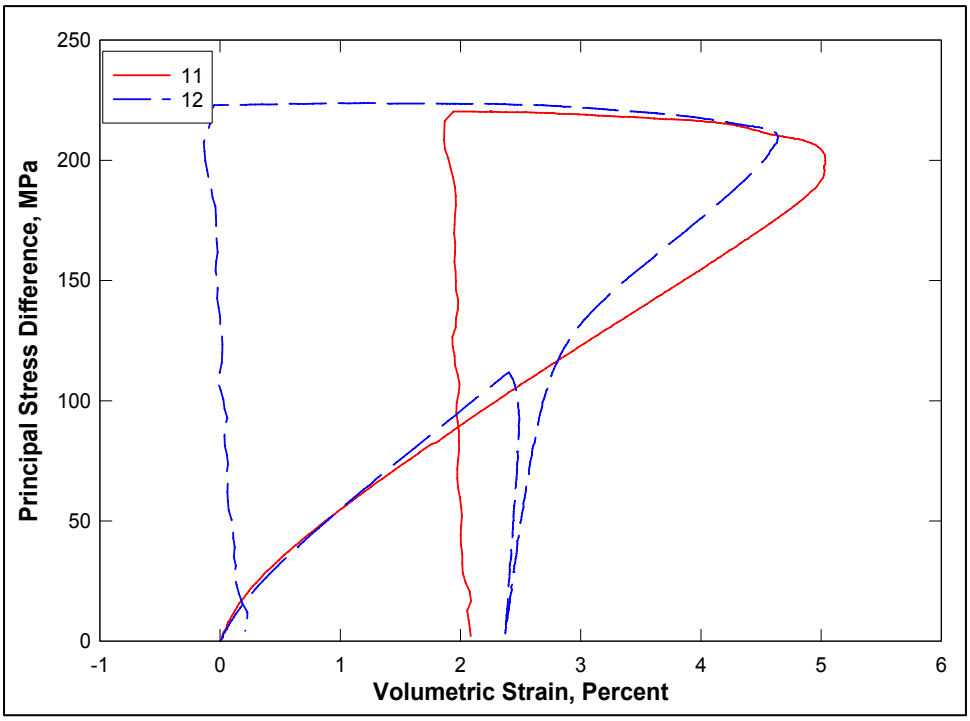

Figure 19. Stress difference-volume strain during shear from TXC tests at a confining pressure of 100 MPa

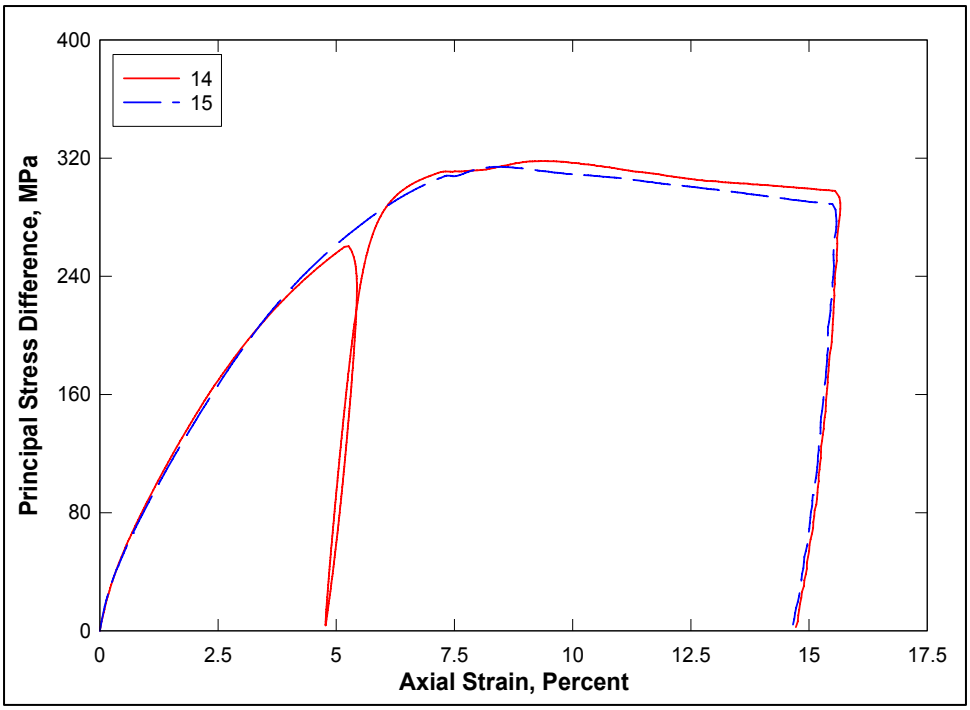

Figure 20. Stress-strain curves from TXC tests at a confining pressure of 200 MPa

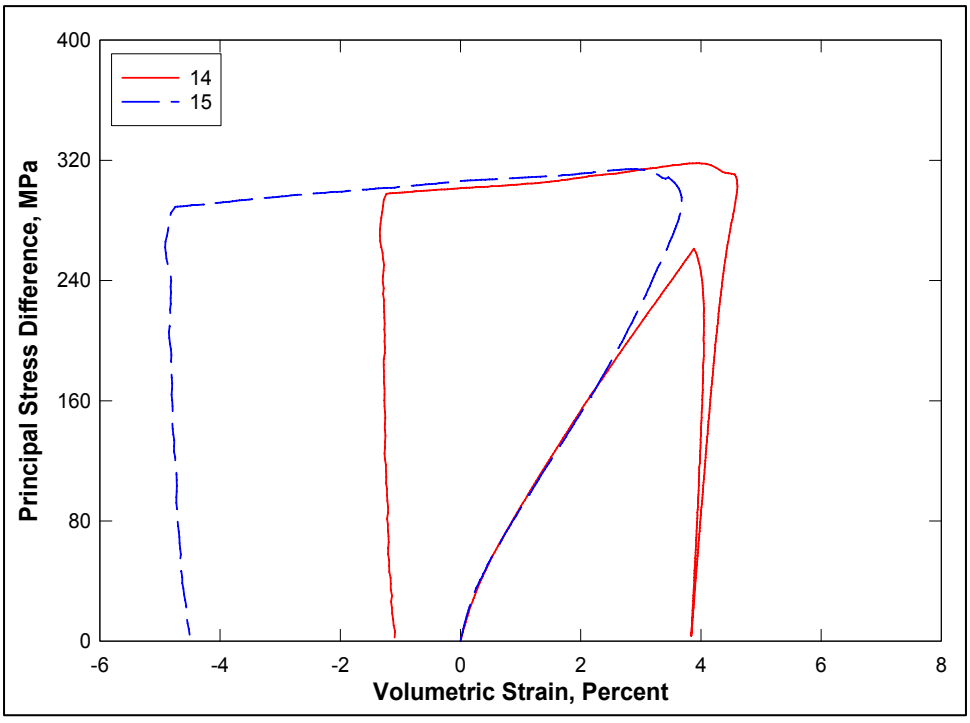

Figure 21. Stress difference-volume strain during shear from TXC tests at a confining pressure of 200 MPa

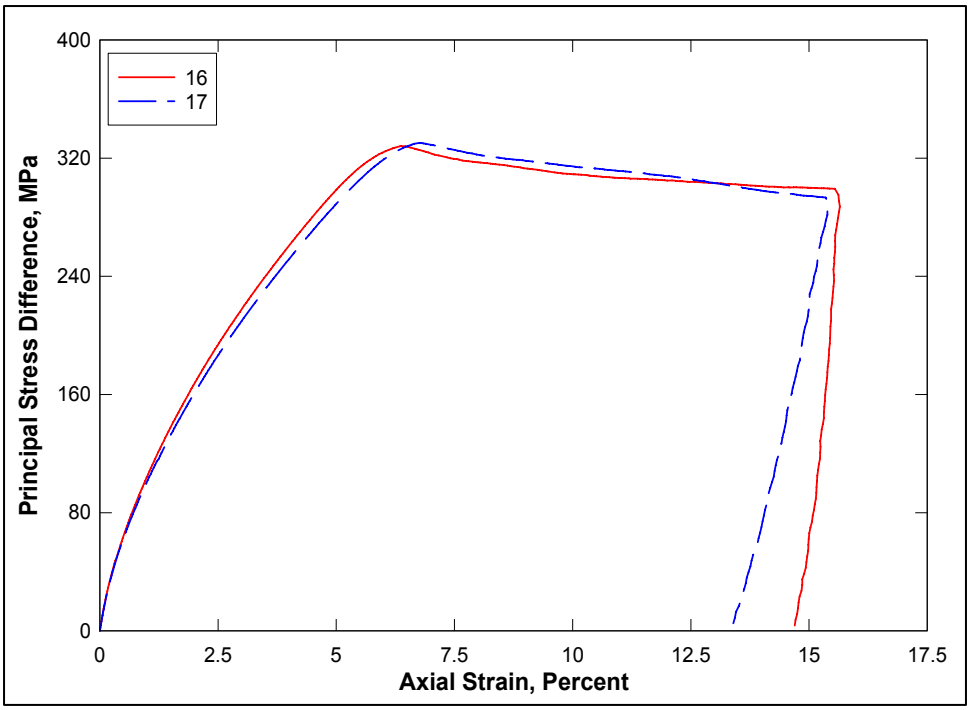

Figure 22. Stress-strain curves from TXC tests at a confining pressure of 300 MPa

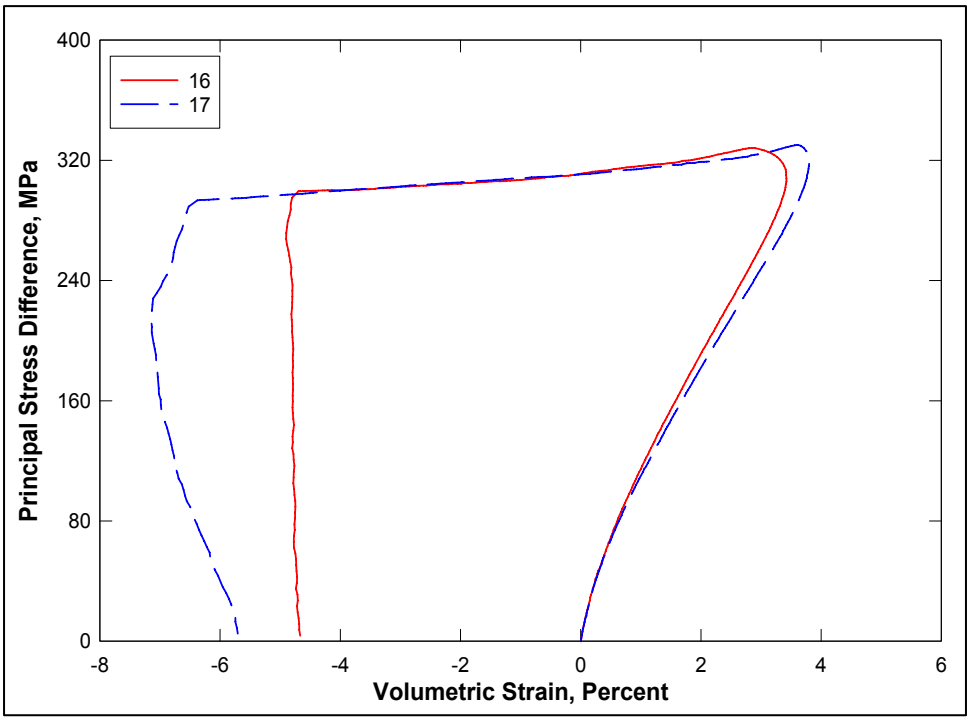

Figure 23. Stress difference-volume strain during shear from TXC tests at a confining pressure of 300 MPa

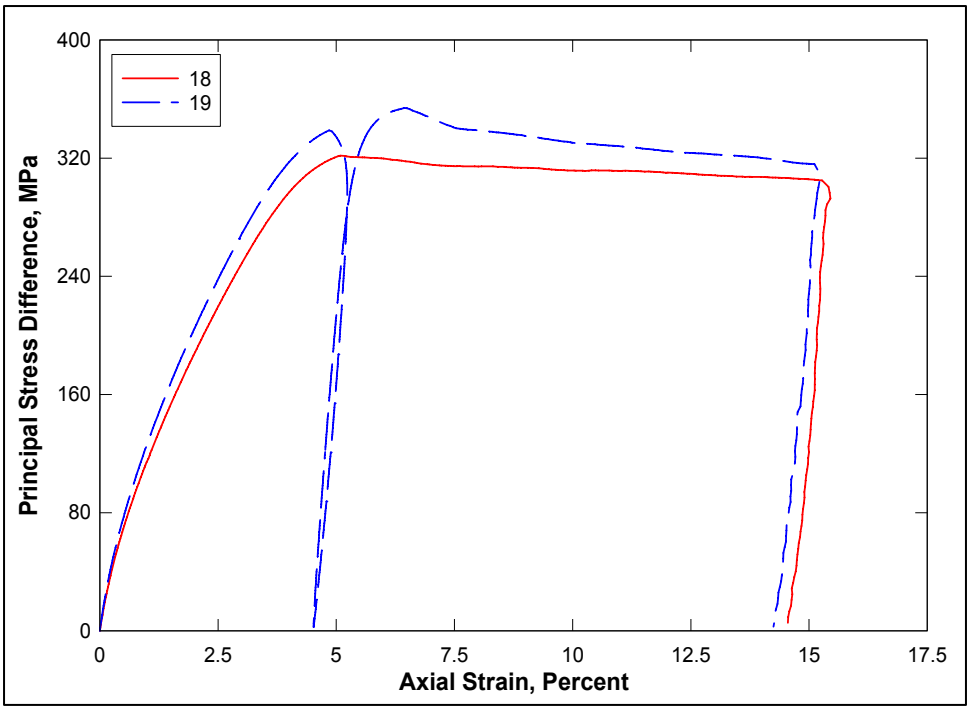

Figure 24. Stress-strain curves from TXC tests at a confining pressure of 400 MPa

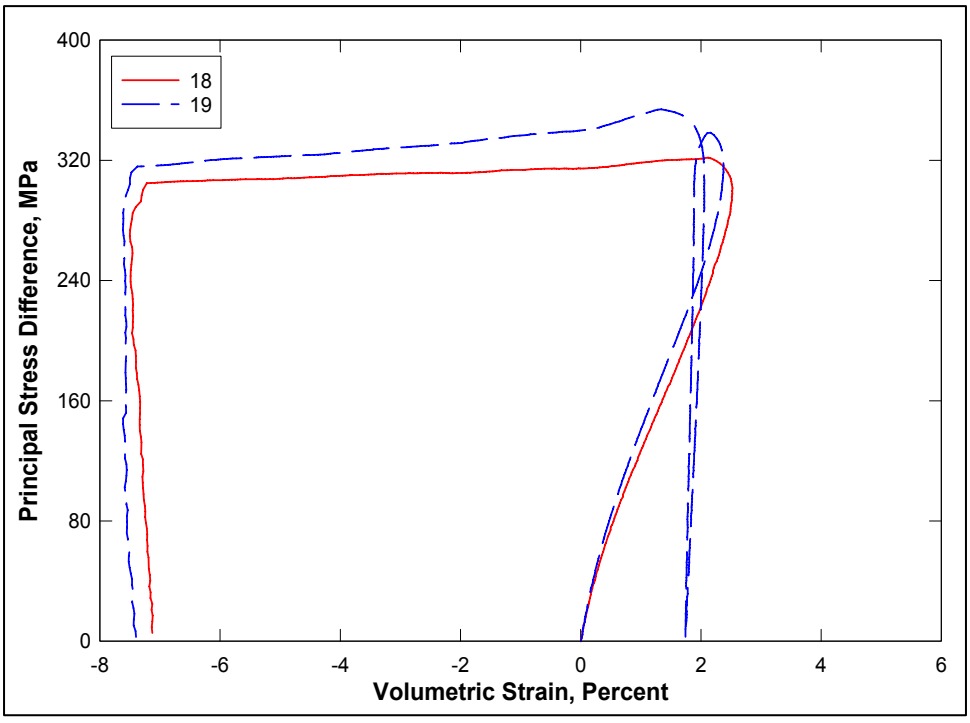

Figure 25. Stress difference-volume strain during shear from TXC tests at a confining pressure of 400 MPa

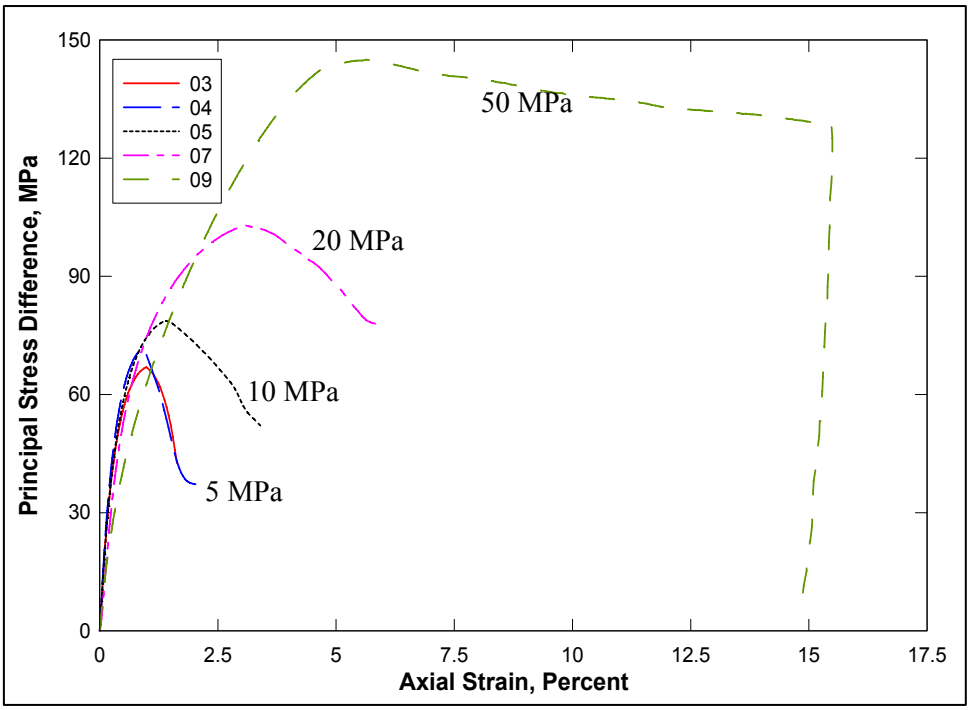

Figure 26. Stress-strain data from TXC non-cyclic tests at confining pressures between 5 and 50 MPa

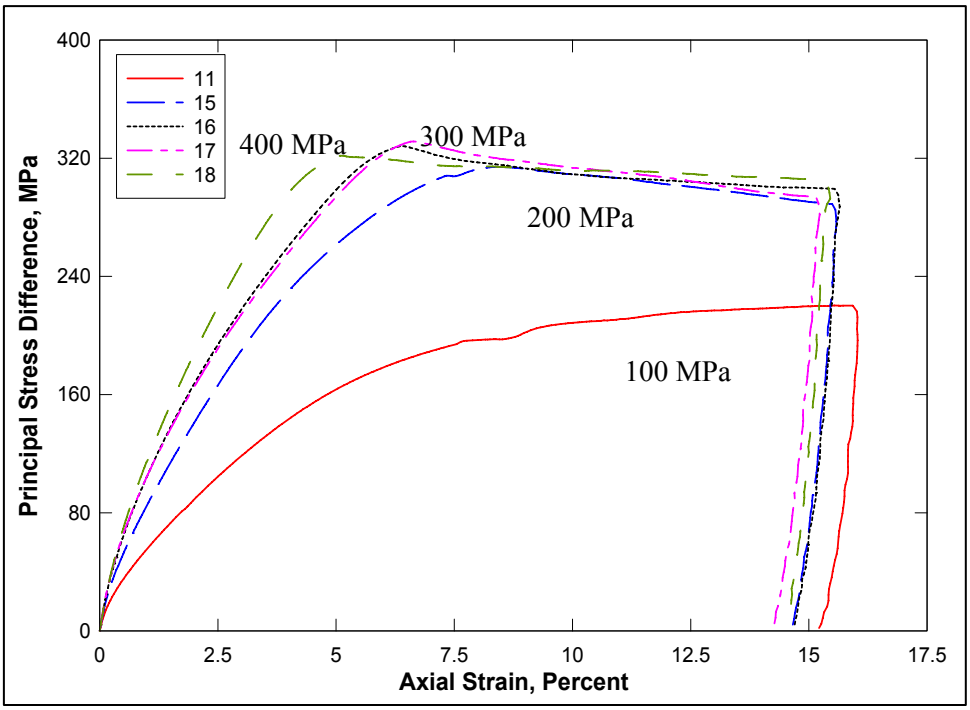

Figure 27. Stress-strain data from TXC non-cyclic tests at confining pressures between 100 and 400 MPa

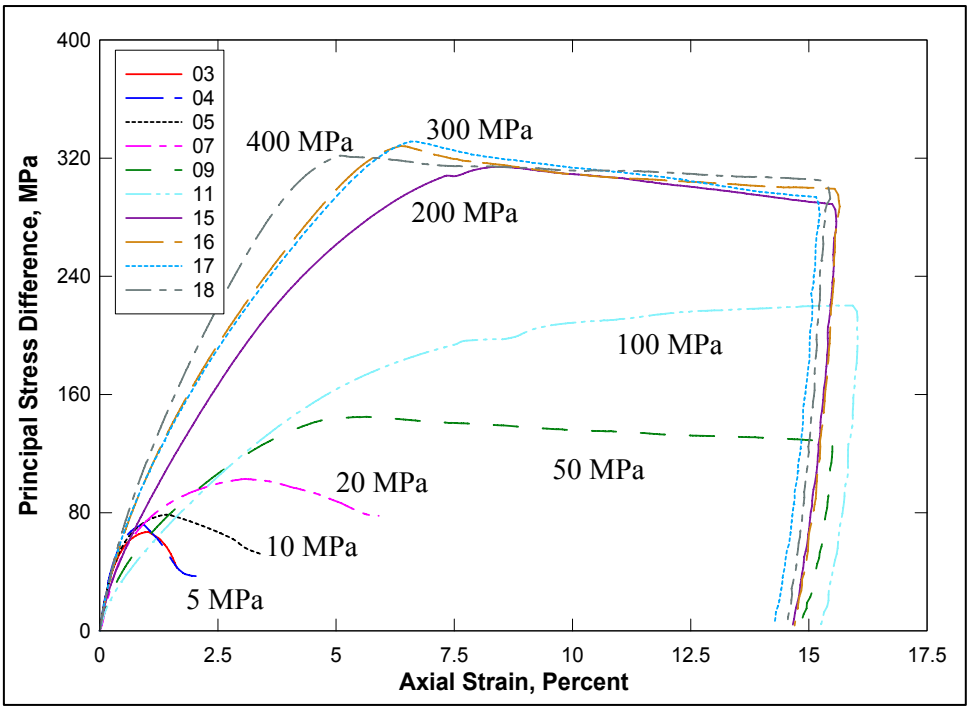

Figure 28. Stress-strain data from non-cyclic TXC tests at confining pressures between 5 and 400 MPa

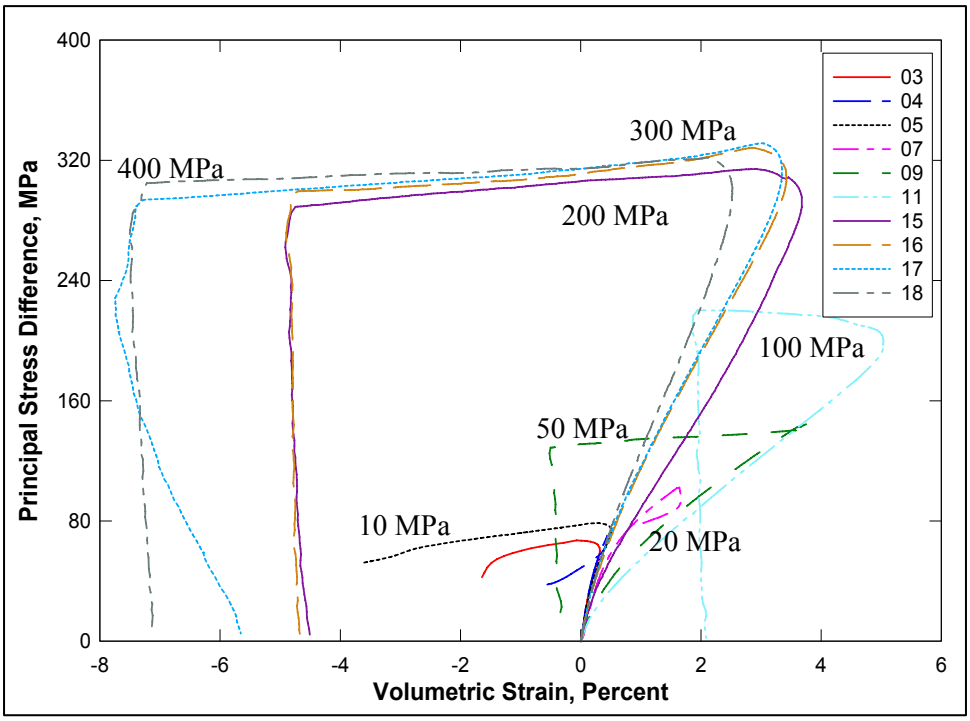

Figure 29. Stress difference-volume strain during shear from non-cyclic TXC tests at confining pressures between 5 and 400 MPa

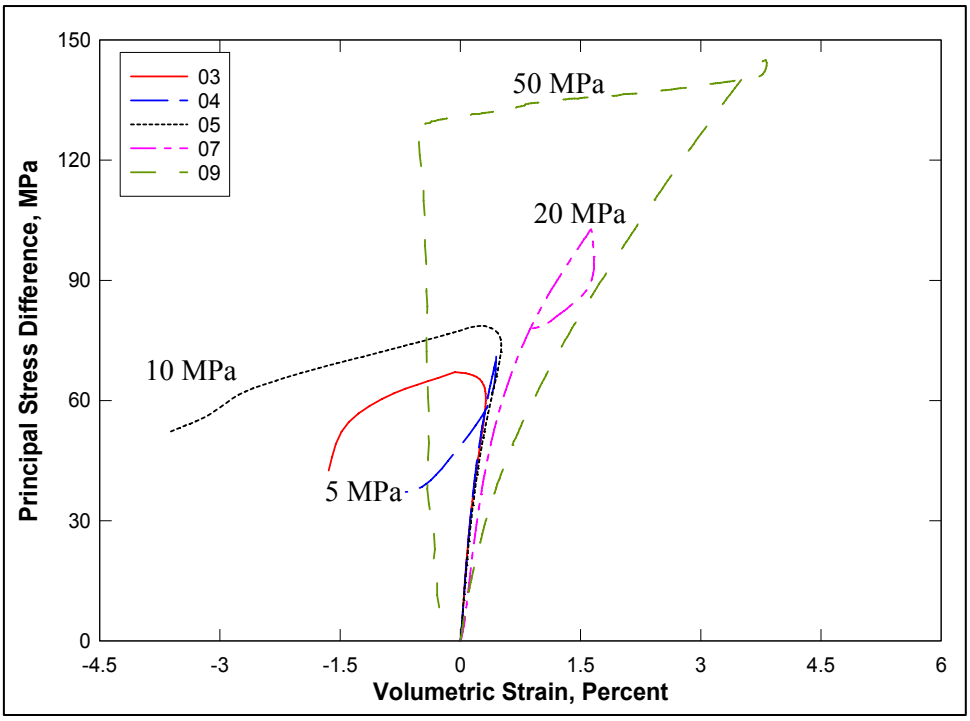

Figure 30. Stress difference-volume strain during shear from TXC non-cyclic tests at confining pressures between 5 and 50 MPa

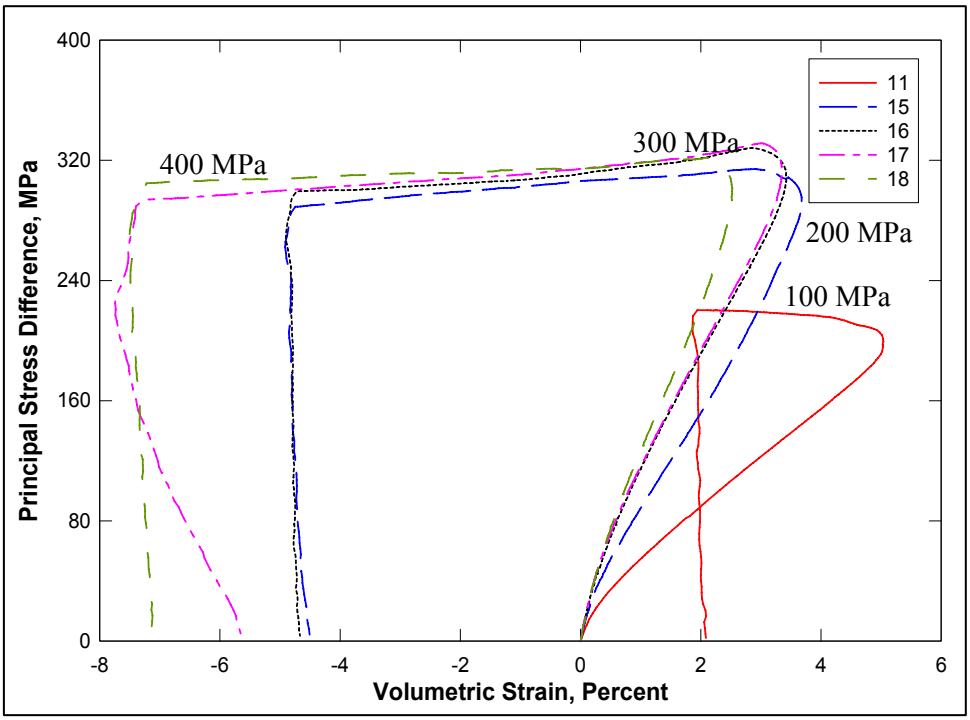

Figure 31. Stress difference-volume strain during shear from TXC non-cyclic tests at confining pressures between 50 and 400 MPa

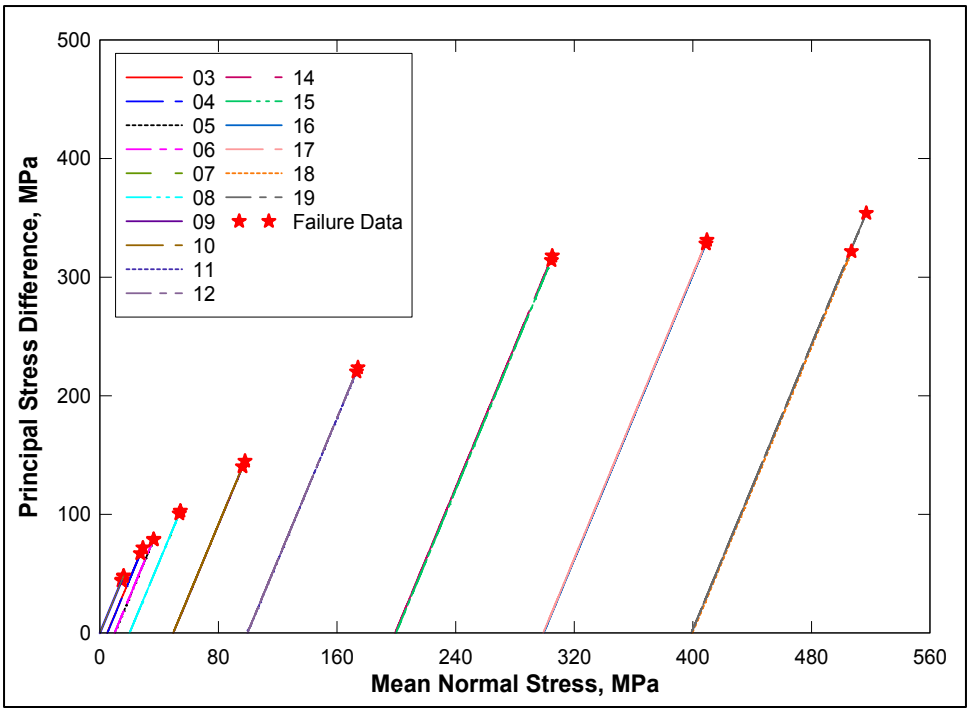

Figure 32. Stress difference-pressure during shear from TXC tests at confining pressures between 5 and 400 MPa

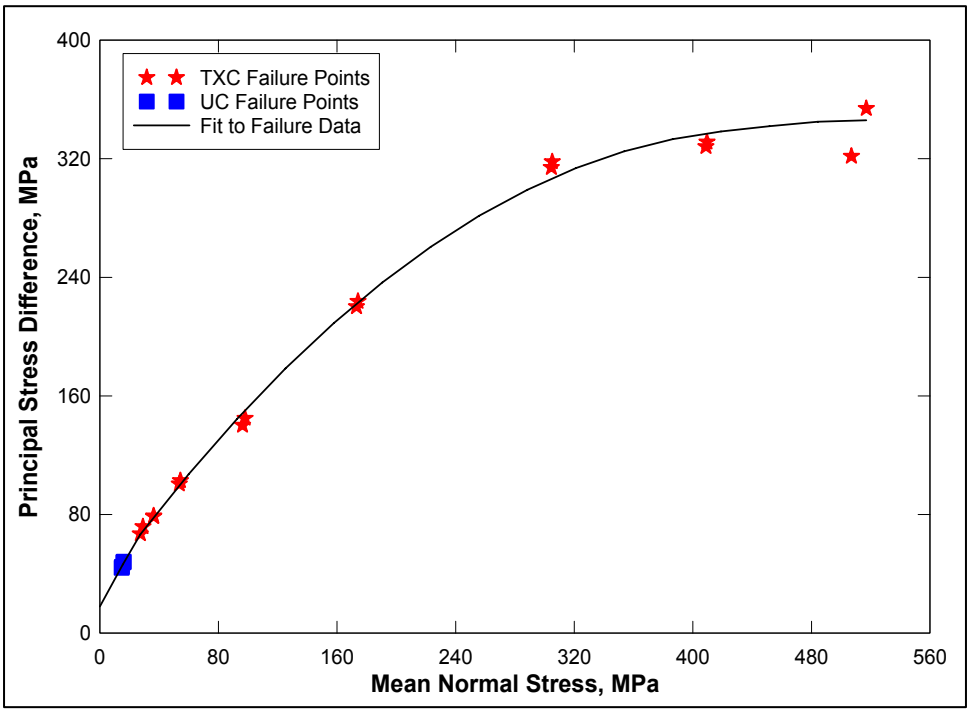

Figure 33. Failure points from UC and TXC tests and recommended failure surface

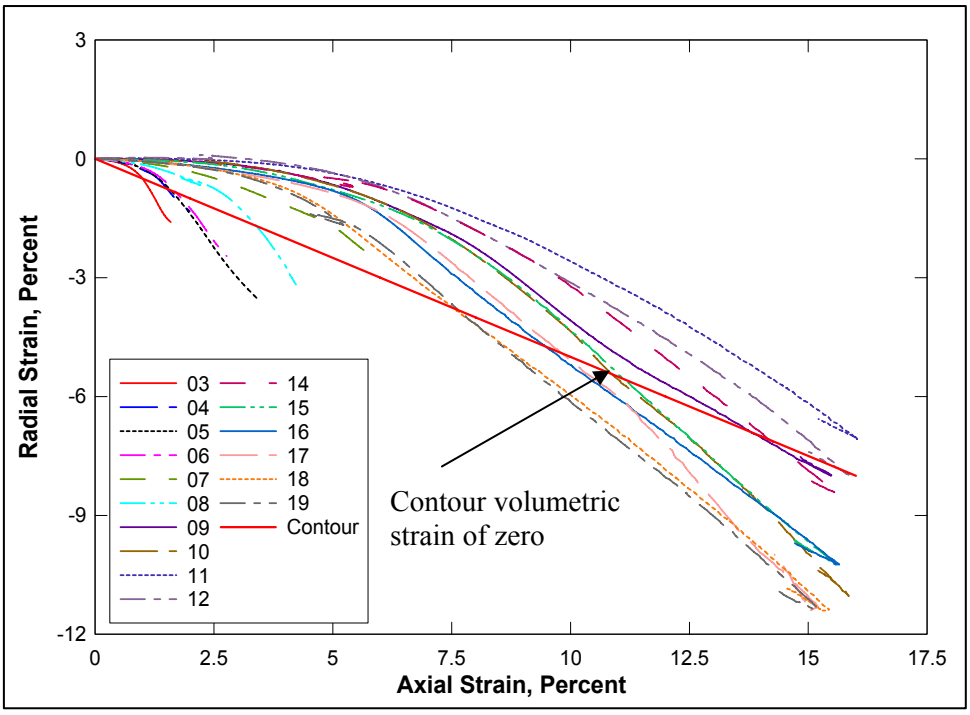

Figure 34. Radial strain-axial strain data during shear from TXC tests at confining pressures between 5 and 400 MPa

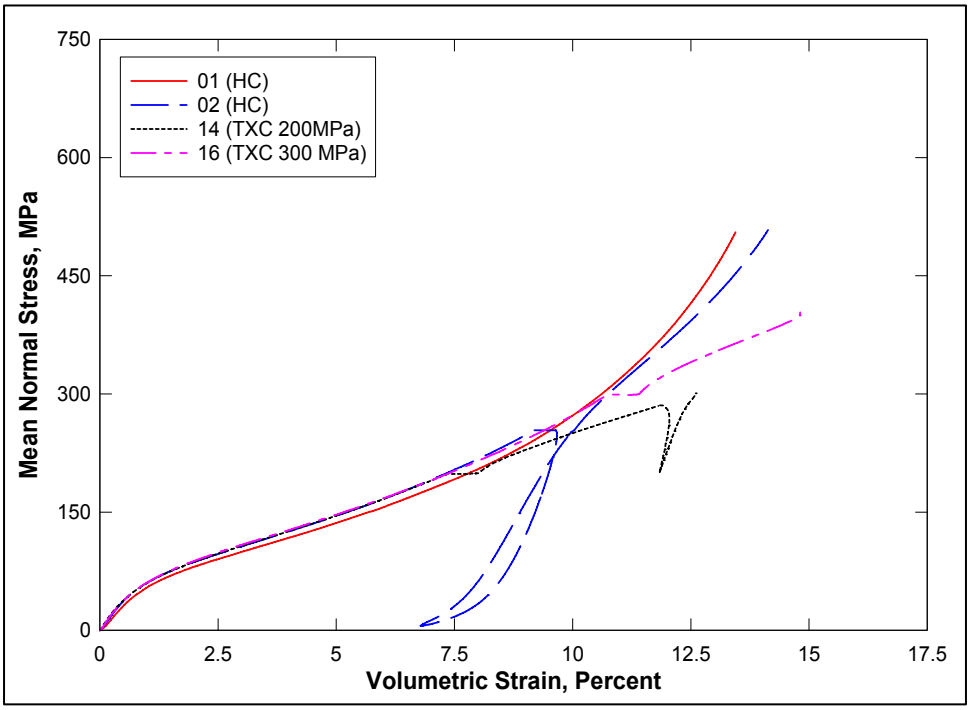

Figure 35. Pressure-volume curves from HC and selected TXC tests

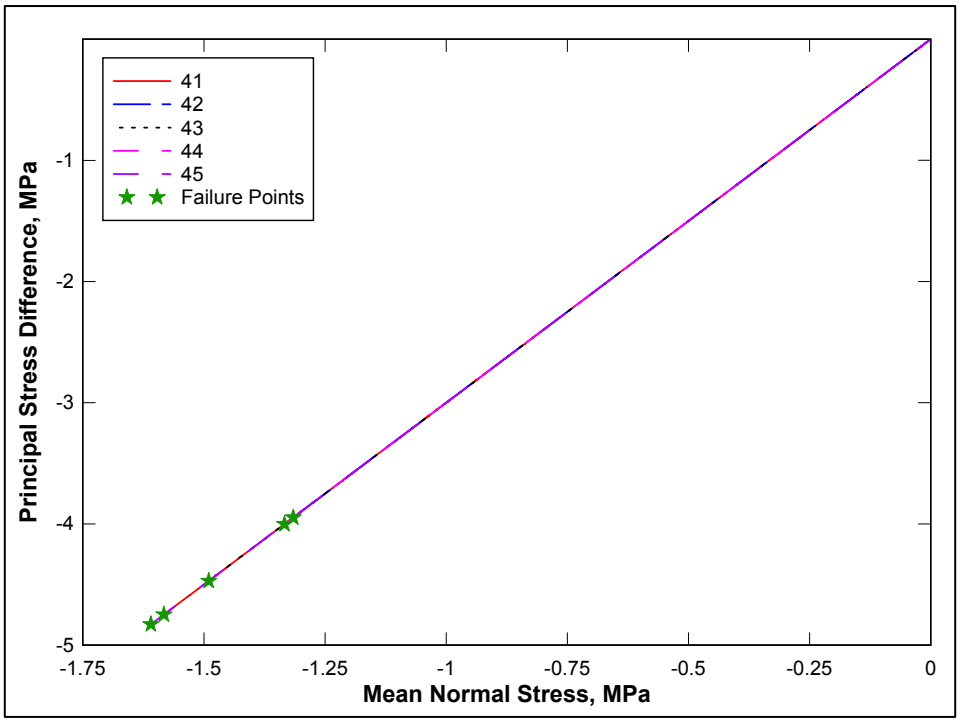

Figure 36. Stress paths and failure points from DP tests

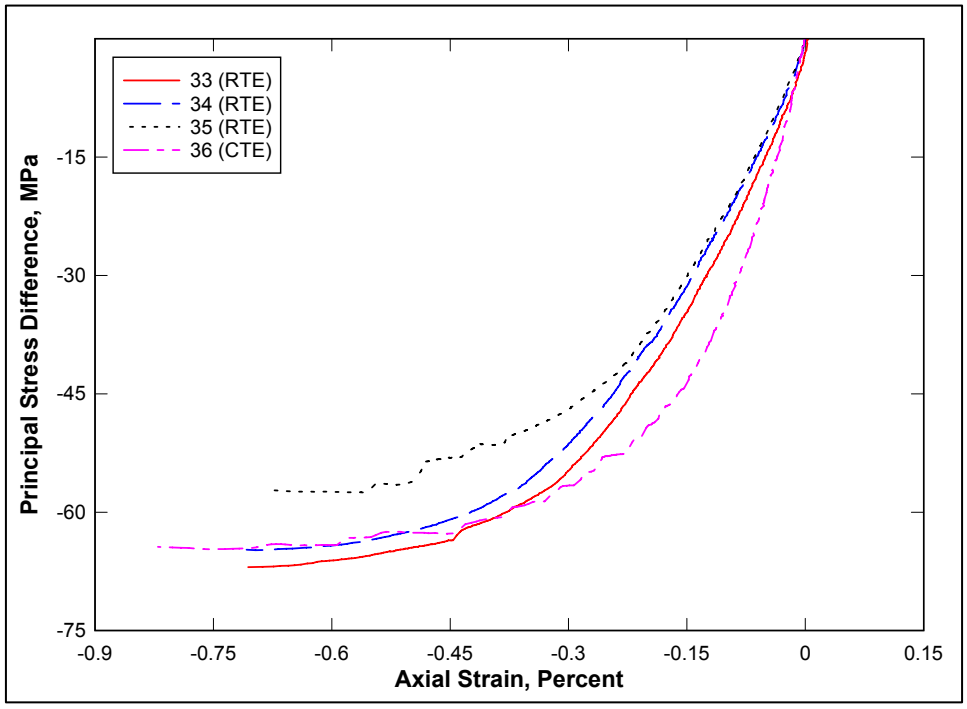

Figure 37. Stress-strain data from RTE tests and a CTE test

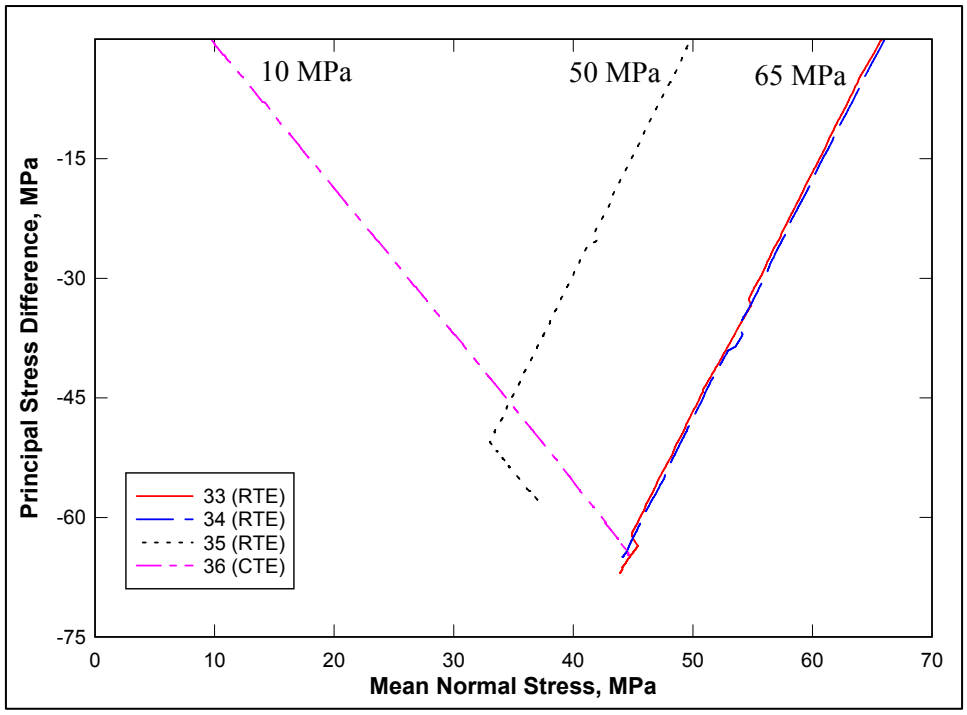

Figure 38. Stress path data from RTE tests and a CTE test

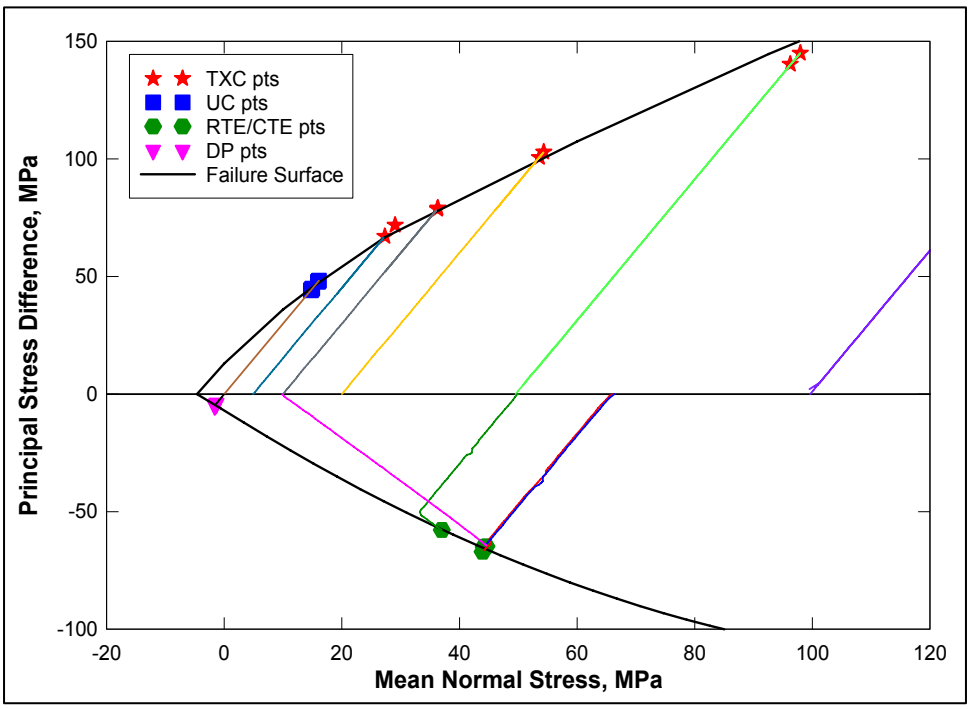

Figure 39. Failure surfaces and stress paths from UC tests, DP tests, RTE tests, CTE test, and the TXC tests between 5 MPa to 100 MPa

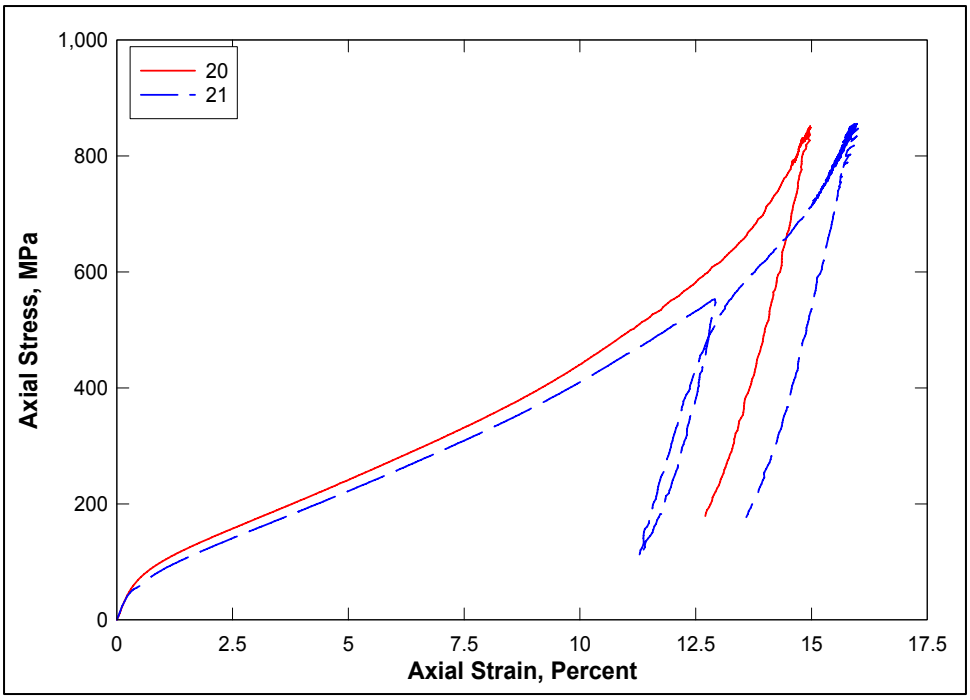

Figure 40. Stress-strain curves from UX tests

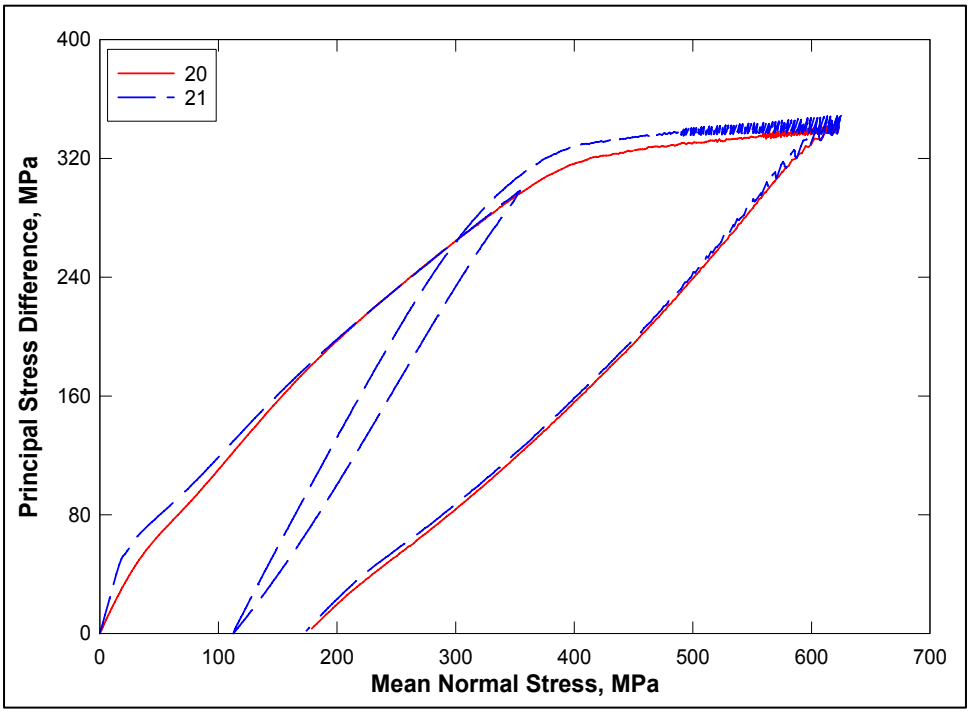

Figure 41. Stress paths from UX tests

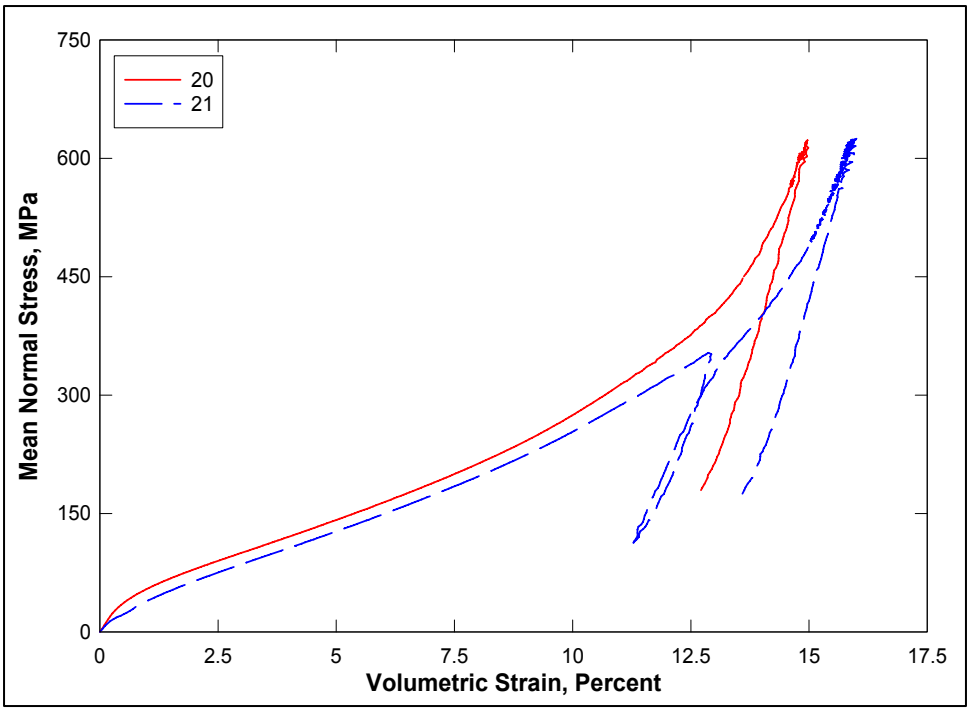

Figure 42. Pressure-volume data from UX tests

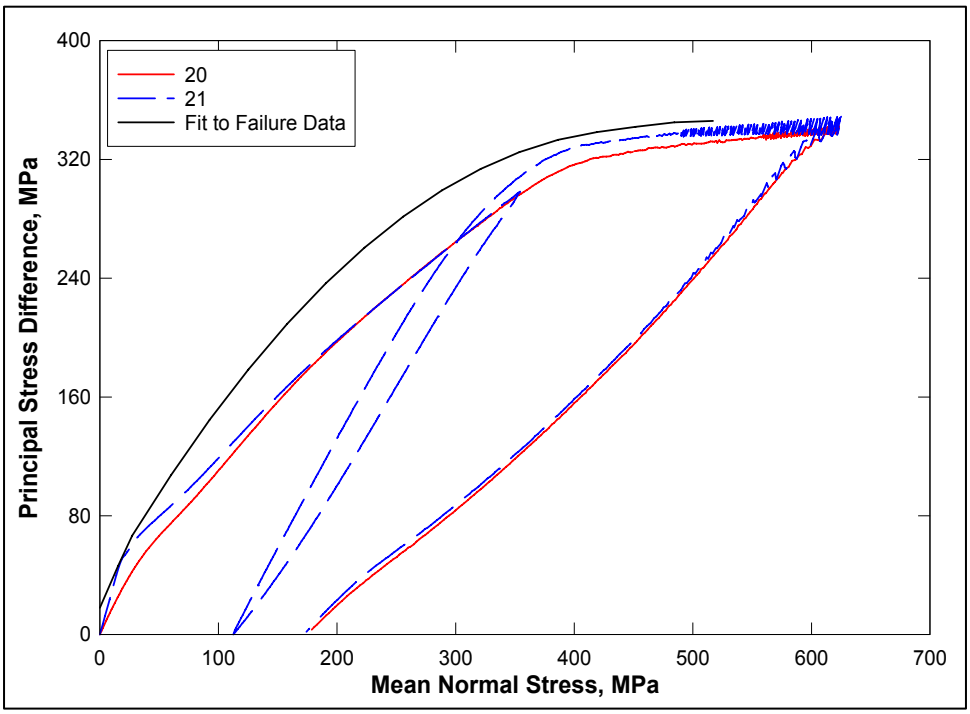

Figure 43. Stress paths from UX tests and failure surface from TXC tests

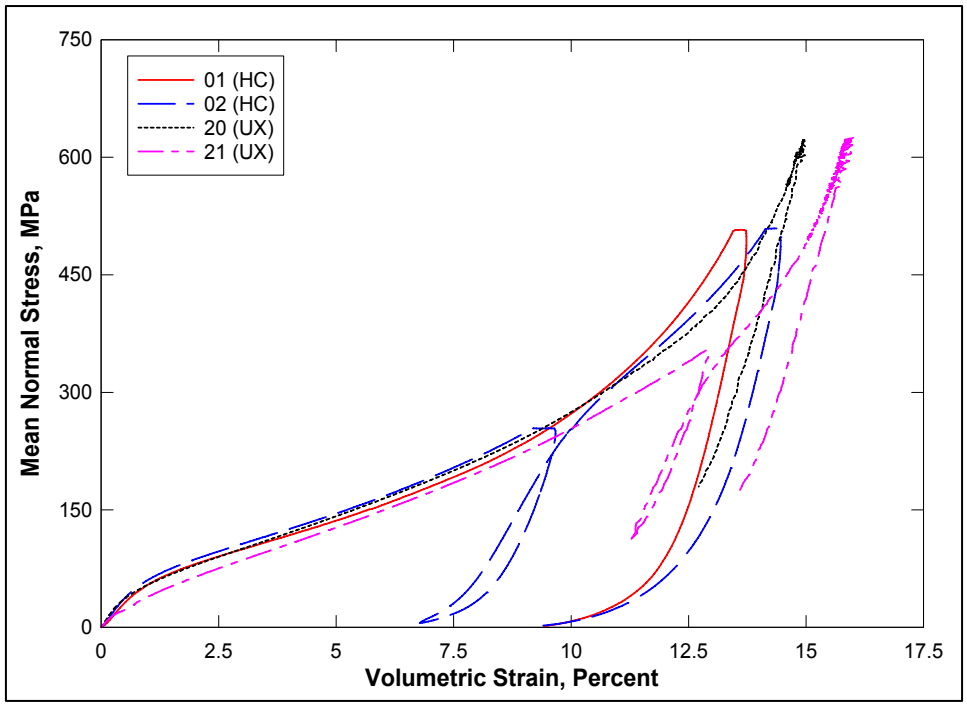

Figure 44. Comparison of pressure-volume data from HC and UX tests

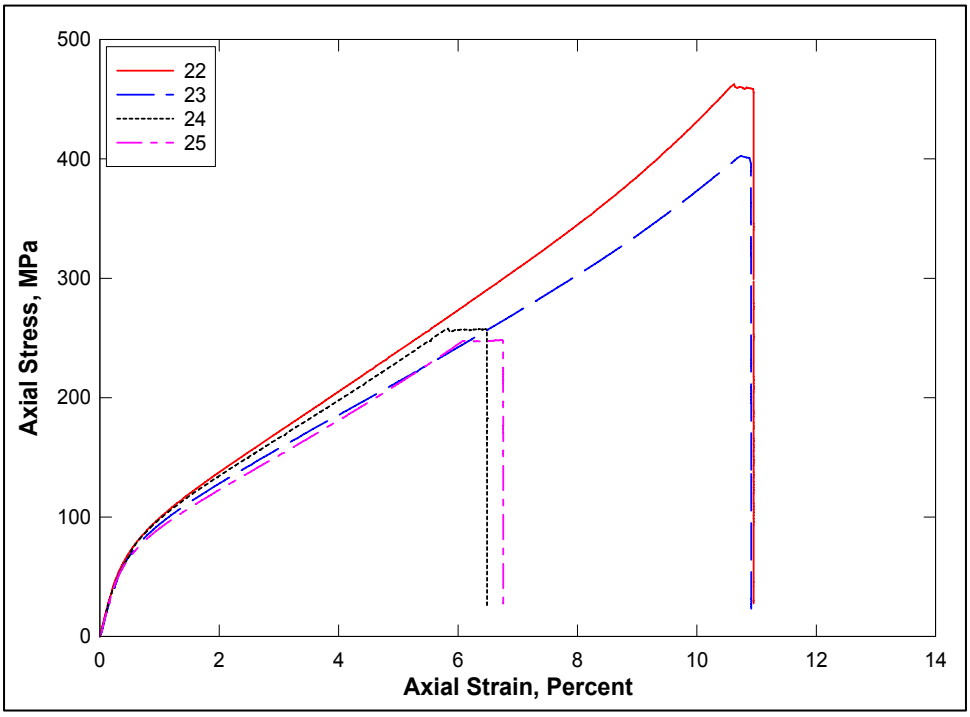

Figure 45. Stress-strain curves from UX/BX tests

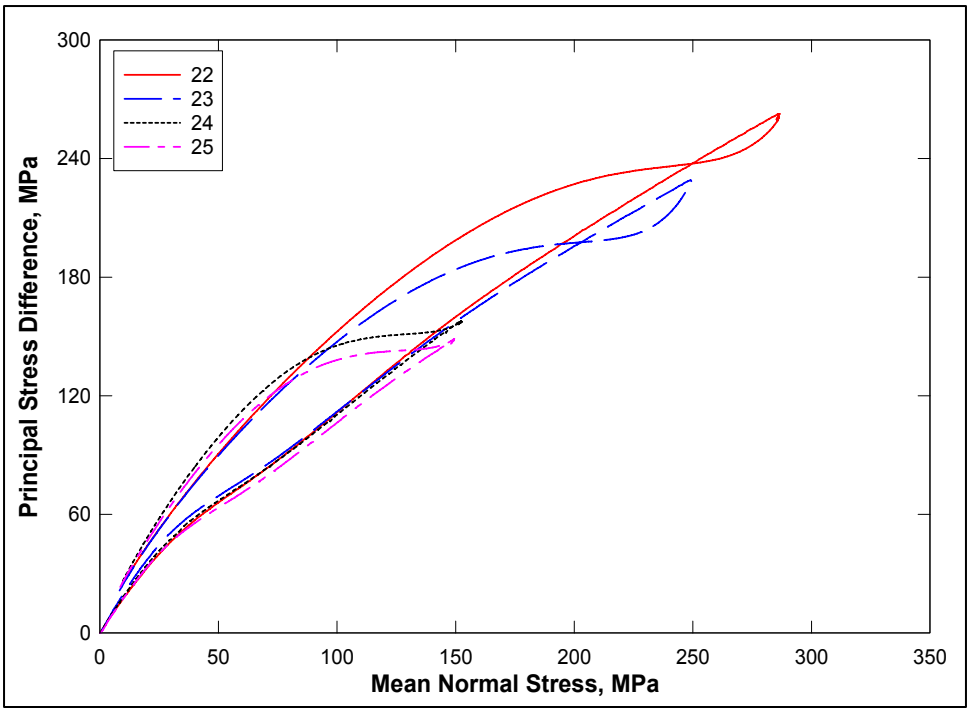

Figure 46. Stress paths from UX/BX tests

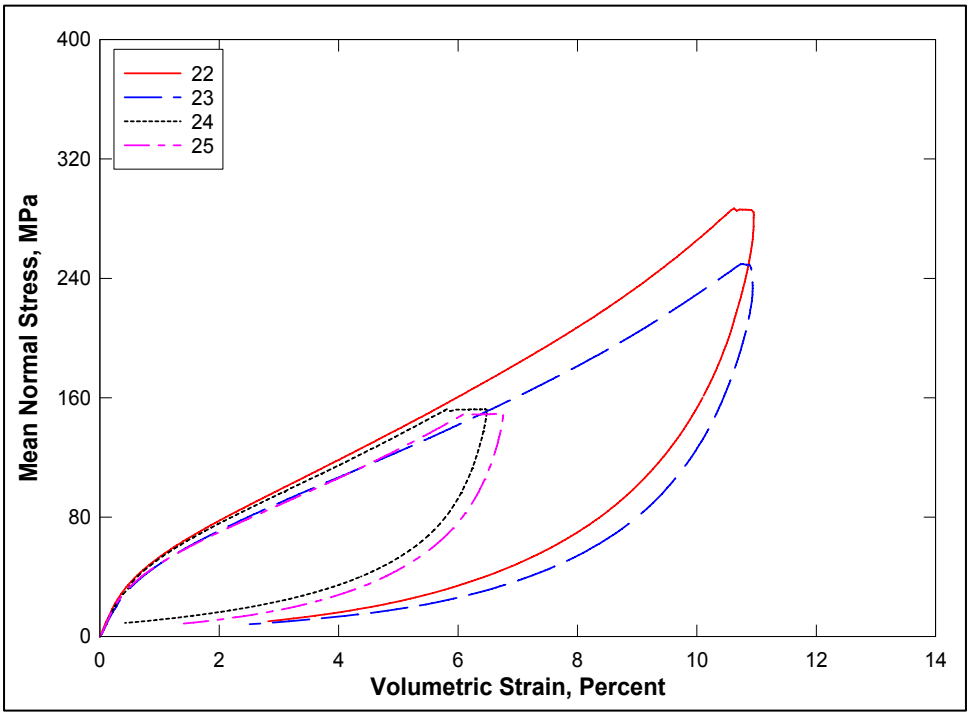

Figure 47. Pressure-volume data from UX/BX tests

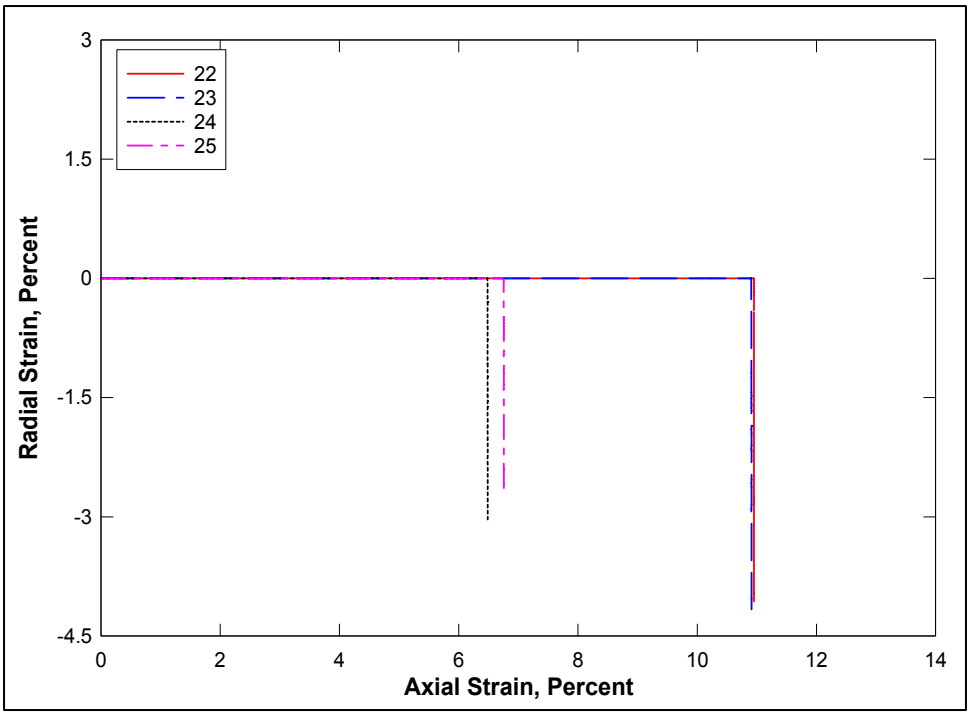

Figure 48. Strain paths from UX/BX tests

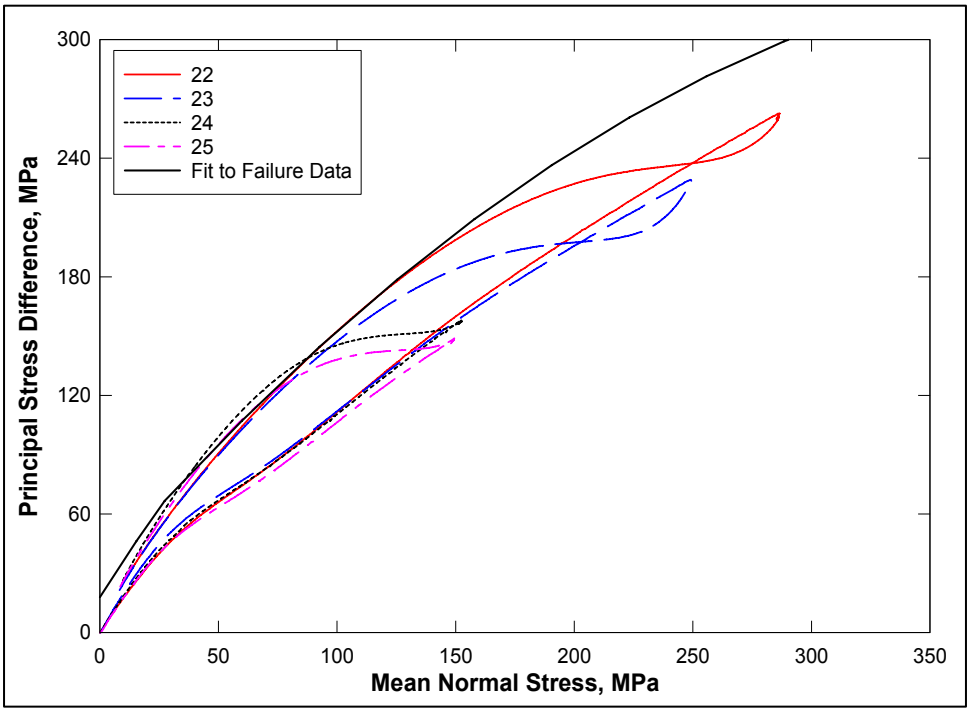

Figure 49. Stress paths from UX/BX tests and failure surface from TXC tests

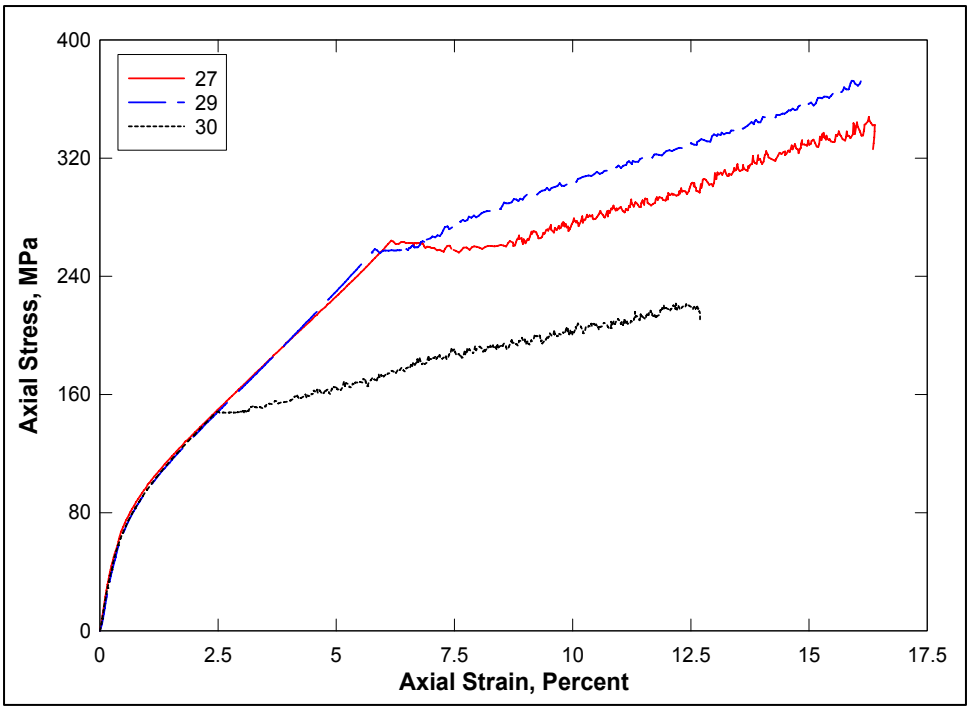

Figure 50. Stress-strain curves from UX/CV tests

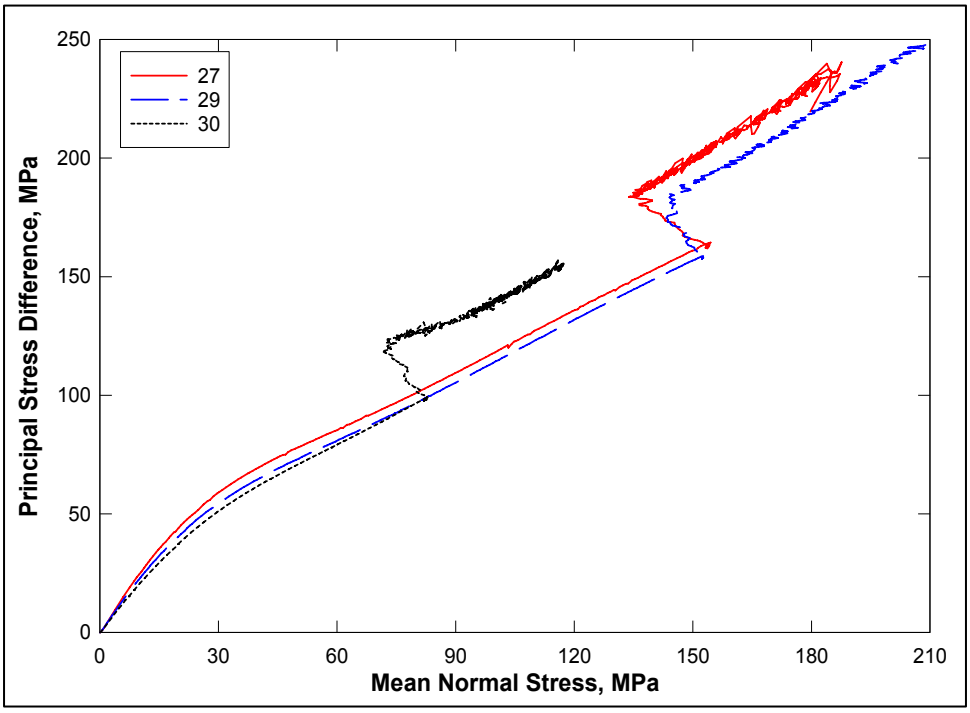

Figure 51. Stress paths from UX/CV tests

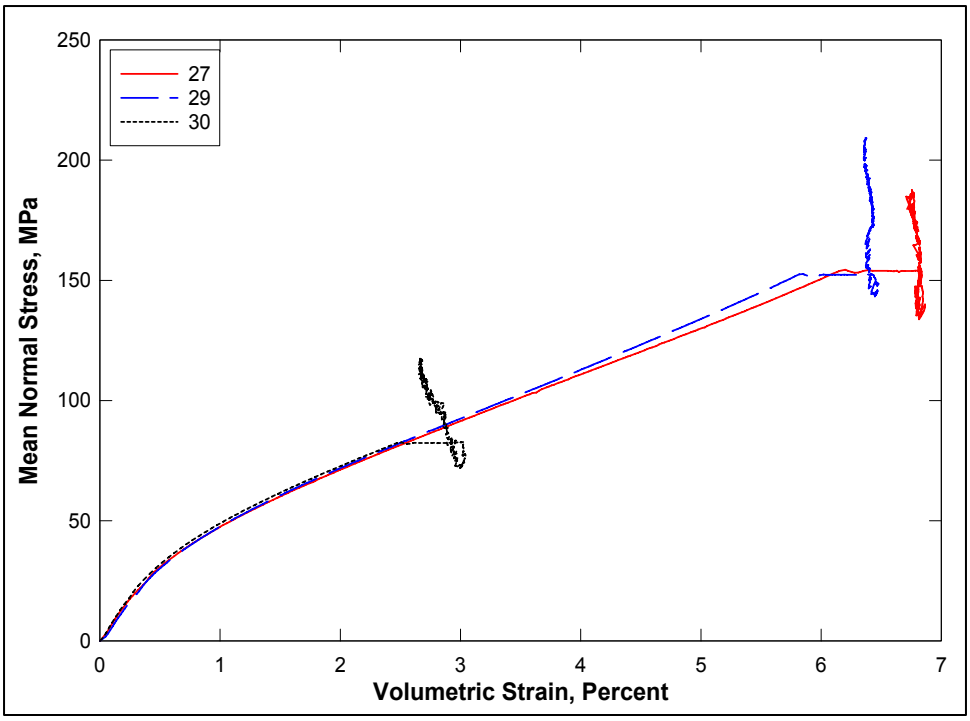

Figure 52. Pressure-volume data from UX/CV tests

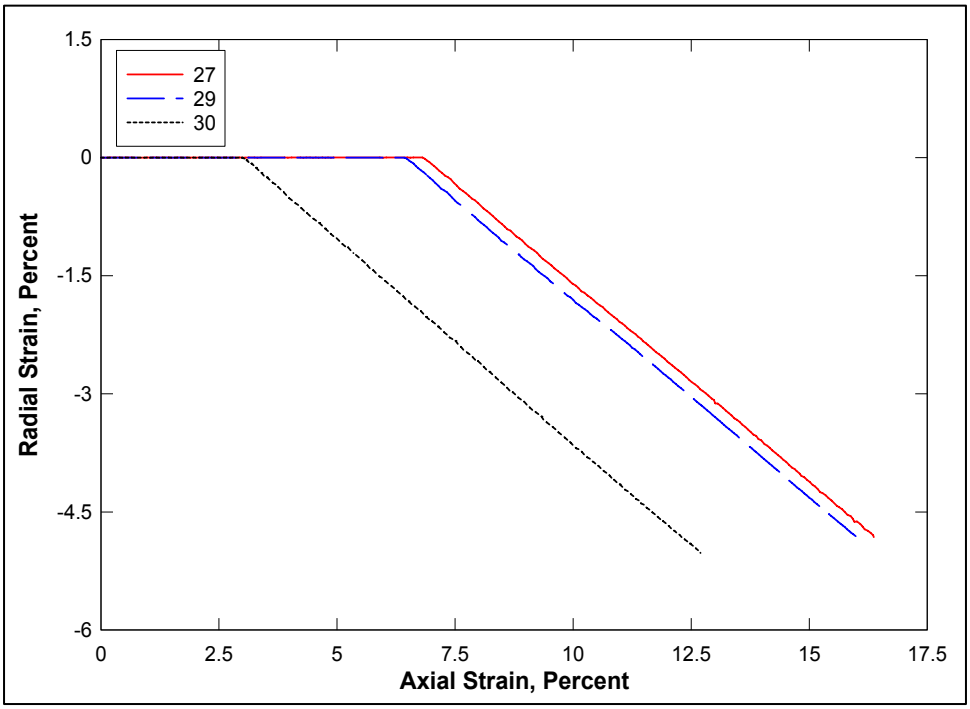

Figure 53. Strain paths from UX/CV tests

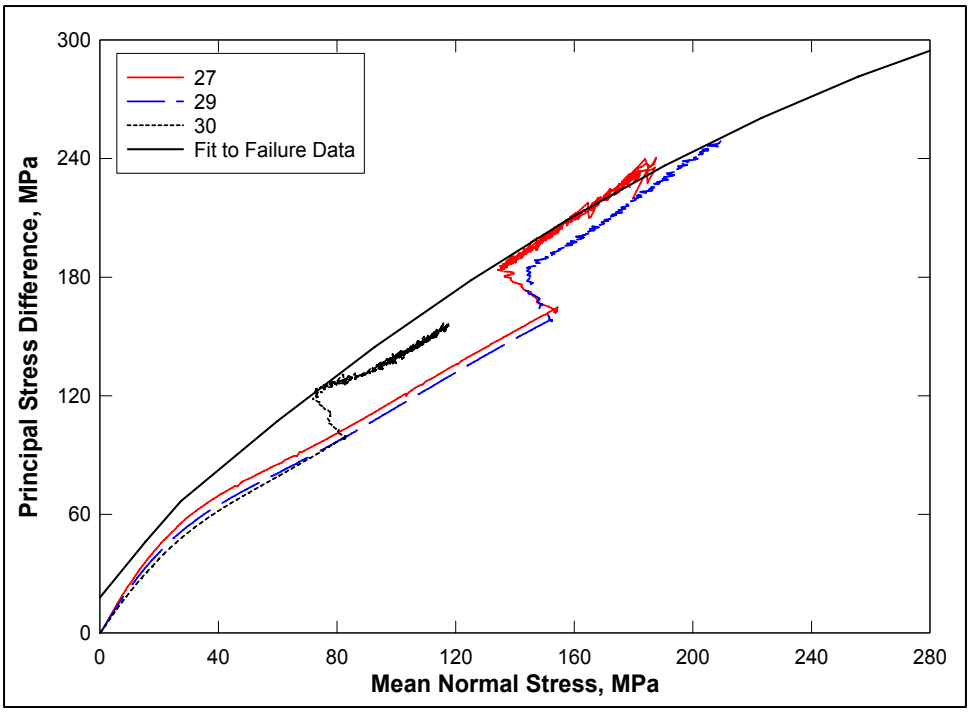

Figure 54. Stress paths from UX/CV tests and failure surface from TXC tests

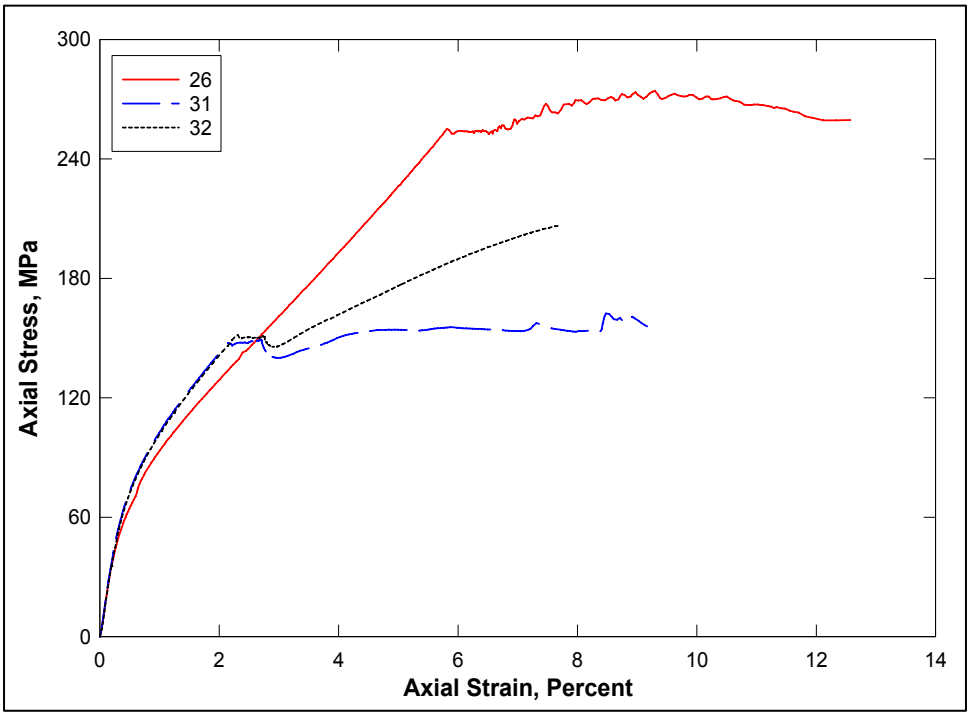

Figure 55. Stress-strain curves from UX/SP tests

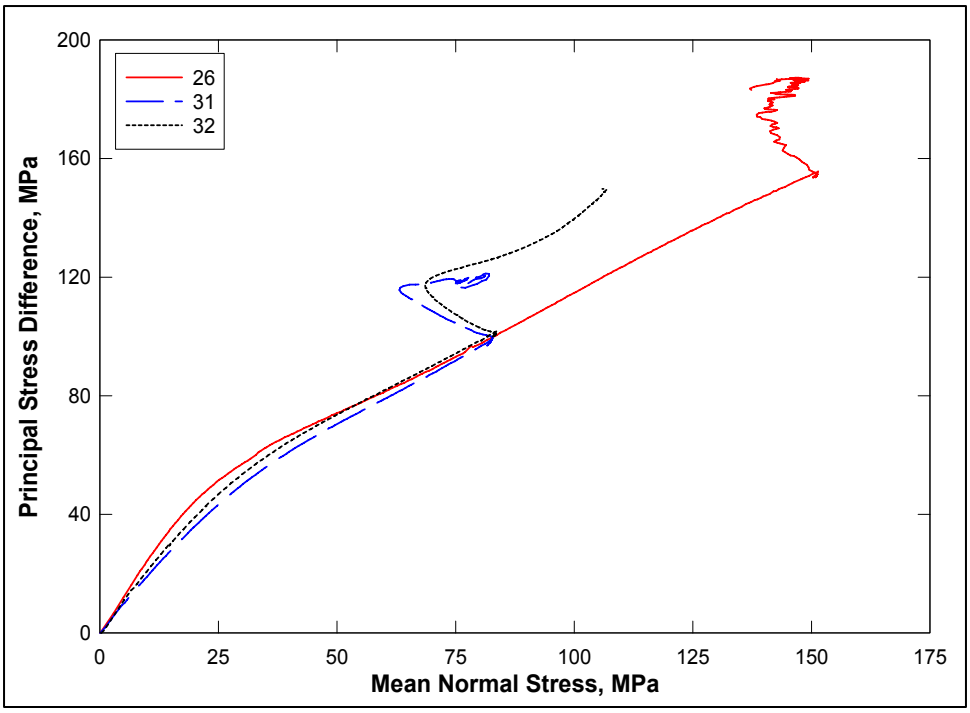

Figure 56. Stress paths from UX/SP tests

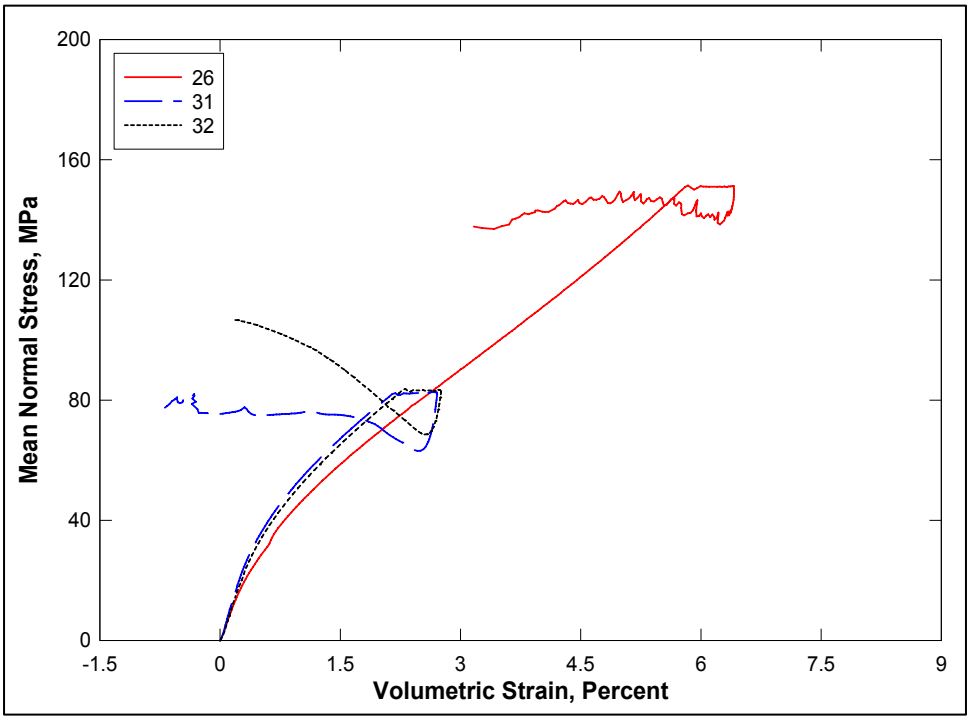

Figure 57. Pressure-volume data from UX/SP tests

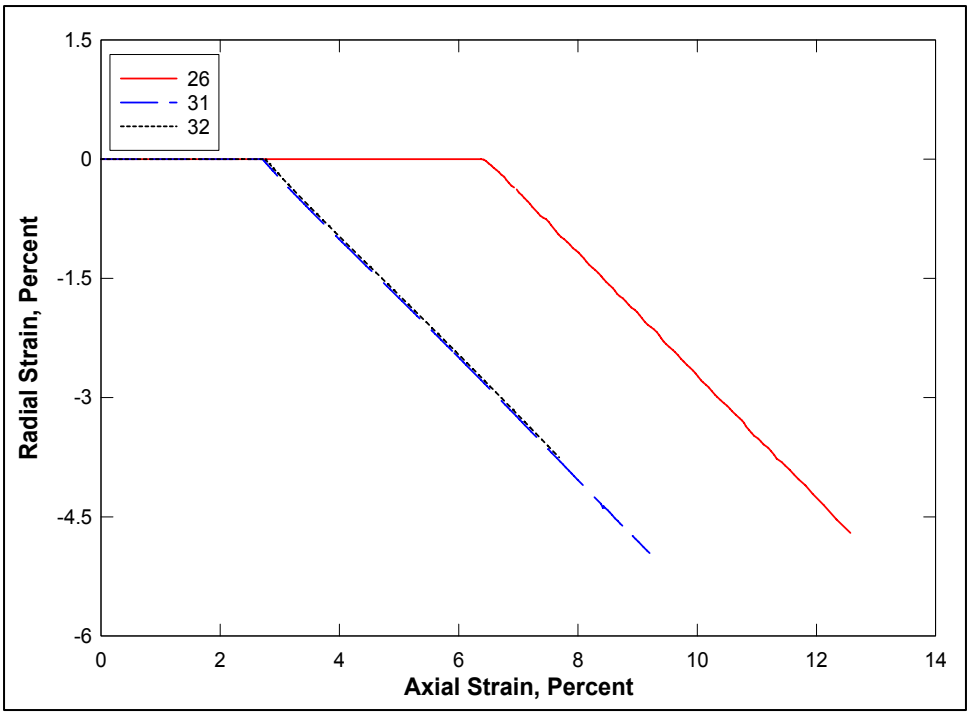

Figure 58. Strain paths from UX/SP tests

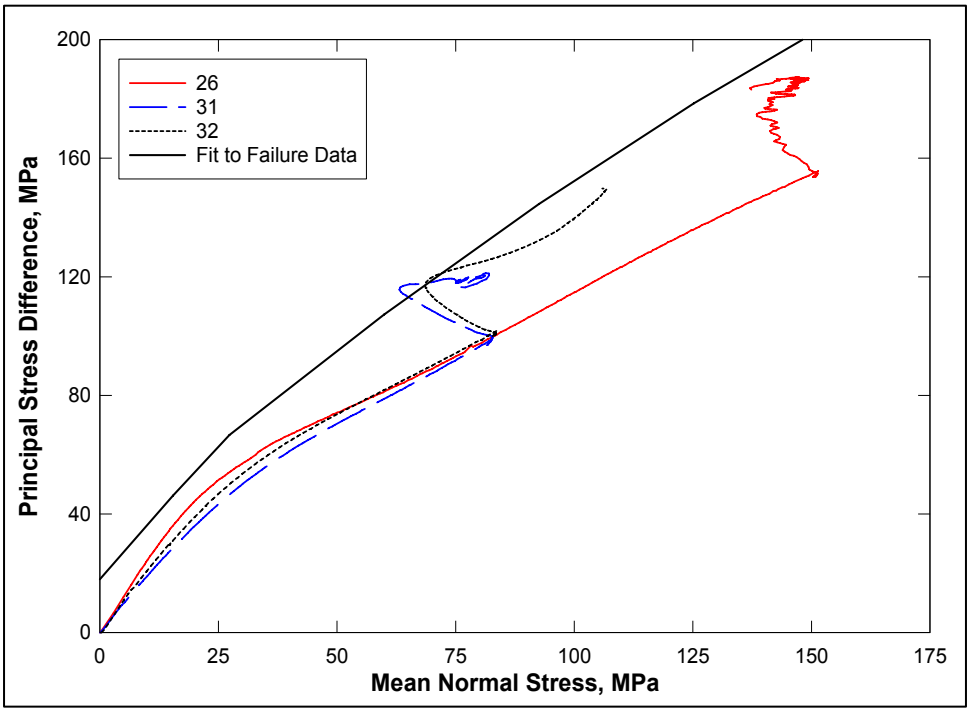

Figure 59. Stress paths from UX/SP tests and failure surface from TXC tests

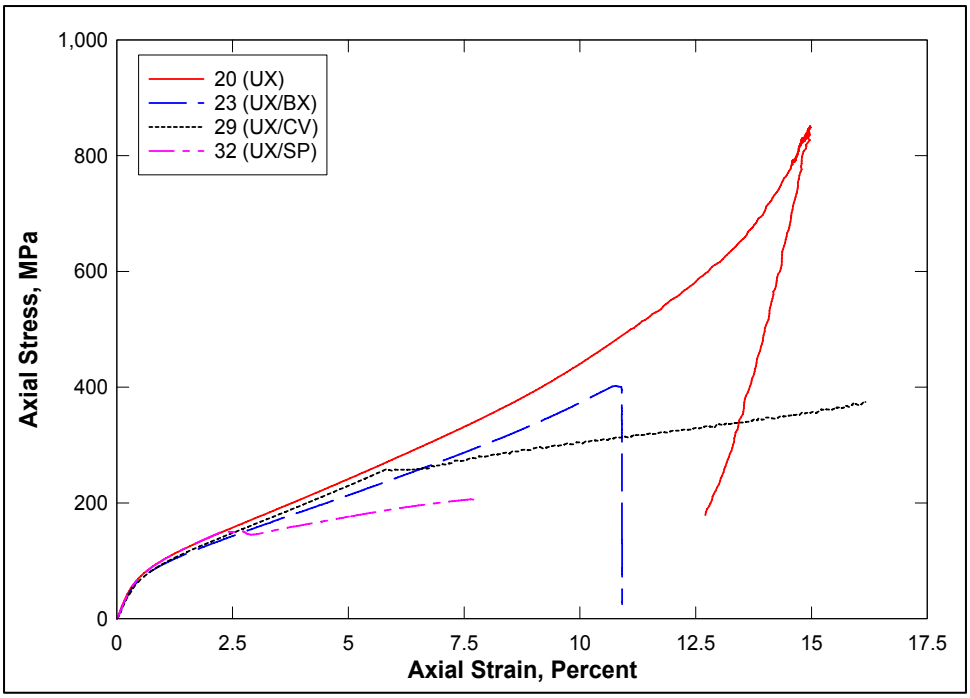

Figure 60. Stress-strain curves from selected UX, UX/BX, UX/CV, and UX/SP tests

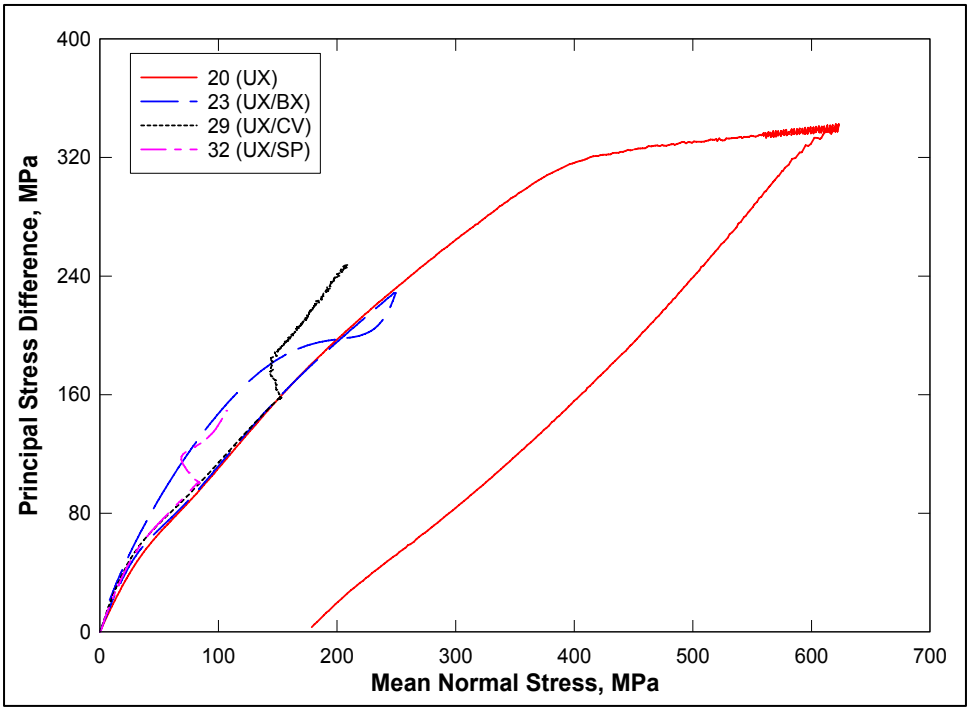

Figure 61. Stress paths from selected UX, UX/BX, UX/CV, and UX/SP tests

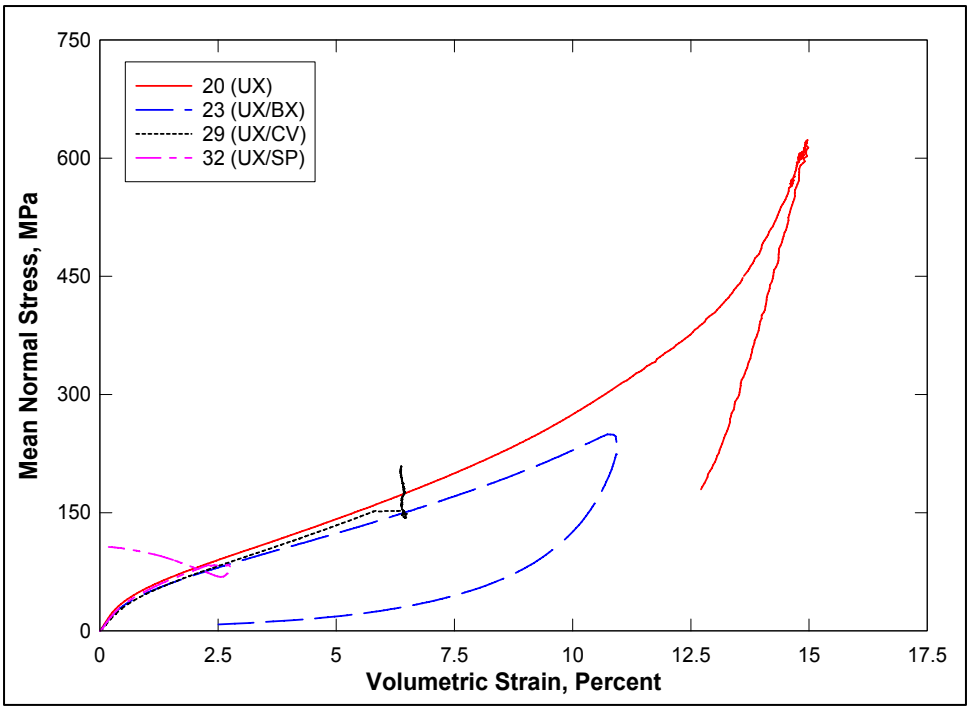

Figure 62. Pressure-volume data from selected UX, UX/BX, UX/CV, and UX/SP tests

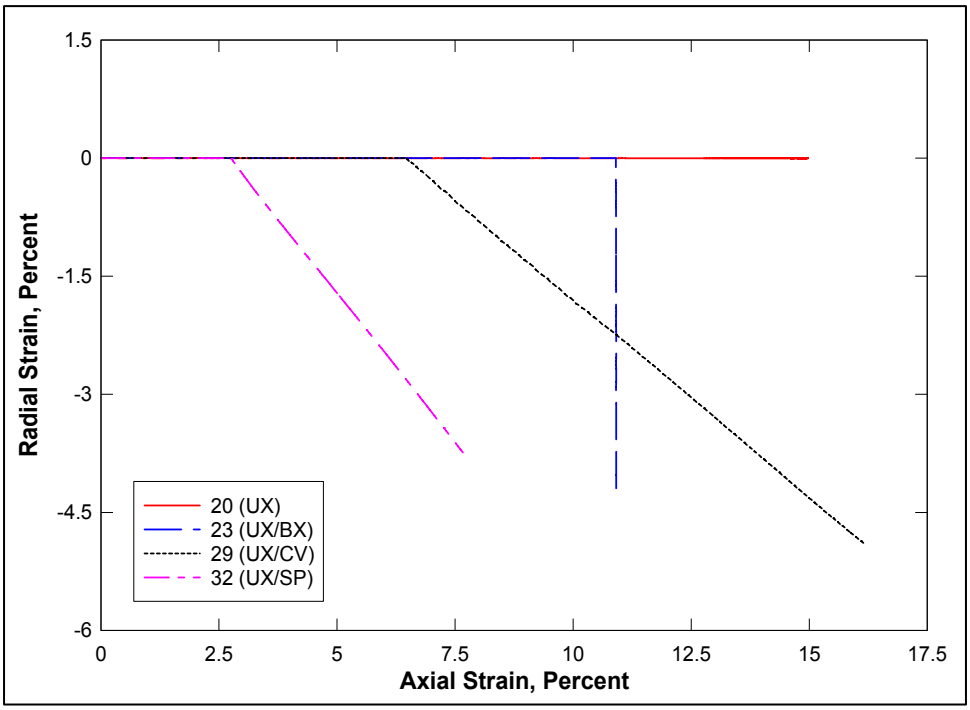

Figure 63. Strain paths from selected UX, UX/BX, UX/CV, and UX/SP tests

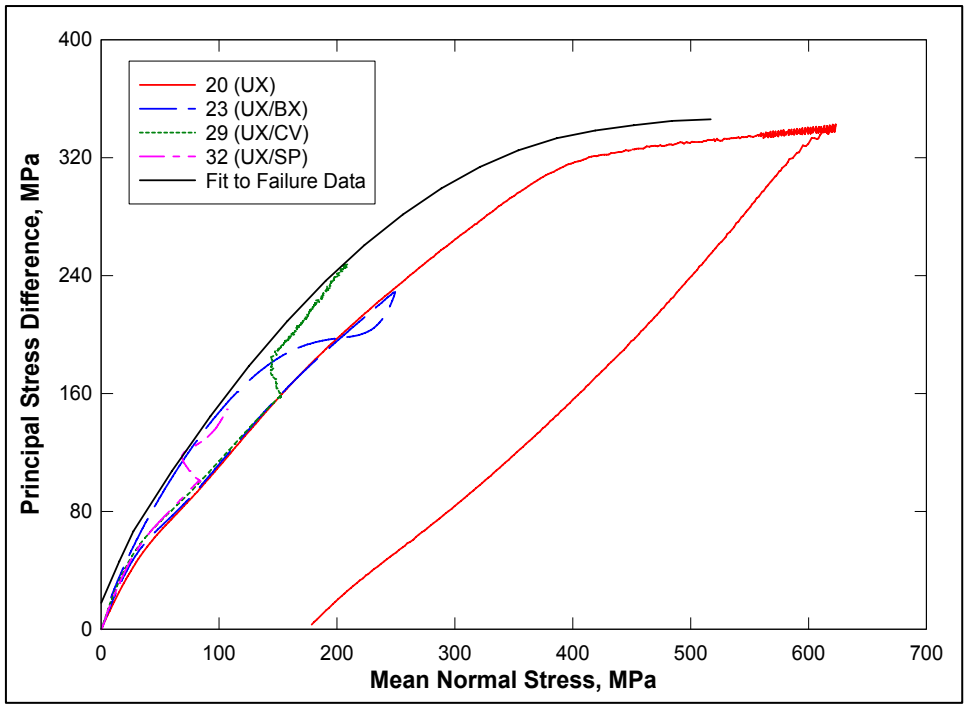

Figure 64. Stress paths from selected UX, UX/BX, UX/CV, and UX/SP tests and failure surface from TXC tests

4 Summary

Personnel in the Geotechnical and Structures Laboratory (GSL) of the U.S. Army Engineer Research and Development Center conducted a laboratory investigation to characterize the strength and constitutive property behavior of fine aggregate cementitious material (FACM). GSL conducted 43 successful mechanical property tests consisting of two hydrostatic compression tests, four unconfined compression tests, 16 triaxial compression tests, two uniaxial strain tests, four uniaxial strain load/biaxial strain unloading tests, three uniaxial strain load/constant volume tests, three uniaxial strain load/constant strain path tests, five direct pull tests, one conventional triaxial extension test, and three reduced triaxial extension tests. In addition to the mechanical property tests, nondestructive pulse-velocity measurements were performed on each specimen.

Results from the laboratory mechanical property tests conducted on the FACM specimens were documented in this report. The TXC tests exhibited a continuous increase in principal stress difference with increasing confining stress. A compression failure surface was developed from the TXC results at eight levels of confining stress and from the results of the unconfined compression tests. The results for RTE and CTE tests along with the DP tests were used to develop a recommended extension failure surface for FACM. Creep was observed during the HC and UX tests. During UX/BX tests, stress relaxation was evident during the change from uniaxial strain loading to biaxial strain unloading. Good agreement was observed between stress paths of the strain path tests and the failure surface from the TXC tests.

References

Akers, S. A., Reed, P. A., and Ehrgott, J. Q. (1986). "WES high-pressure uniaxial strain and triaxial shear test equipment," Miscellaneous Paper SL-86-11, U.S. Army Engineer Waterways Experiment Station, Vicksburg, MS.

American Society for Testing and Materials. (2002). *2002 Annual Book of ASTM Standards*, Philadelphia, PA.

a. Designation C 39-01. "Standard test method for compressive strength of concrete specimens."
b. Designation C 42-99. "Standard test method for obtaining and testing drilled cores and sawed beams of concrete."
c. Designation C 597-97. "Standard test method for pulse velocity through concrete."
d. Designation C 801-98. "Standard test method for determining the mechanical properties of hardened concrete under triaxial loads."
e. Designation D 2216-98. "Standard test method for laboratory determination of water (moisture) content of soil and rock by mass."
f. Designation D 4543-01. "Standard test method for preparing rock core specimens and determining dimensional and shape tolerances."

Bishop, A. W., and Henkel, D. J. (1962). *The measurement of soil properties in the triaxial test.* Edward Arnold, Ltd., London, pp 72-74.

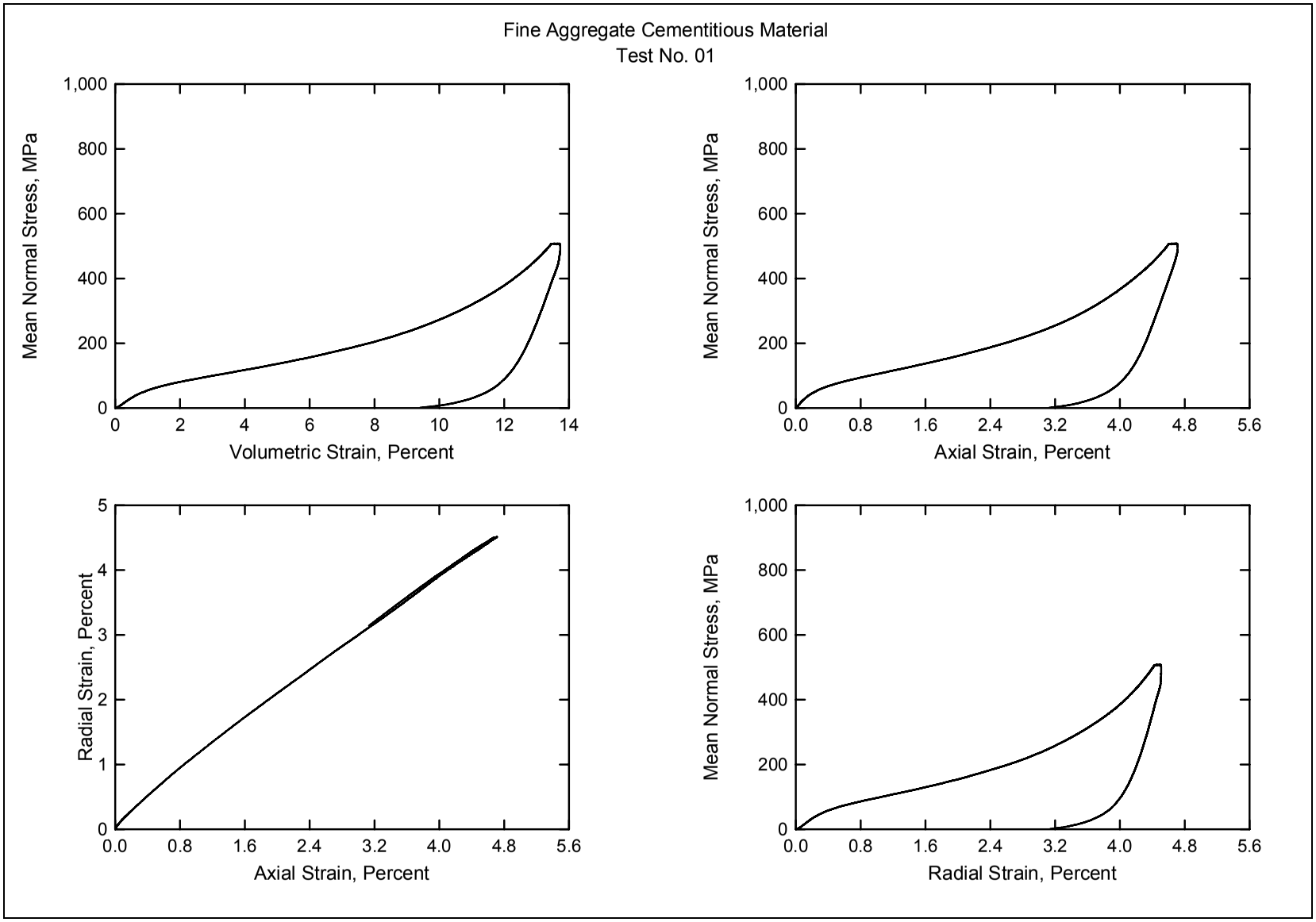
Fine Aggregate Cementitious Material
Test No. 01
Mean Normal Stress, MPa
1,000
800
600
400
200
0
0
2
4
6
8
10
12
14
Volumetric Strain, Percent
Mean Normal Stress, MPa
1,000
800
600
400
200
0
0.0
0.8
1.6
2.4
3.2
4.0
4.8
5.6
Axial Strain, Percent
Radial Strain, Percent
5
4
3
2
1
0
0.0
0.8
1.6
2.4
3.2
4.0
4.8
5.6
Axial Strain, Percent
Mean Normal Stress, MPa
1,000
800
600
400
200
0
0.0
0.8
1.6
2.4
3.2
4.0
4.8
5.6
Radial Strain, Percent

Plate 1

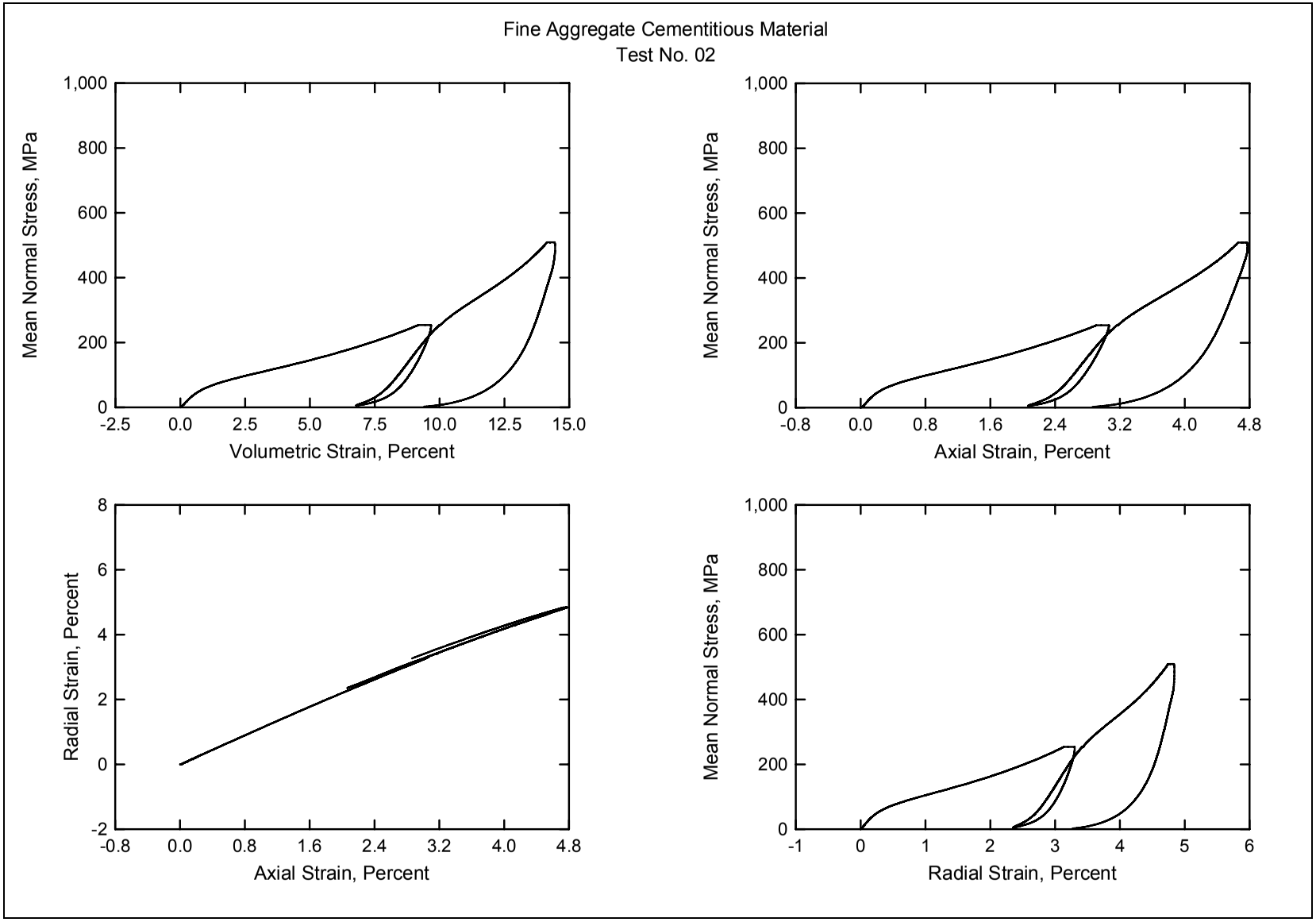
Fine Aggregate Cementitious Material
Test No. 02
Mean Normal Stress, MPa
1,000
800
600
400
200
0
-2.5
0.0
2.5
5.0
7.5
10.0
12.5
15.0
Volumetric Strain, Percent
Mean Normal Stress, MPa
1,000
800
600
400
200
0
-0.8
0.0
0.8
1.6
2.4
3.2
4.0
4.8
Axial Strain, Percent
Radial Strain, Percent
8
6
4
2
0
-2
-0.8
0.0
0.8
1.6
2.4
3.2
4.0
4.8
Axial Strain, Percent
Mean Normal Stress, MPa
1,000
800
600
400
200
0
-1
0
1
2
3
4
5
6
Radial Strain, Percent

Plate 2

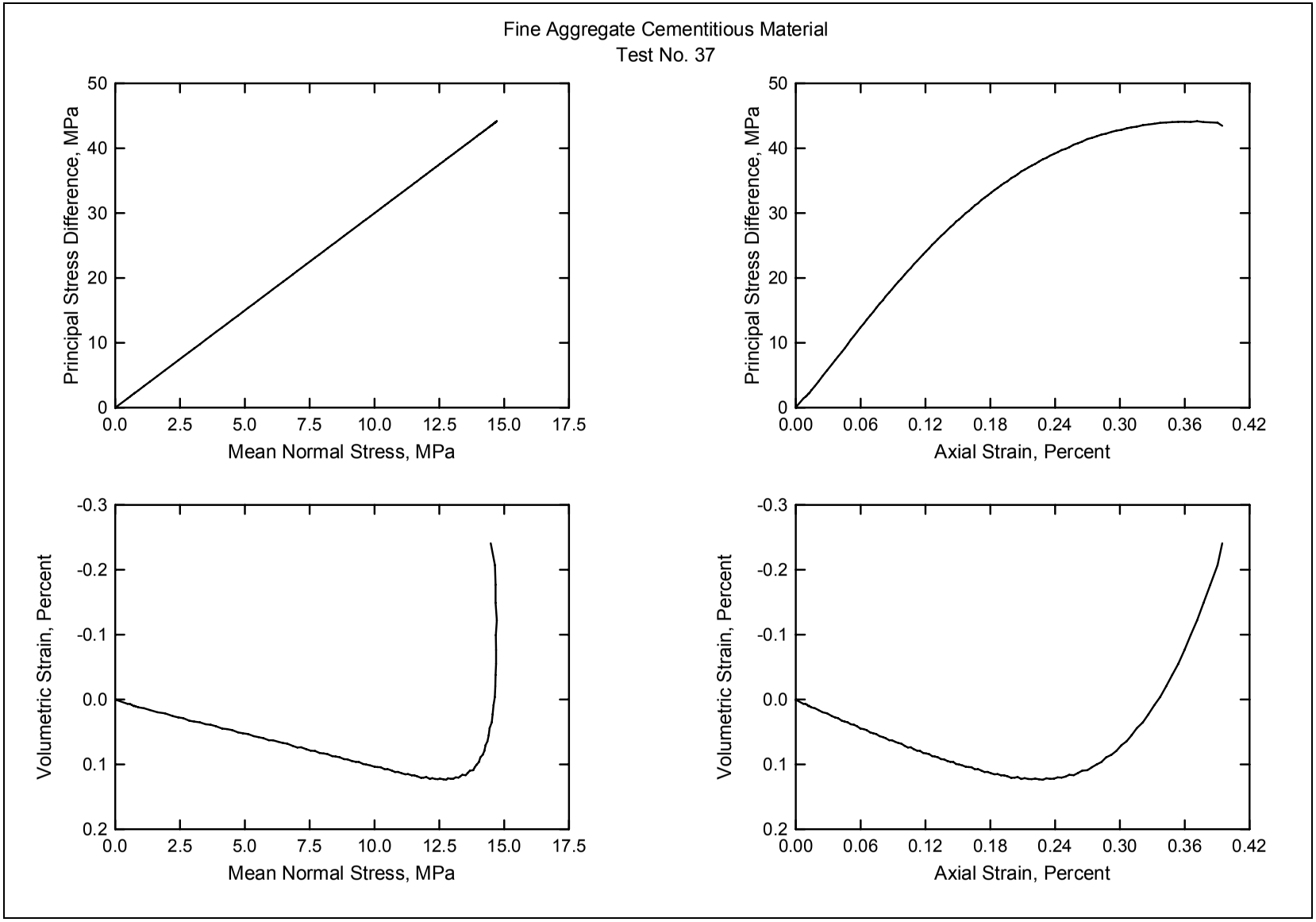
Fine Aggregate Cementitious Material
Test No. 37
Principal Stress Difference, MPa
Mean Normal Stress, MPa
Principal Stress Difference, MPa
Axial Strain, Percent
Volumetric Strain, Percent
Mean Normal Stress, MPa
Volumetric Strain, Percent
Axial Strain, Percent

Plate 3

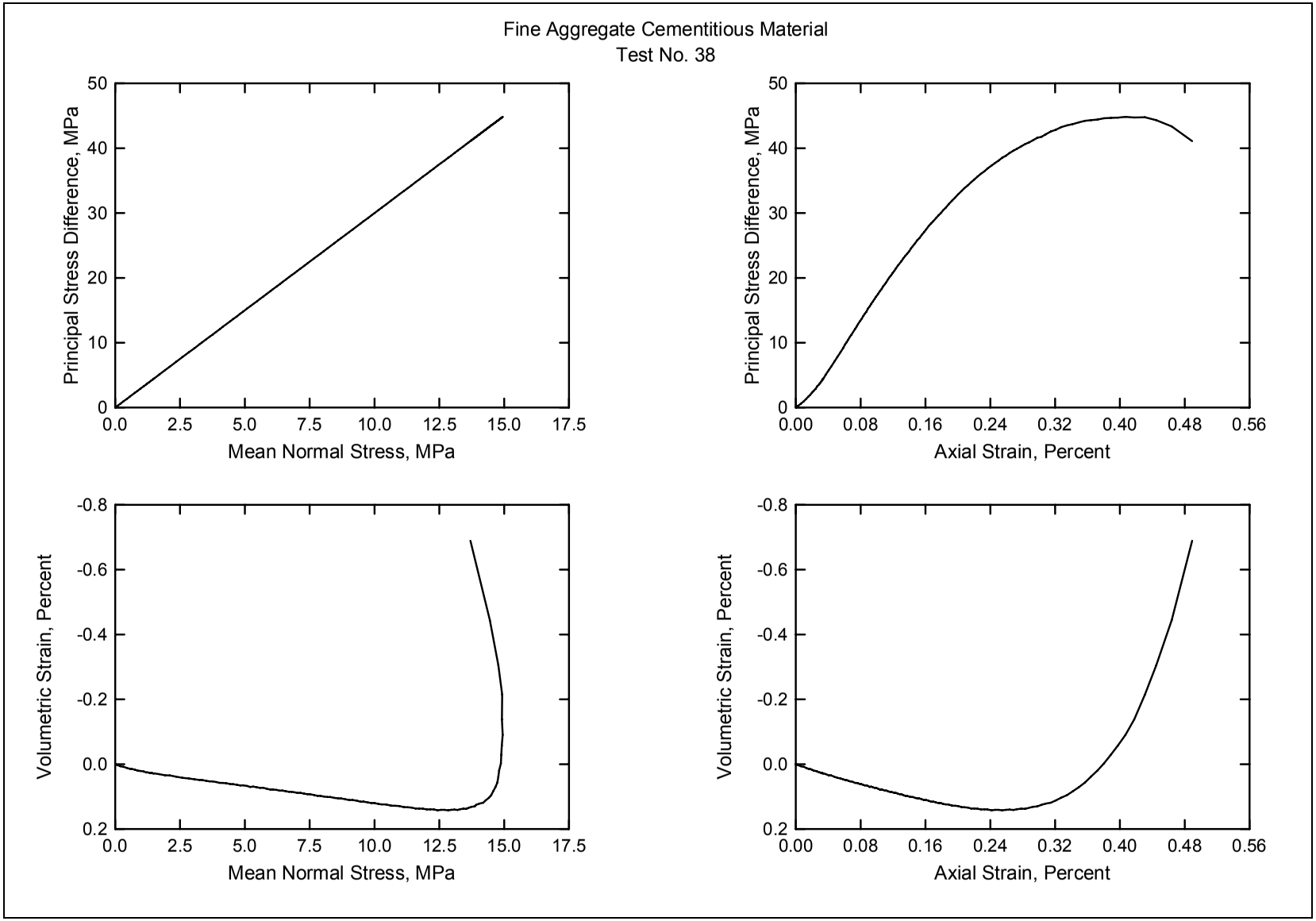
Fine Aggregate Cementitious Material
Test No. 38
Principal Stress Difference, MPa
Mean Normal Stress, MPa
Principal Stress Difference, MPa
Axial Strain, Percent
Volumetric Strain, Percent
Mean Normal Stress, MPa
Volumetric Strain, Percent
Axial Strain, Percent

Plate 4

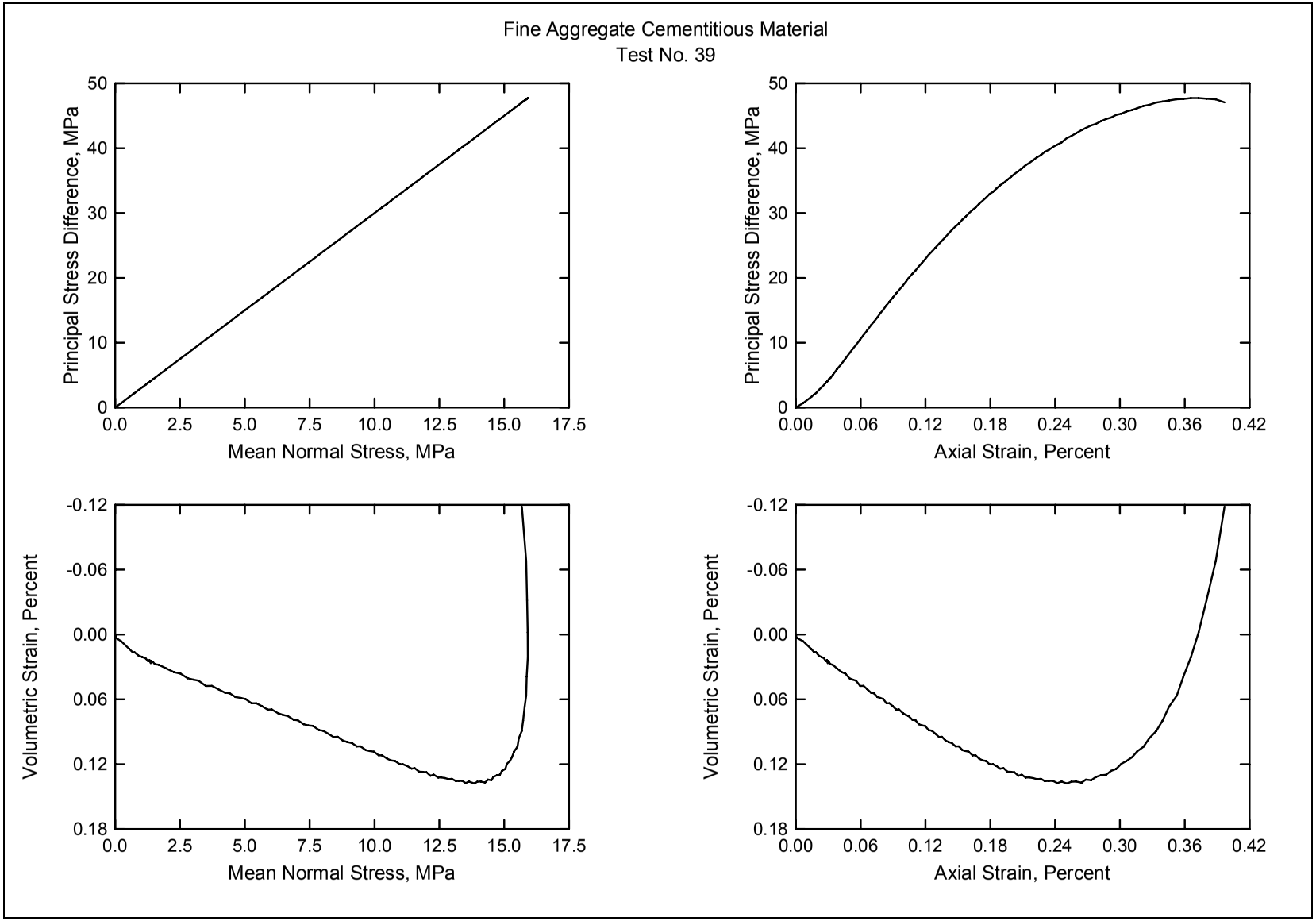
Fine Aggregate Cementitious Material
Test No. 39
Principal Stress Difference, MPa
Mean Normal Stress, MPa
Principal Stress Difference, MPa
Axial Strain, Percent
Volumetric Strain, Percent
Mean Normal Stress, MPa
Volumetric Strain, Percent
Axial Strain, Percent

Plate 5

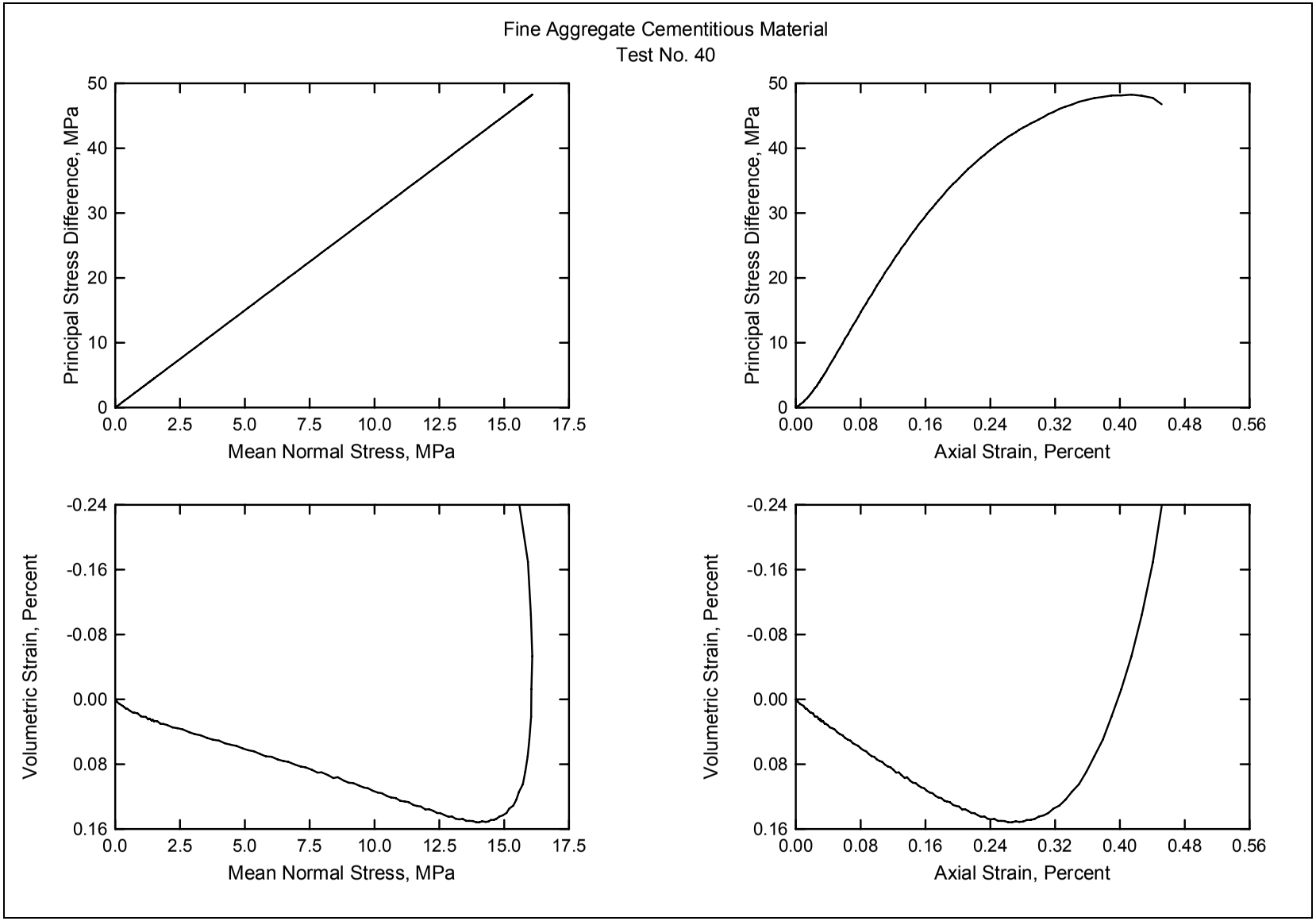
Fine Aggregate Cementitious Material
Test No. 40
Principal Stress Difference, MPa
Mean Normal Stress, MPa
Principal Stress Difference, MPa
Axial Strain, Percent
Volumetric Strain, Percent
Mean Normal Stress, MPa
Volumetric Strain, Percent
Axial Strain, Percent

Plate 6

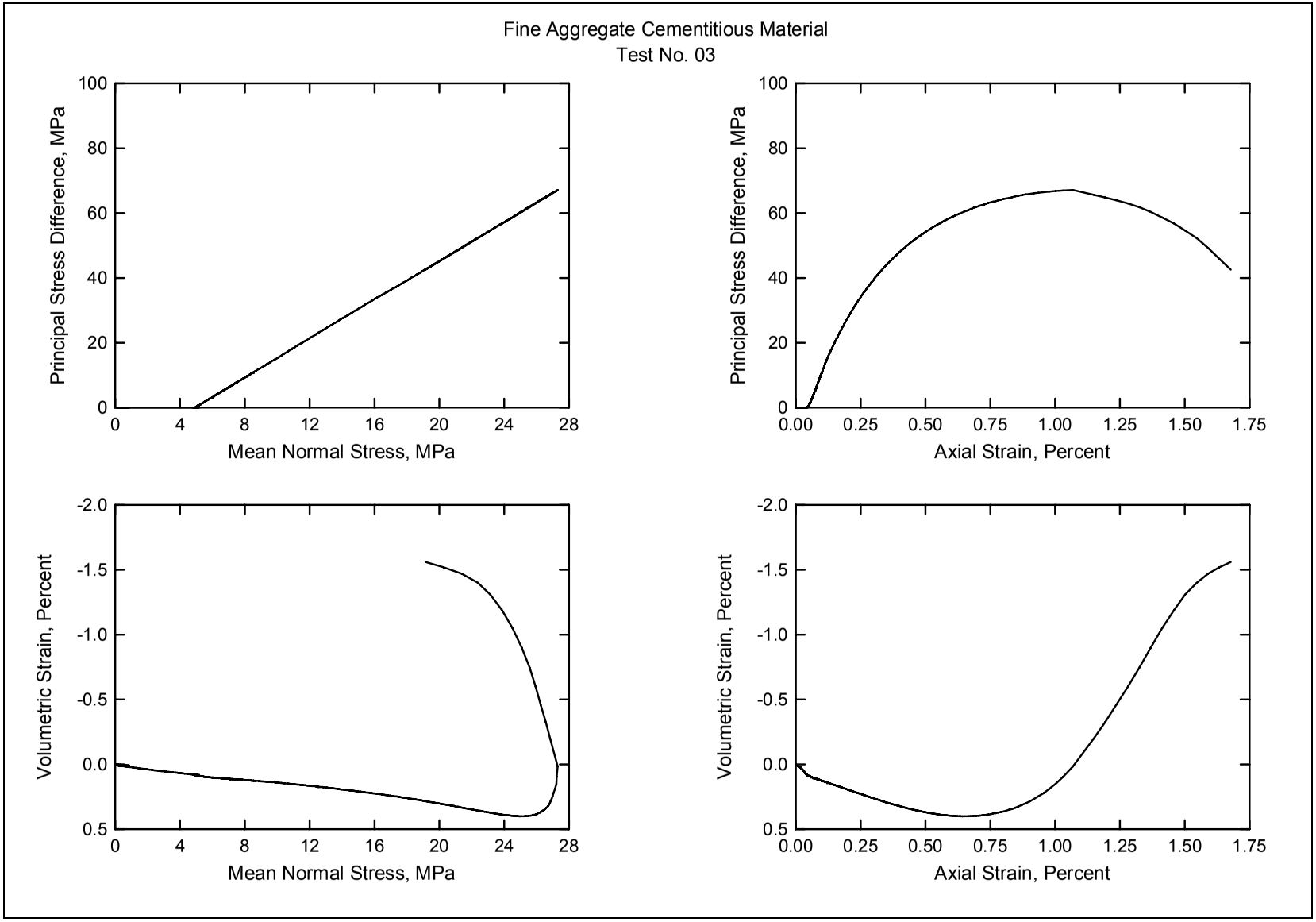
Fine Aggregate Cementitious Material
Test No. 03
Principal Stress Difference, MPa
Mean Normal Stress, MPa
Principal Stress Difference, MPa
Axial Strain, Percent
Volumetric Strain, Percent
Mean Normal Stress, MPa
Volumetric Strain, Percent
Axial Strain, Percent

Plate 7

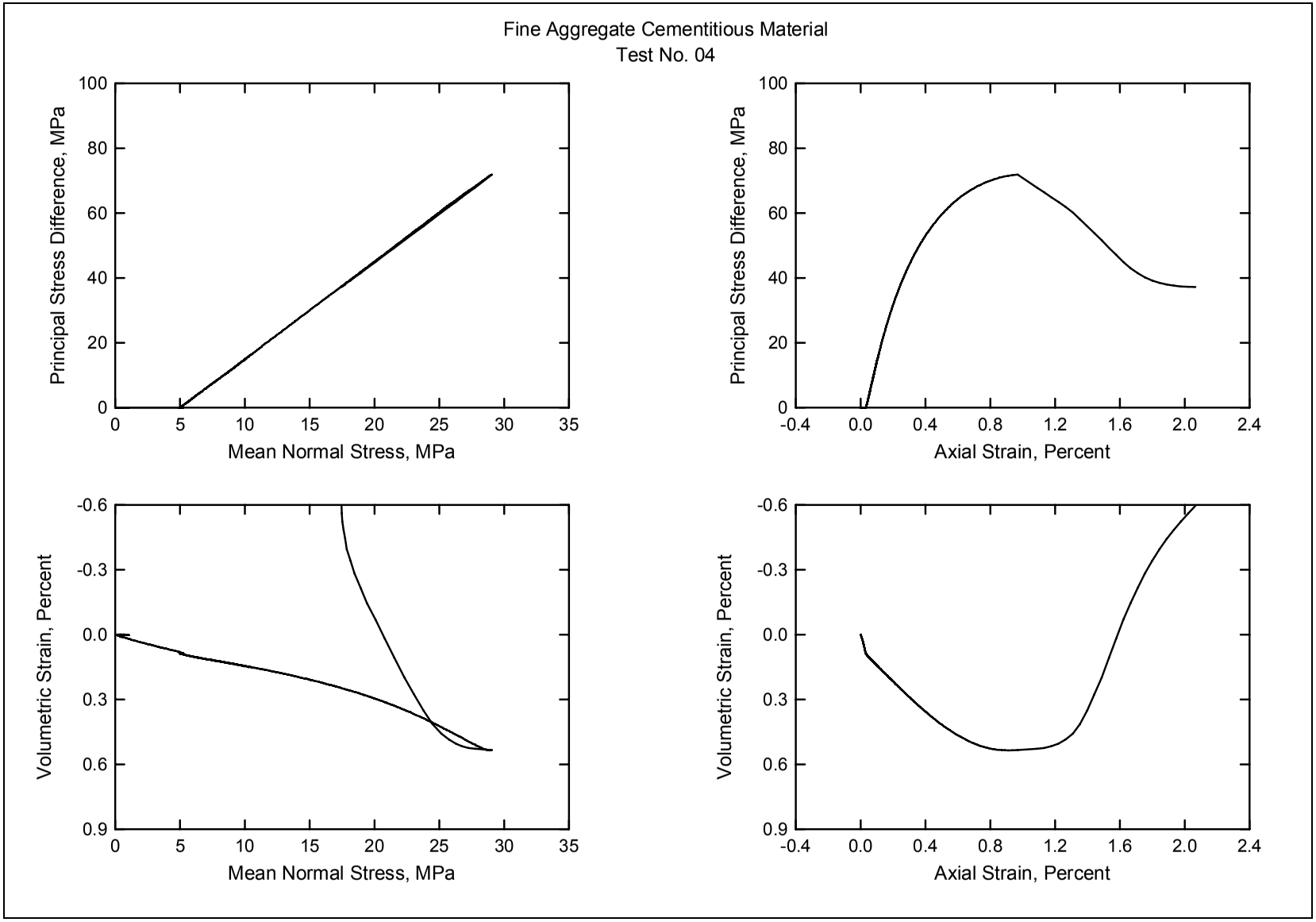
Fine Aggregate Cementitious Material
Test No. 04
Principal Stress Difference, MPa
Mean Normal Stress, MPa
Principal Stress Difference, MPa
Axial Strain, Percent
Volumetric Strain, Percent
Mean Normal Stress, MPa
Volumetric Strain, Percent
Axial Strain, Percent

Plate 8

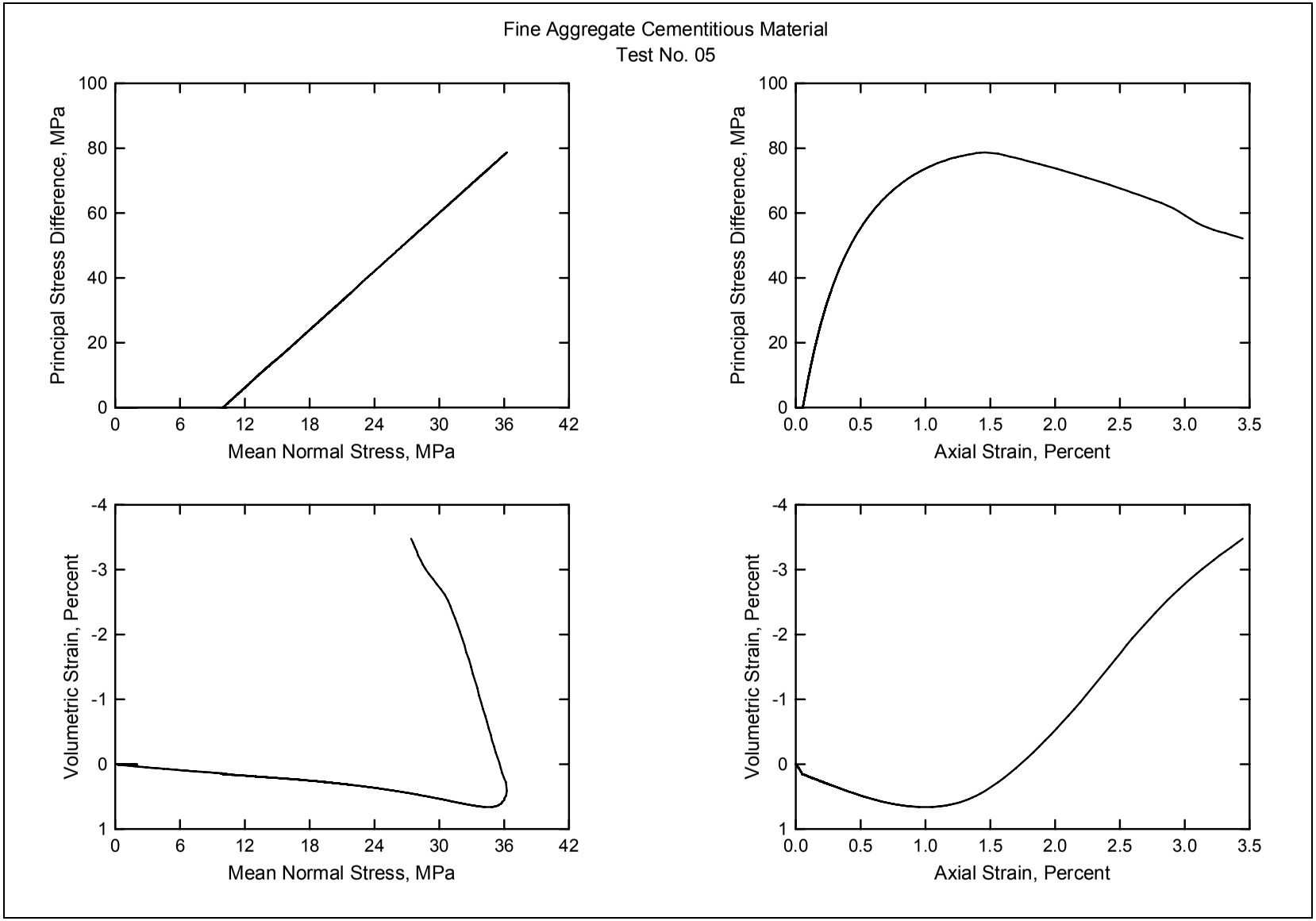
Fine Aggregate Cementitious Material
Test No. 05
Principal Stress Difference, MPa
Mean Normal Stress, MPa
Principal Stress Difference, MPa
Axial Strain, Percent
Volumetric Strain, Percent
Mean Normal Stress, MPa
Volumetric Strain, Percent
Axial Strain, Percent

Plate 9

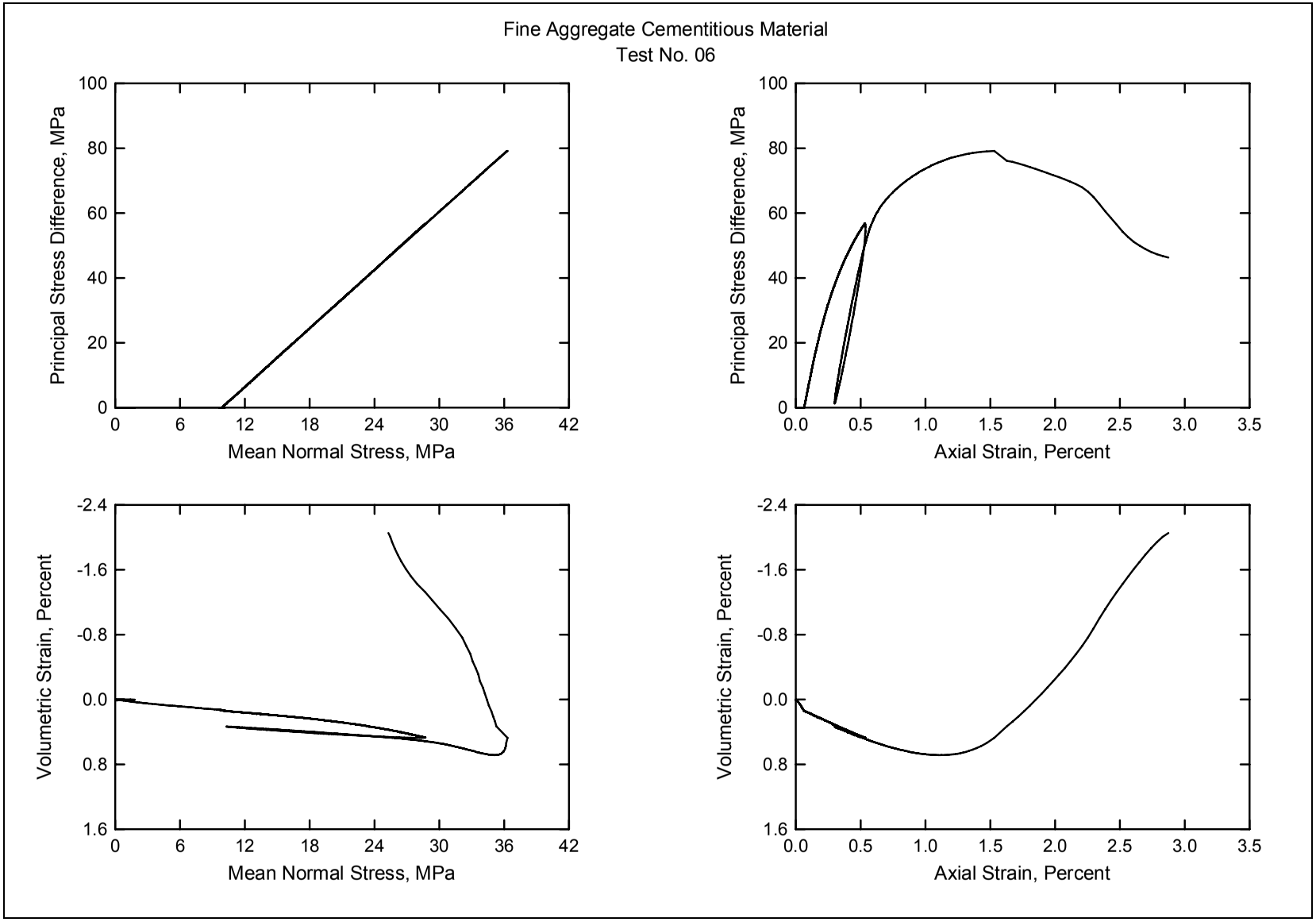
Fine Aggregate Cementitious Material
Test No. 06
Principal Stress Difference, MPa
Mean Normal Stress, MPa
Principal Stress Difference, MPa
Axial Strain, Percent
Volumetric Strain, Percent
Mean Normal Stress, MPa
Volumetric Strain, Percent
Axial Strain, Percent

Plate 10

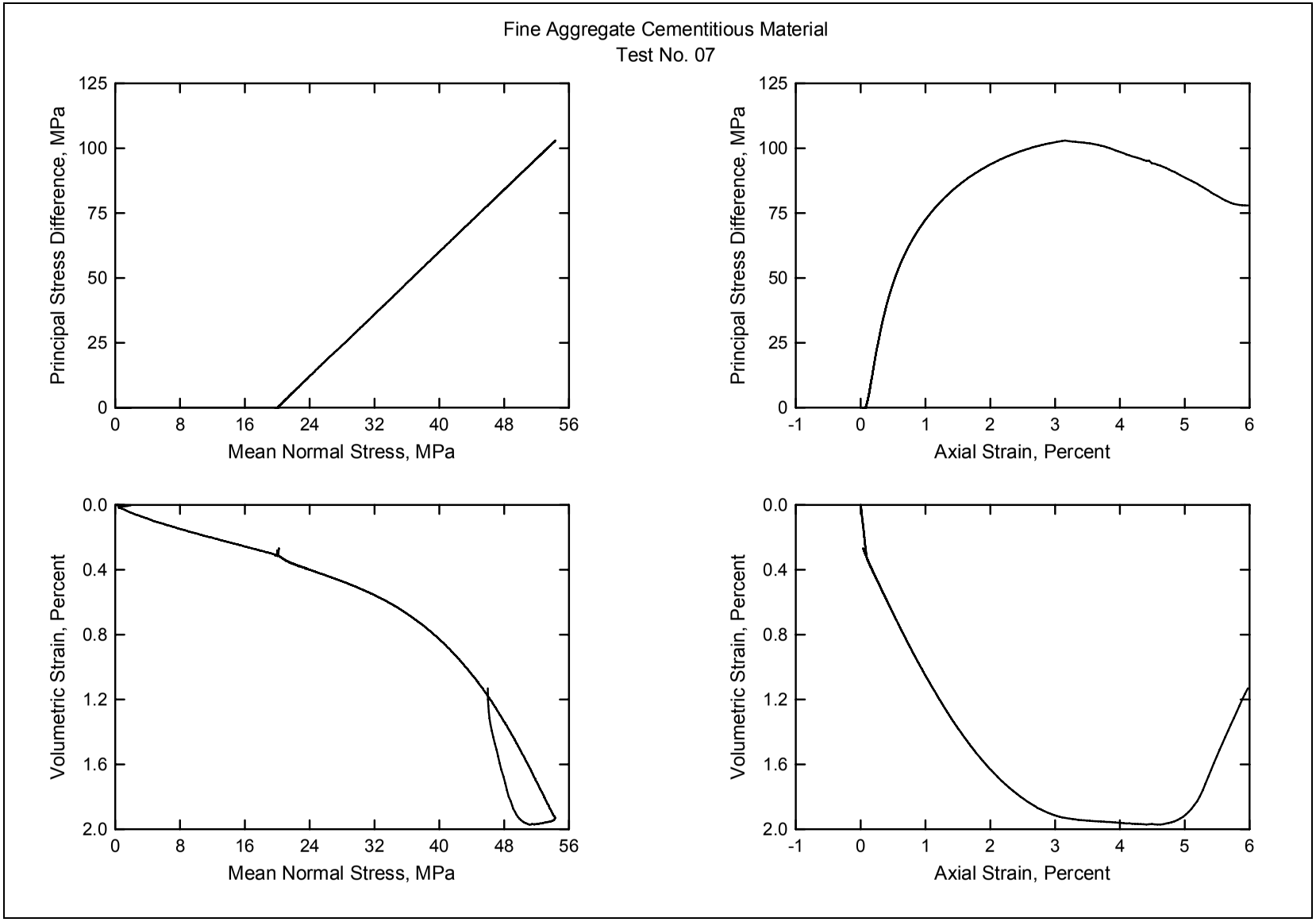
Fine Aggregate Cementitious Material
Test No. 07
Principal Stress Difference, MPa
Mean Normal Stress, MPa
Principal Stress Difference, MPa
Axial Strain, Percent
Volumetric Strain, Percent
Mean Normal Stress, MPa
Volumetric Strain, Percent
Axial Strain, Percent

Plate 11

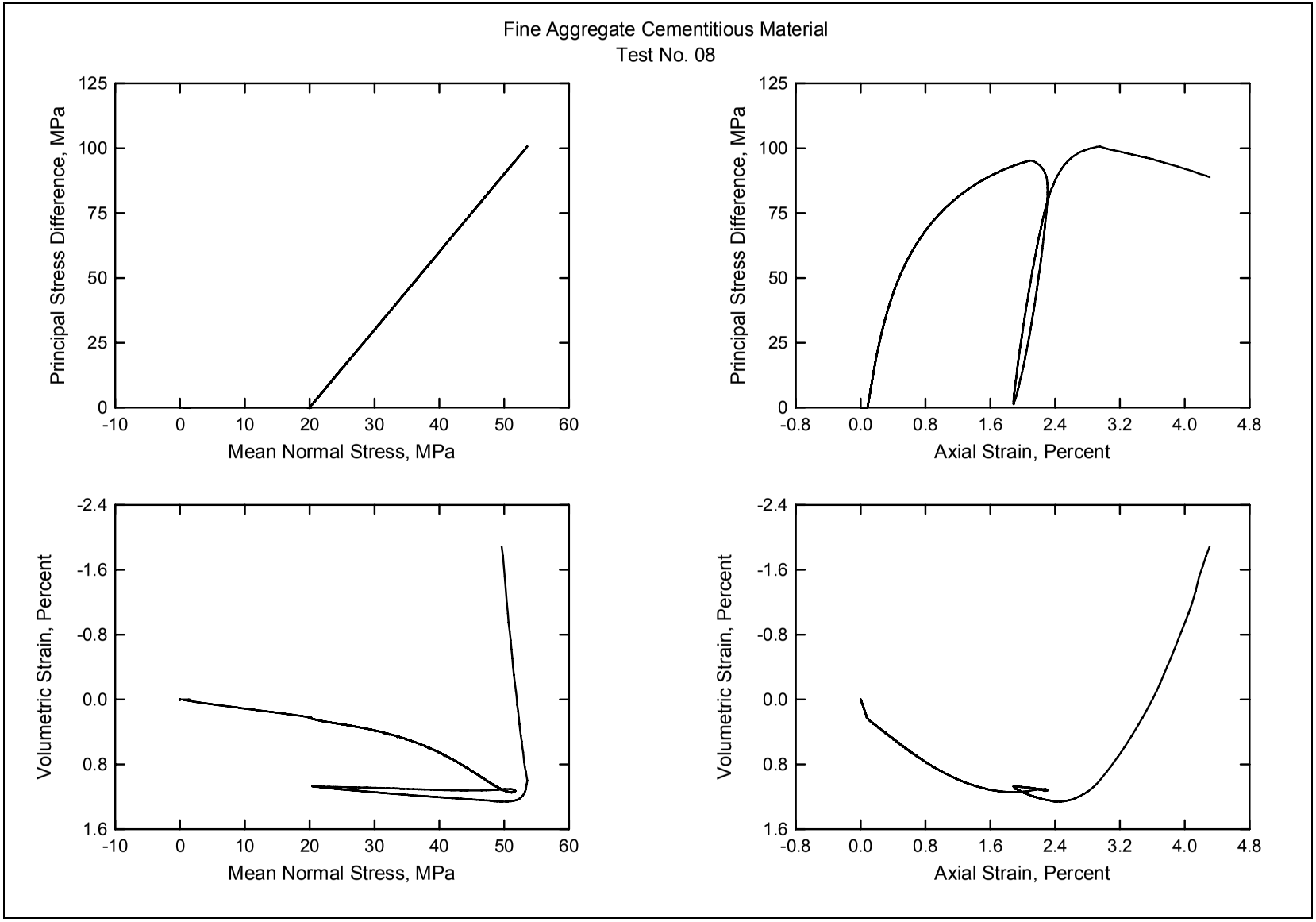
Fine Aggregate Cementitious Material
Test No. 08
Principal Stress Difference, MPa
125
100
75
50
25
0
-10
0
10
20
30
40
50
60
Mean Normal Stress, MPa
Principal Stress Difference, MPa
125
100
75
50
25
0
-0.8
0.0
0.8
1.6
2.4
3.2
4.0
4.8
Axial Strain, Percent
Volumetric Strain, Percent
-2.4
-1.6
-0.8
0.0
0.8
1.6
-10
0
10
20
30
40
50
60
Mean Normal Stress, MPa
Volumetric Strain, Percent
-2.4
-1.6
-0.8
0.0
0.8
1.6
-0.8
0.0
0.8
1.6
2.4
3.2
4.0
4.8
Axial Strain, Percent

Plate 12

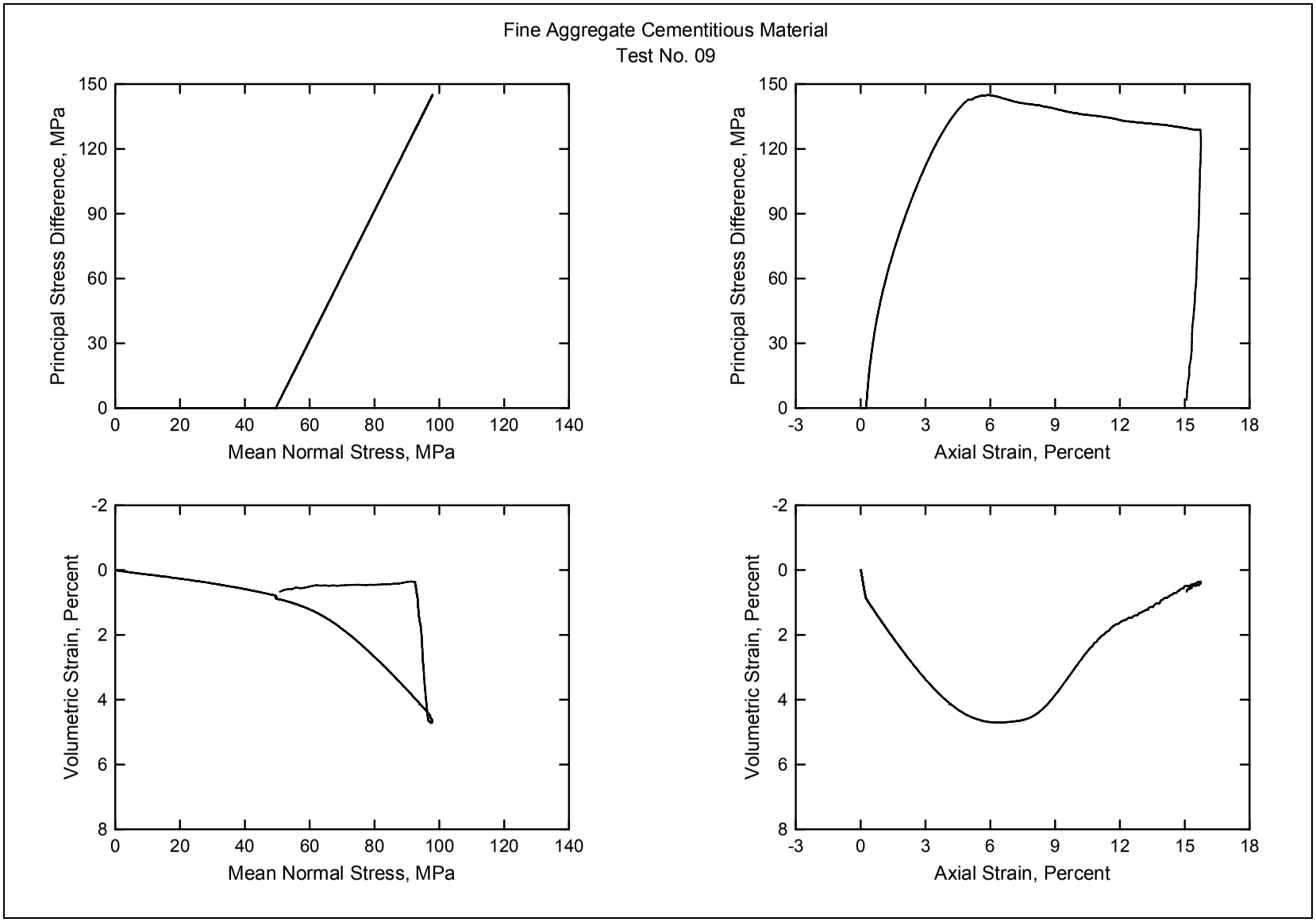
Fine Aggregate Cementitious Material
Test No. 09
Principal Stress Difference, MPa
Mean Normal Stress, MPa
Principal Stress Difference, MPa
Axial Strain, Percent
Volumetric Strain, Percent
Mean Normal Stress, MPa
Volumetric Strain, Percent
Axial Strain, Percent

Plate 13

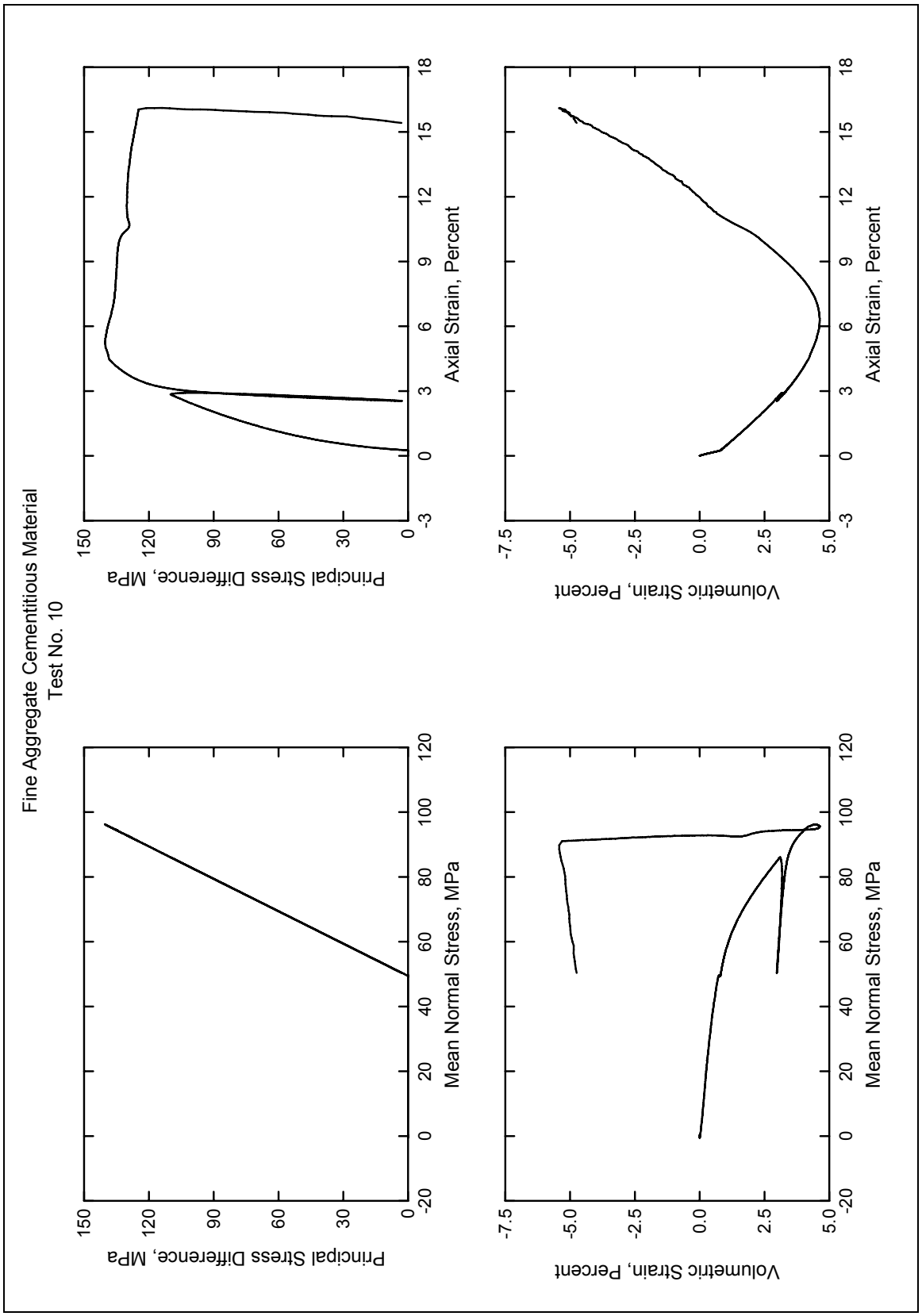
Fine Aggregate Cementitious Material
Test No. 10
Principal Stress Difference, MPa
Axial Strain, Percent
Volumetric Strain, Percent
Axial Strain, Percent
Principal Stress Difference, MPa
Mean Normal Stress, MPa
Volumetric Strain, Percent
Mean Normal Stress, MPa

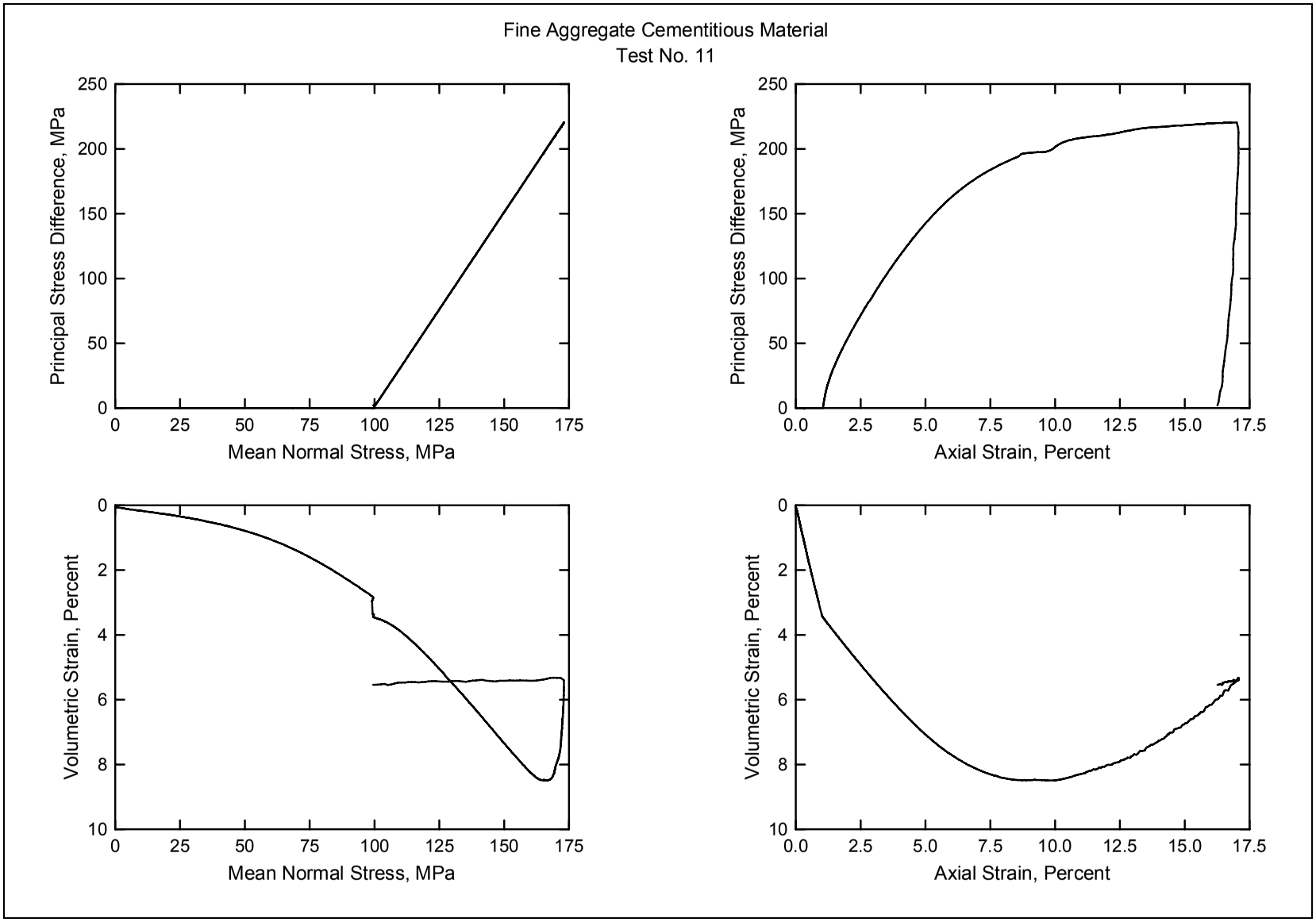
Fine Aggregate Cementitious Material
Test No. 11
Principal Stress Difference, MPa
Mean Normal Stress, MPa
Principal Stress Difference, MPa
Axial Strain, Percent
Volumetric Strain, Percent
Mean Normal Stress, MPa
Volumetric Strain, Percent
Axial Strain, Percent

Plate 15

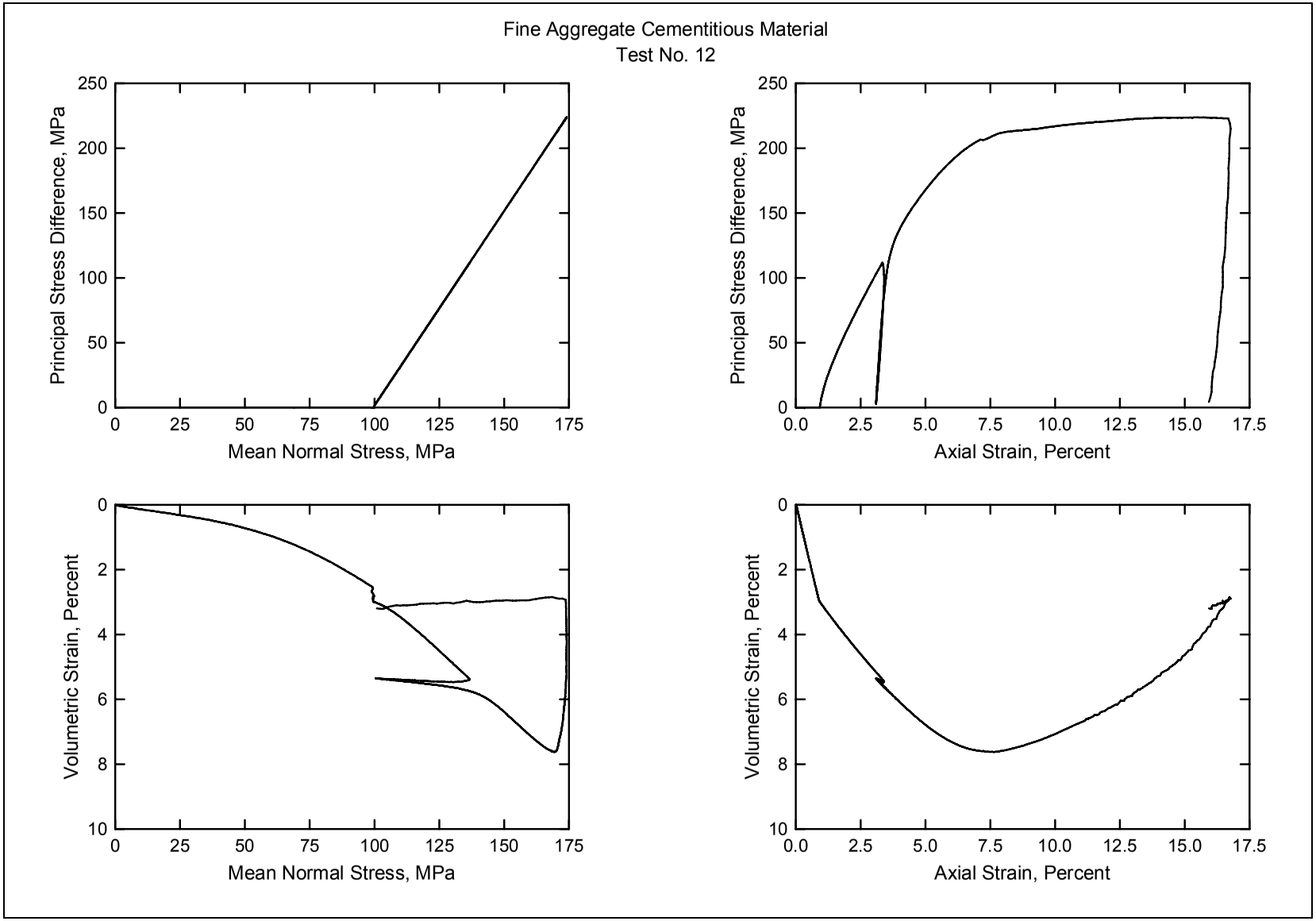
Fine Aggregate Cementitious Material
Test No. 12
Principal Stress Difference, MPa
Mean Normal Stress, MPa
Principal Stress Difference, MPa
Axial Strain, Percent
Volumetric Strain, Percent
Mean Normal Stress, MPa
Volumetric Strain, Percent
Axial Strain, Percent

Plate 16

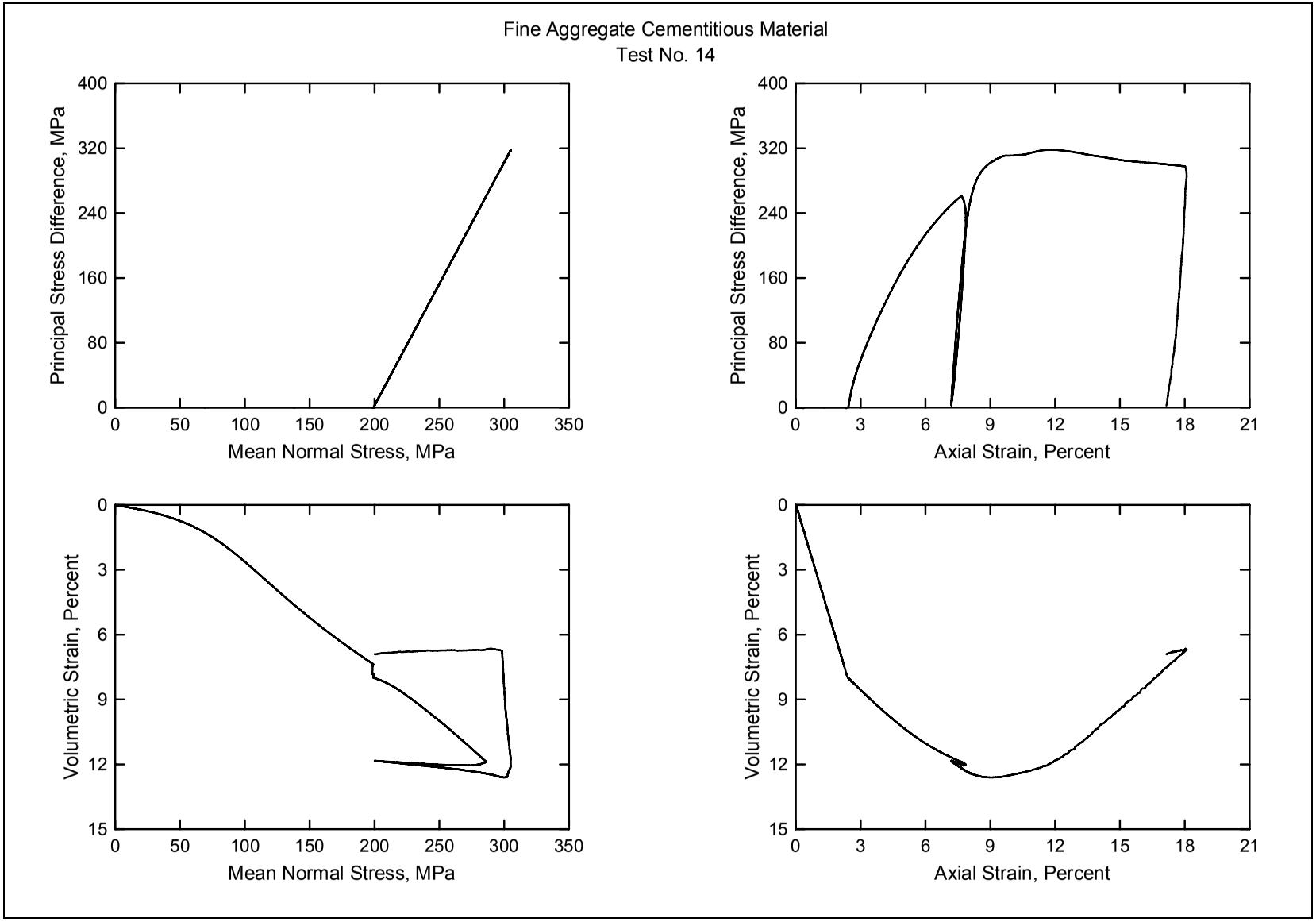
Fine Aggregate Cementitious Material
Test No. 14
Principal Stress Difference, MPa
Mean Normal Stress, MPa
Principal Stress Difference, MPa
Axial Strain, Percent
Volumetric Strain, Percent
Mean Normal Stress, MPa
Volumetric Strain, Percent
Axial Strain, Percent

Plate 17

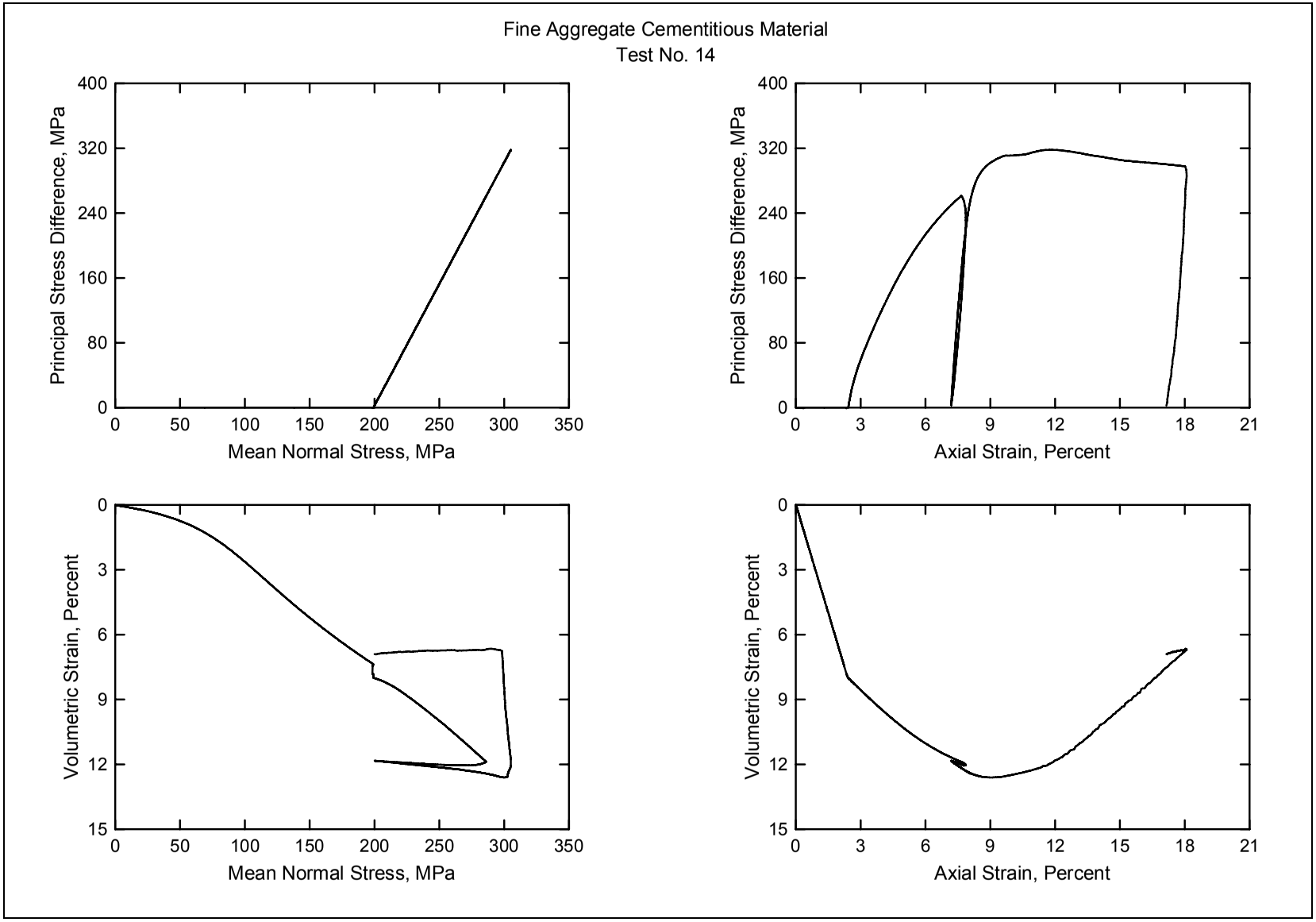
Fine Aggregate Cementitious Material
Test No. 14
Principal Stress Difference, MPa
Mean Normal Stress, MPa
Principal Stress Difference, MPa
Axial Strain, Percent
Volumetric Strain, Percent
Mean Normal Stress, MPa
Volumetric Strain, Percent
Axial Strain, Percent

Plate 18

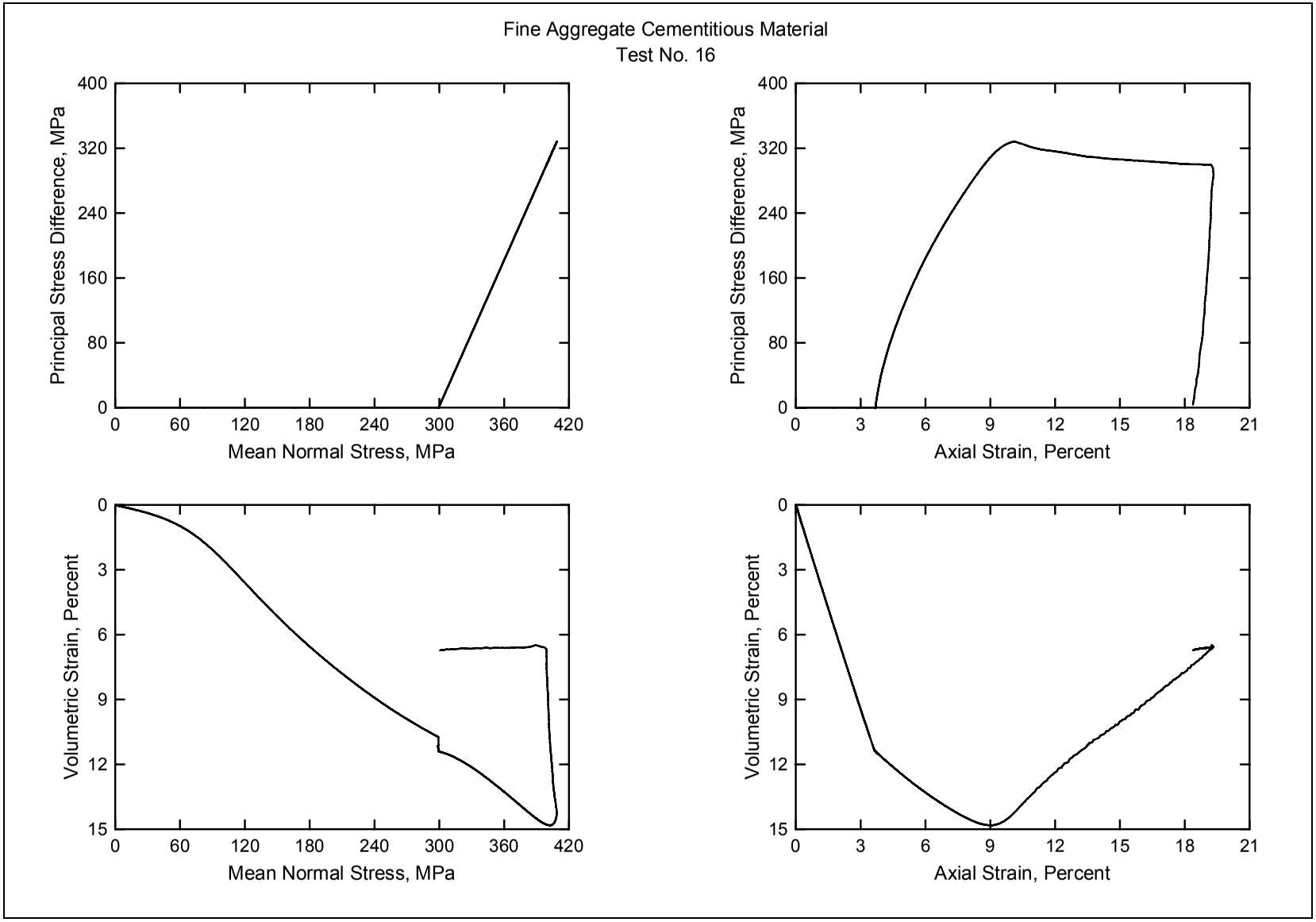
Fine Aggregate Cementitious Material
Test No. 16
Principal Stress Difference, MPa
Mean Normal Stress, MPa
Principal Stress Difference, MPa
Axial Strain, Percent
Volumetric Strain, Percent
Mean Normal Stress, MPa
Volumetric Strain, Percent
Axial Strain, Percent

Plate 19

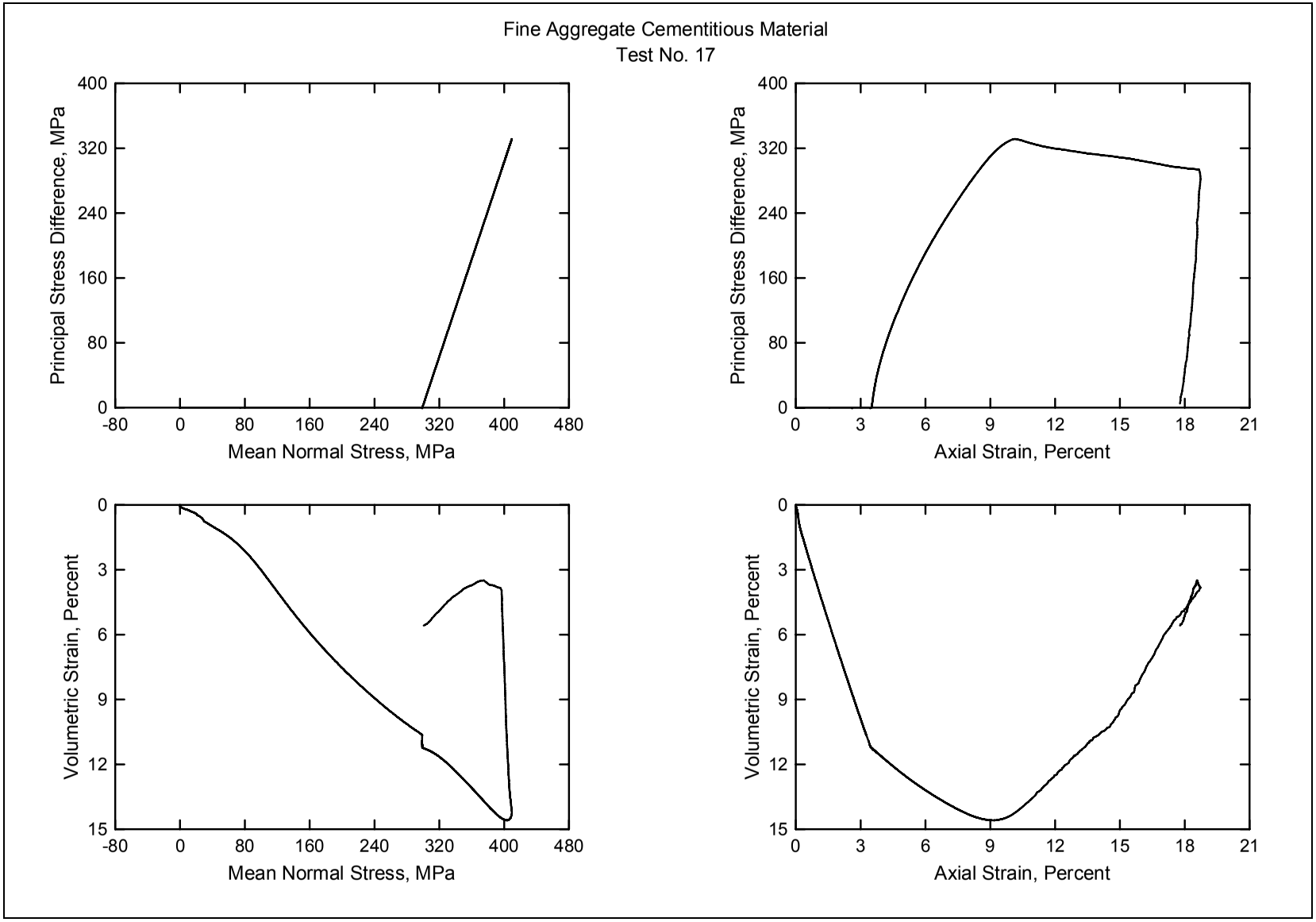
Fine Aggregate Cementitious Material
Test No. 17
Principal Stress Difference, MPa
Mean Normal Stress, MPa
Principal Stress Difference, MPa
Axial Strain, Percent
Volumetric Strain, Percent
Mean Normal Stress, MPa
Volumetric Strain, Percent
Axial Strain, Percent

Plate 20

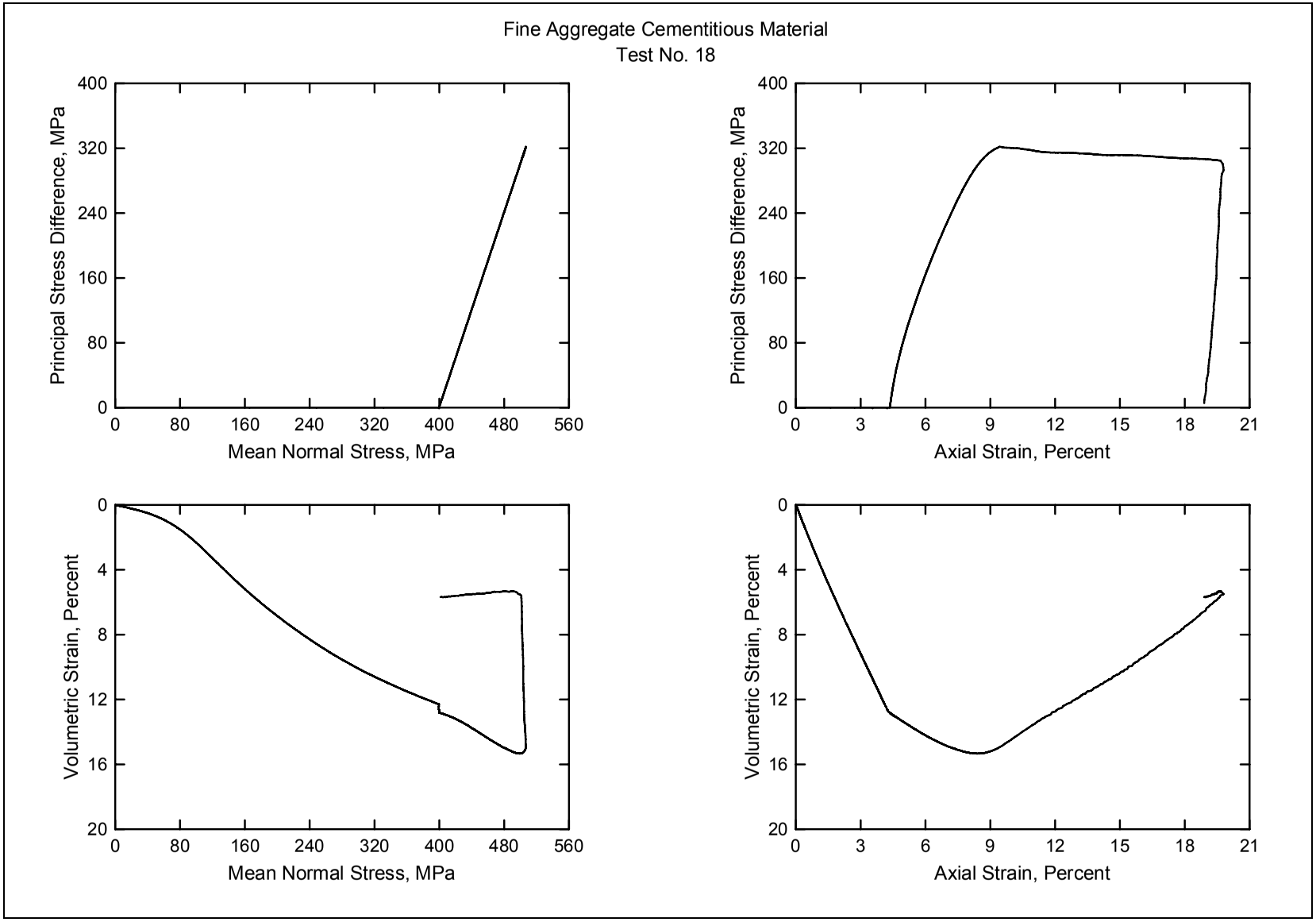
Fine Aggregate Cementitious Material
Test No. 18
Principal Stress Difference, MPa
Mean Normal Stress, MPa
Principal Stress Difference, MPa
Axial Strain, Percent
Volumetric Strain, Percent
Mean Normal Stress, MPa
Volumetric Strain, Percent
Axial Strain, Percent

Plate 21

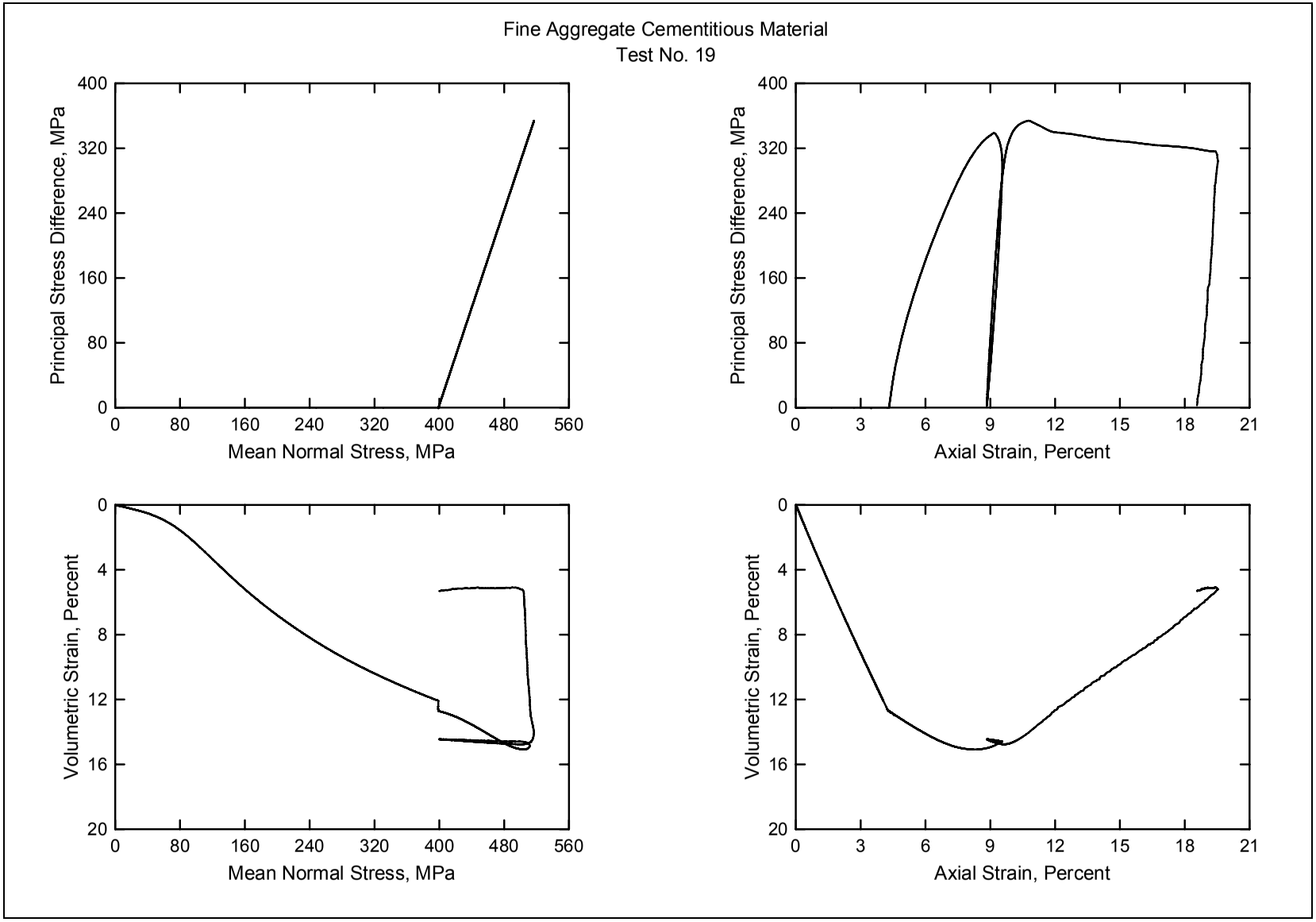
Fine Aggregate Cementitious Material
Test No. 19
Principal Stress Difference, MPa
Mean Normal Stress, MPa
Principal Stress Difference, MPa
Axial Strain, Percent
Volumetric Strain, Percent
Mean Normal Stress, MPa
Volumetric Strain, Percent
Axial Strain, Percent

Plate 22

Fine Aggregate Cementitious Material

Test No. 33

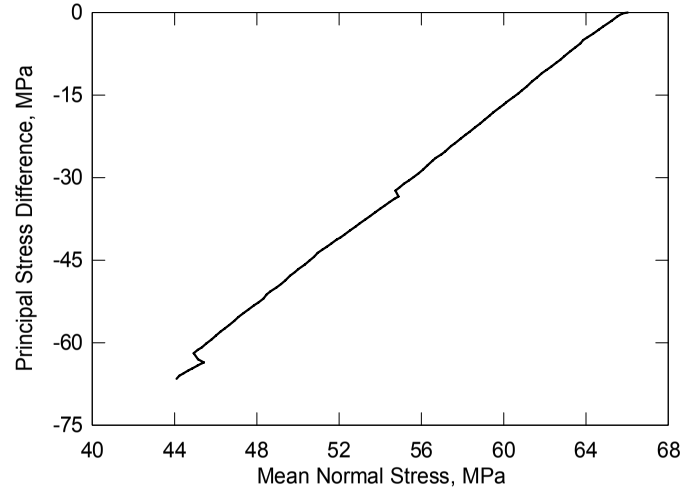

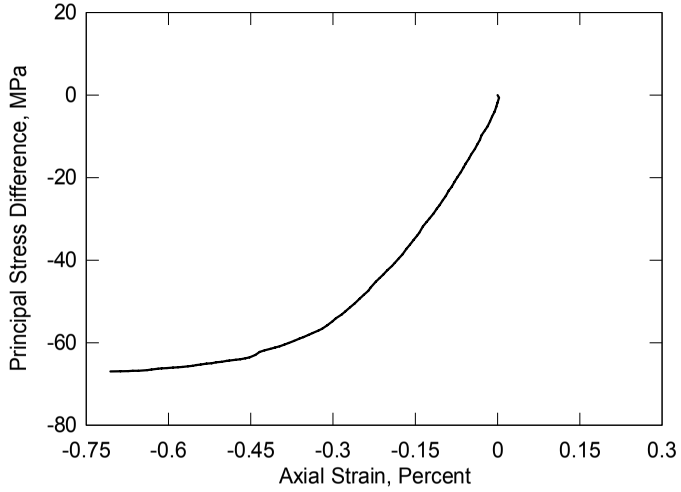

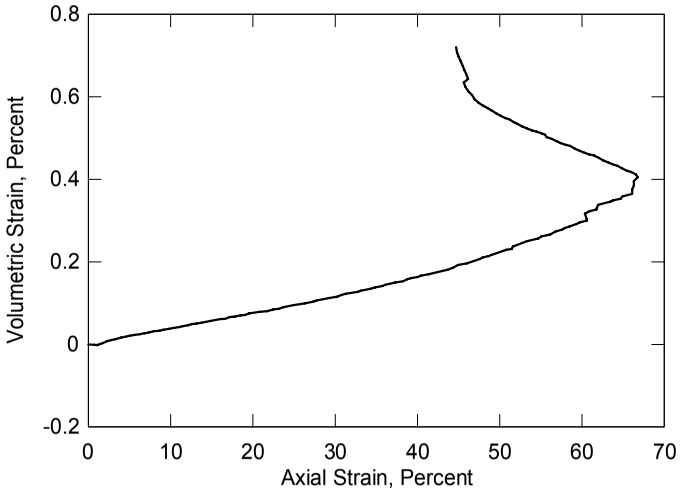

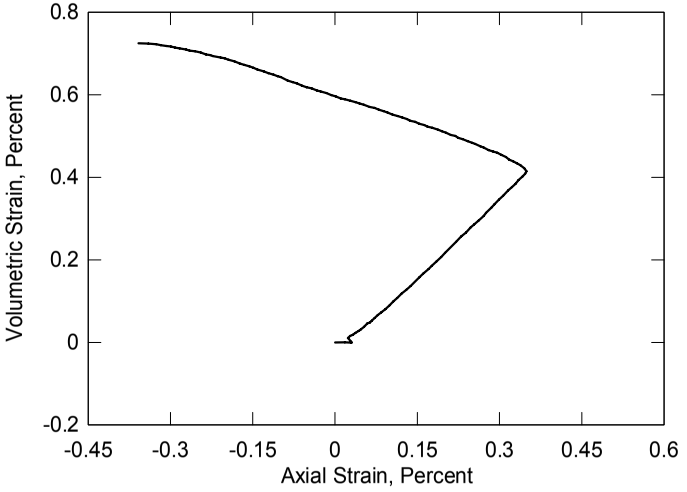

Plate 23

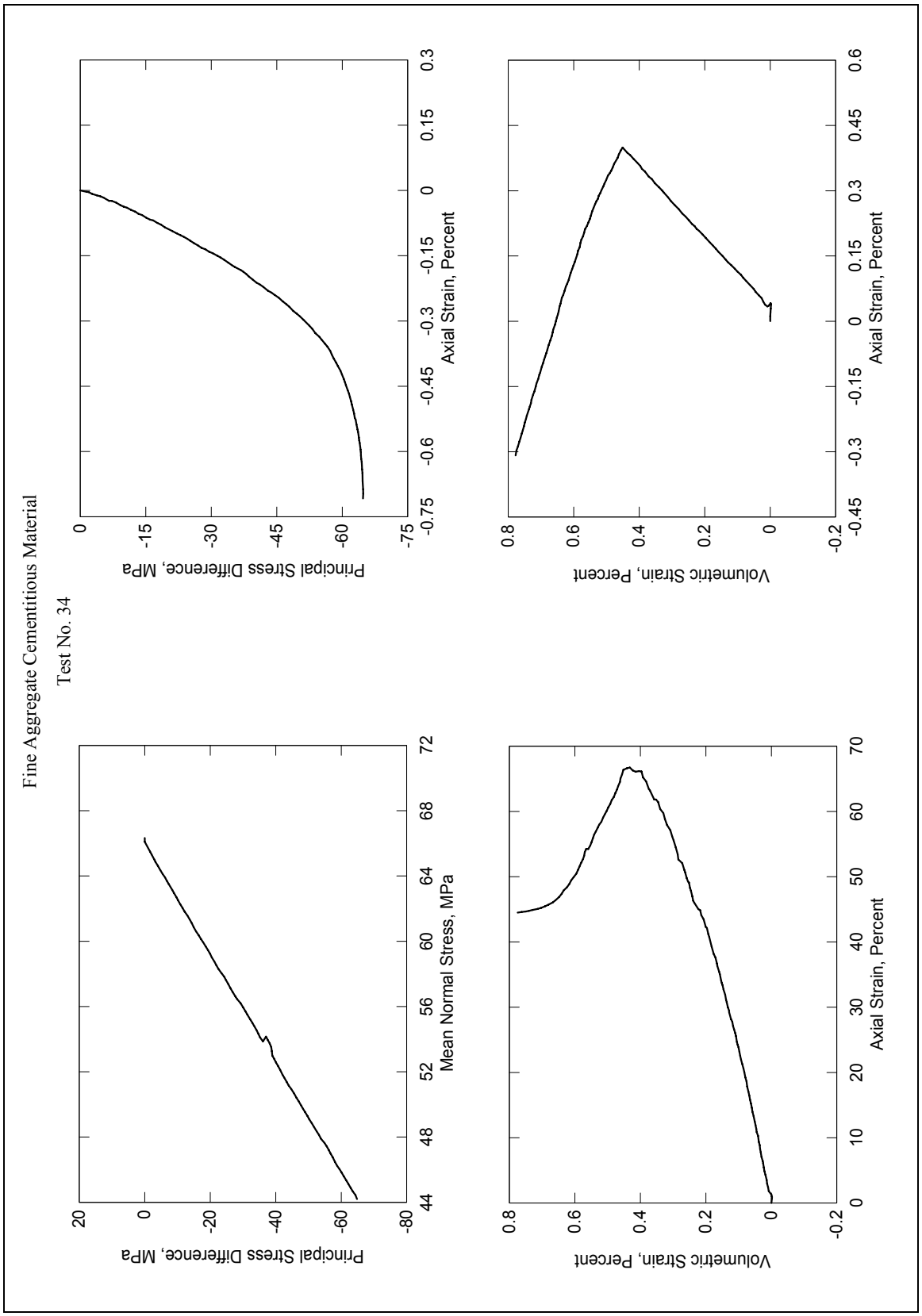
Fine Aggregate Cementitious Material
Test No. 34
Principal Stress Difference, MPa
Mean Normal Stress, MPa
Principal Stress Difference, MPa
Axial Strain, Percent
Volumetric Strain, Percent
Axial Strain, Percent
Volumetric Strain, Percent
Axial Strain, Percent

Plate 24

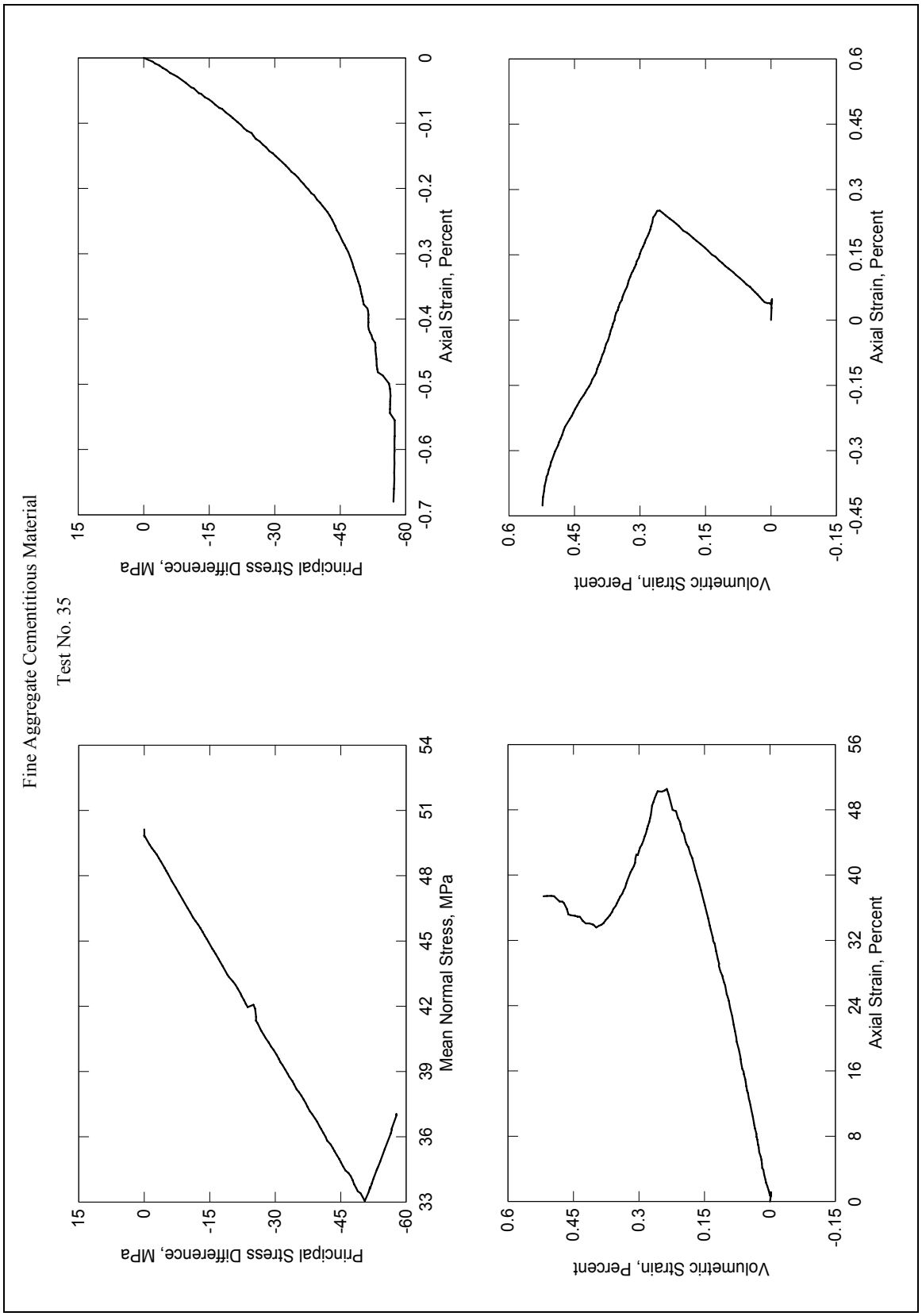
Fine Aggregate Cementitious Material
Test No. 35
Principal Stress Difference, MPa
Mean Normal Stress, MPa
Principal Stress Difference, MPa
Axial Strain, Percent
Volumetric Strain, Percent
Axial Strain, Percent
Volumetric Strain, Percent
Axial Strain, Percent

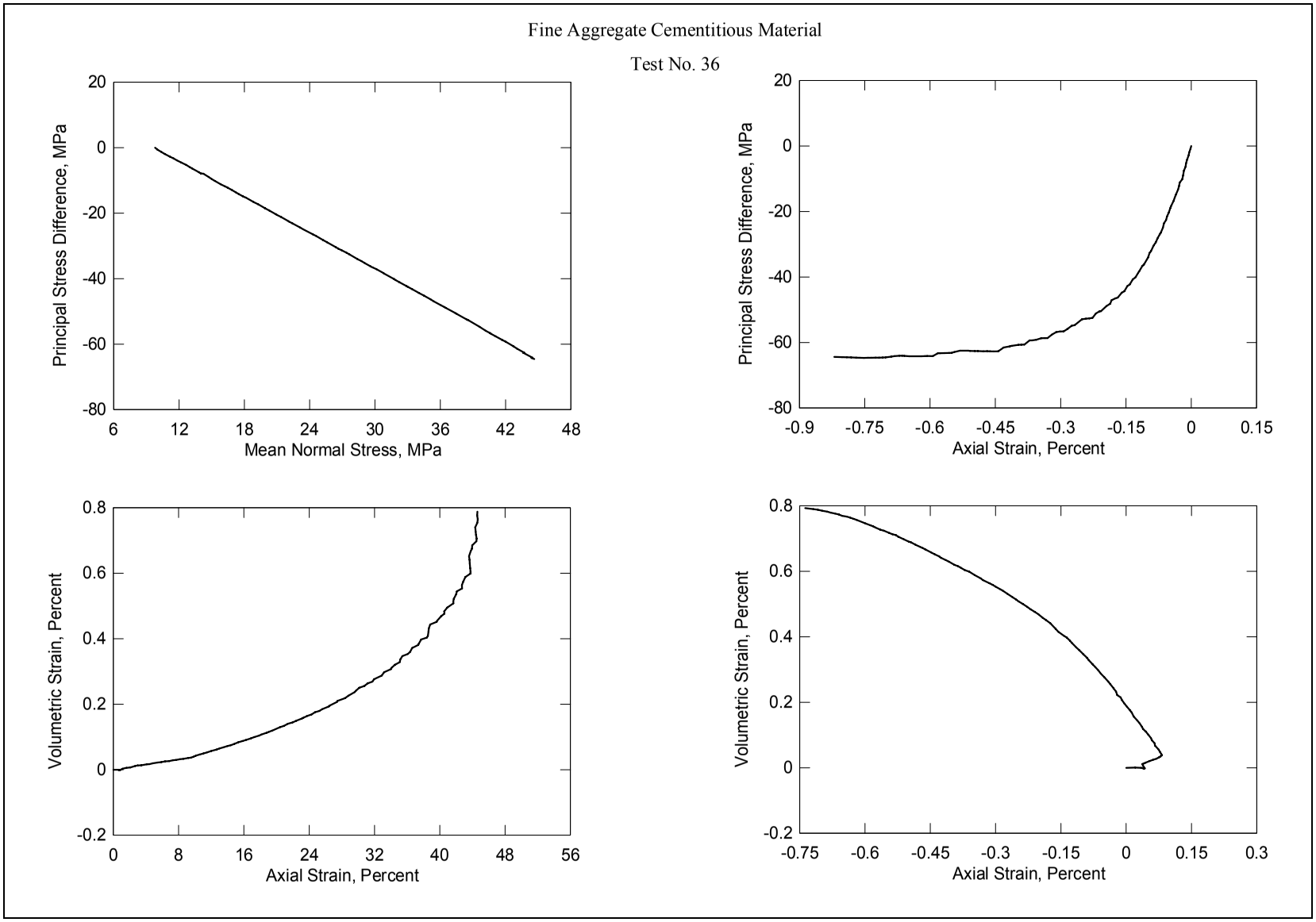
Fine Aggregate Cementitious Material
Test No. 36
Principal Stress Difference, MPa
Mean Normal Stress, MPa
Principal Stress Difference, MPa
Axial Strain, Percent
Volumetric Strain, Percent
Axial Strain, Percent
Volumetric Strain, Percent
Axial Strain, Percent

Plate 26

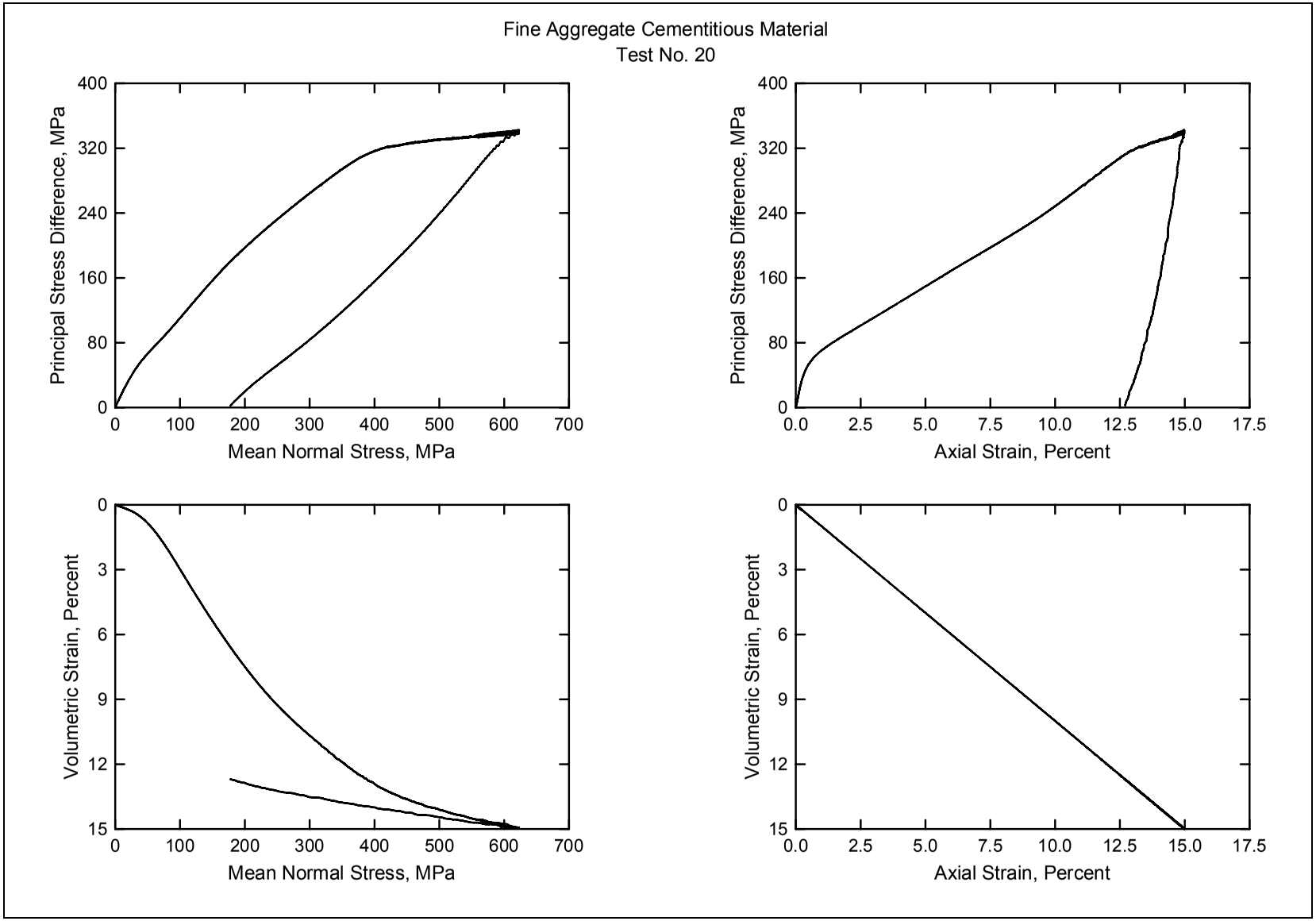
Fine Aggregate Cementitious Material
Test No. 20
Principal Stress Difference, MPa
Mean Normal Stress, MPa
Principal Stress Difference, MPa
Axial Strain, Percent
Volumetric Strain, Percent
Mean Normal Stress, MPa
Volumetric Strain, Percent
Axial Strain, Percent

Plate 27

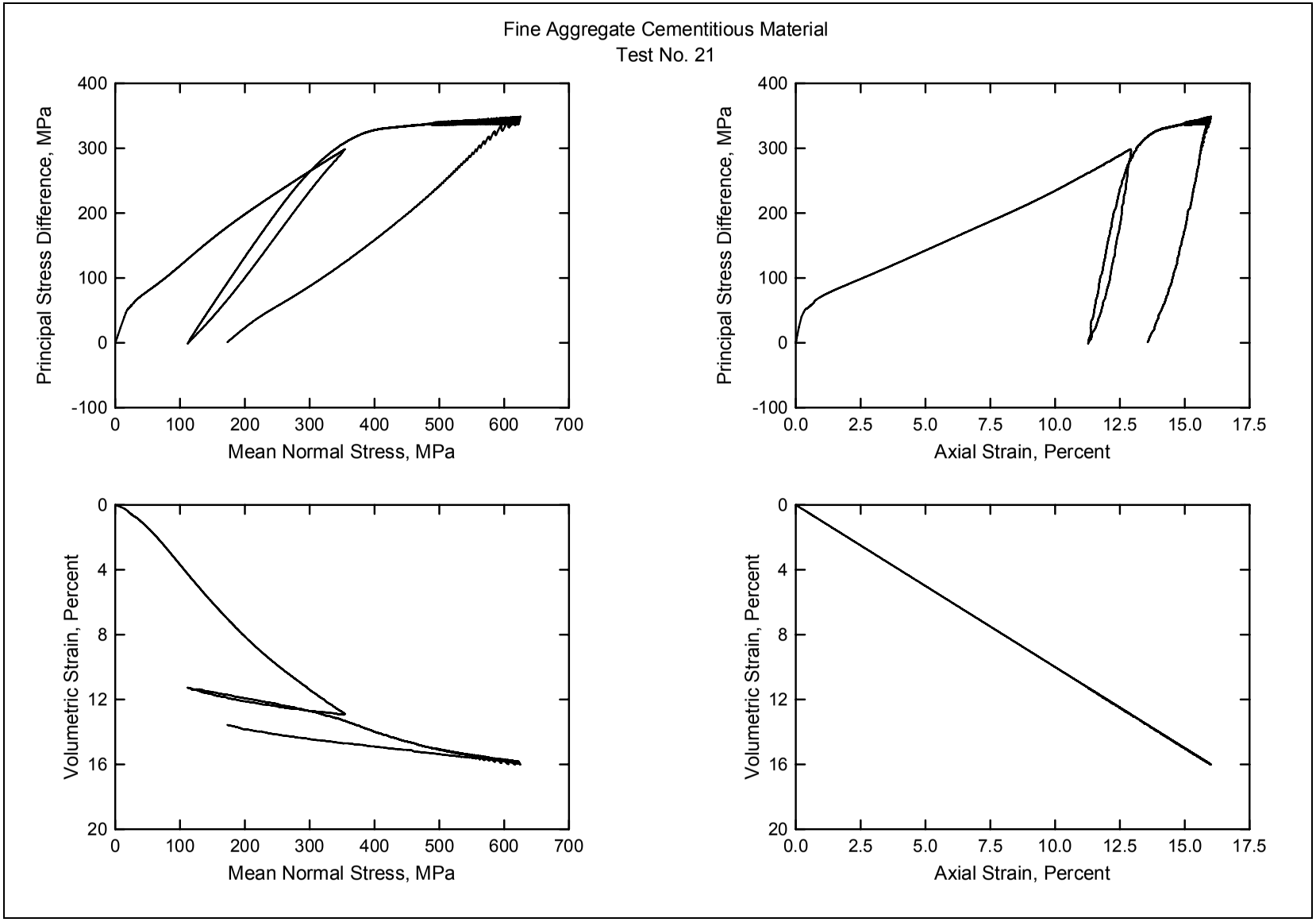
Fine Aggregate Cementitious Material
Test No. 21
Principal Stress Difference, MPa
Mean Normal Stress, MPa
Principal Stress Difference, MPa
Axial Strain, Percent
Volumetric Strain, Percent
Mean Normal Stress, MPa
Volumetric Strain, Percent
Axial Strain, Percent

Plate 28

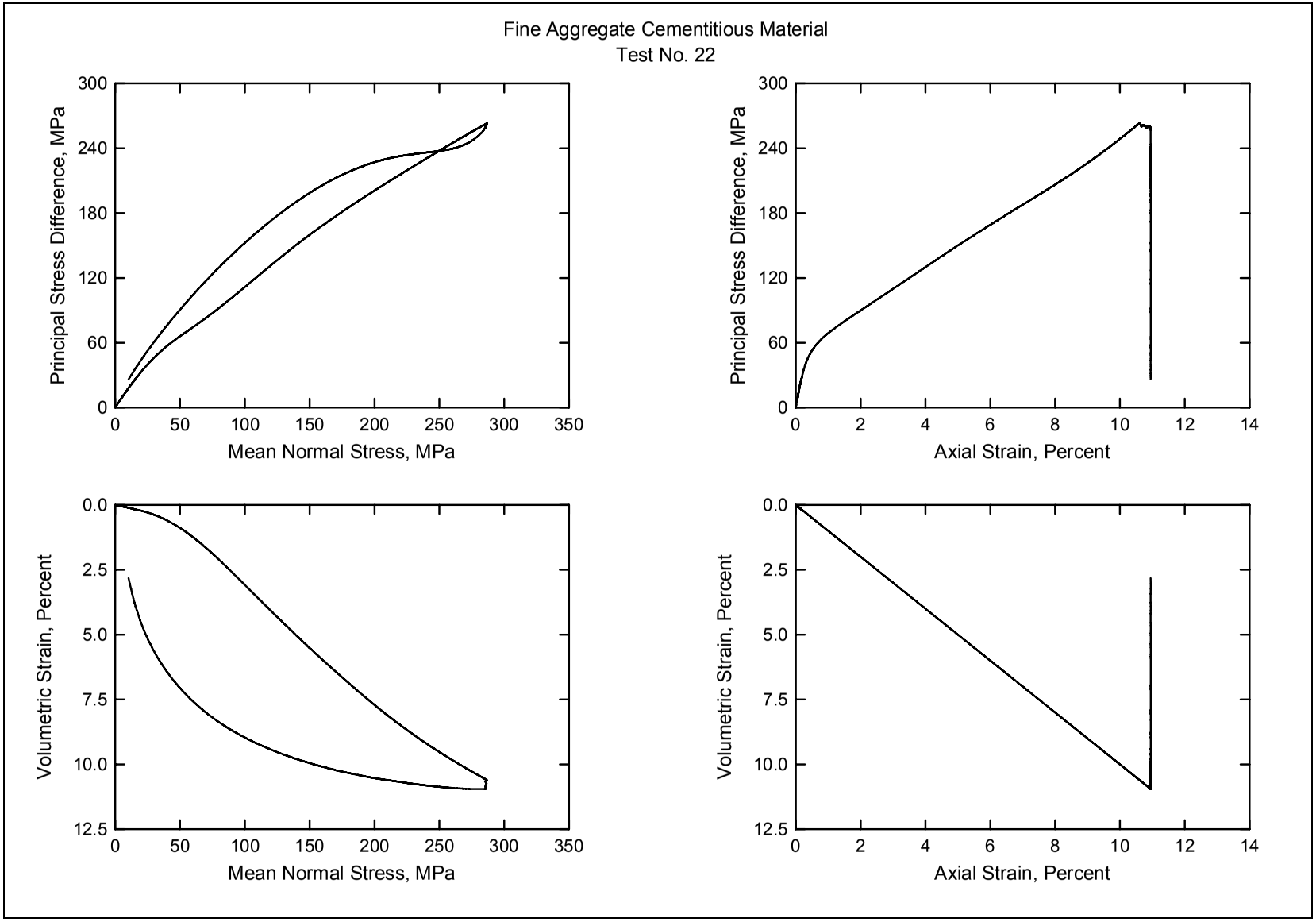
Fine Aggregate Cementitious Material
Test No. 22
Principal Stress Difference, MPa
Mean Normal Stress, MPa
Principal Stress Difference, MPa
Axial Strain, Percent
Volumetric Strain, Percent
Mean Normal Stress, MPa
Volumetric Strain, Percent
Axial Strain, Percent

Plate 29

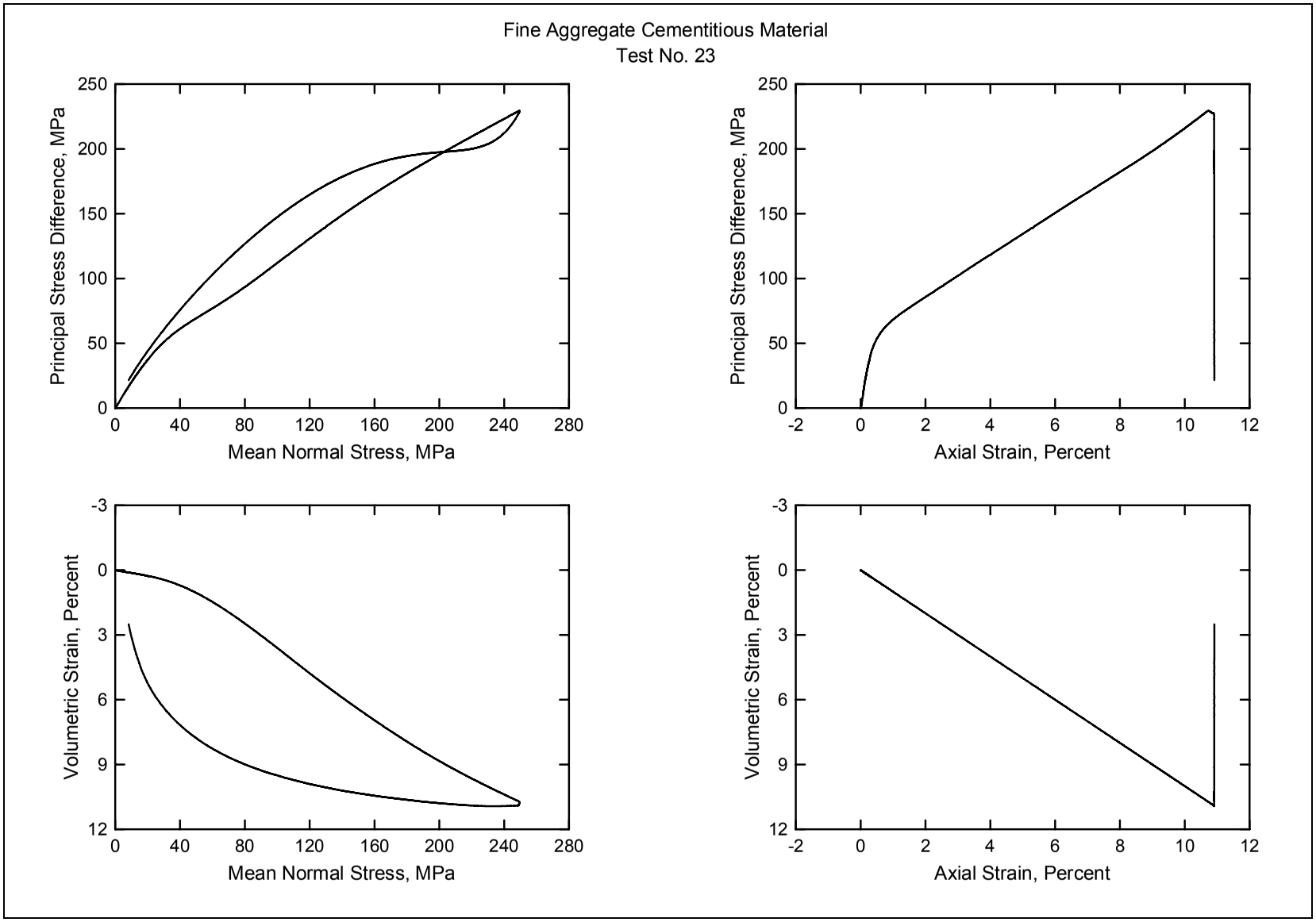
Fine Aggregate Cementitious Material
Test No. 23
Principal Stress Difference, MPa
Mean Normal Stress, MPa
Principal Stress Difference, MPa
Axial Strain, Percent
Volumetric Strain, Percent
Mean Normal Stress, MPa
Volumetric Strain, Percent
Axial Strain, Percent

Plate 30

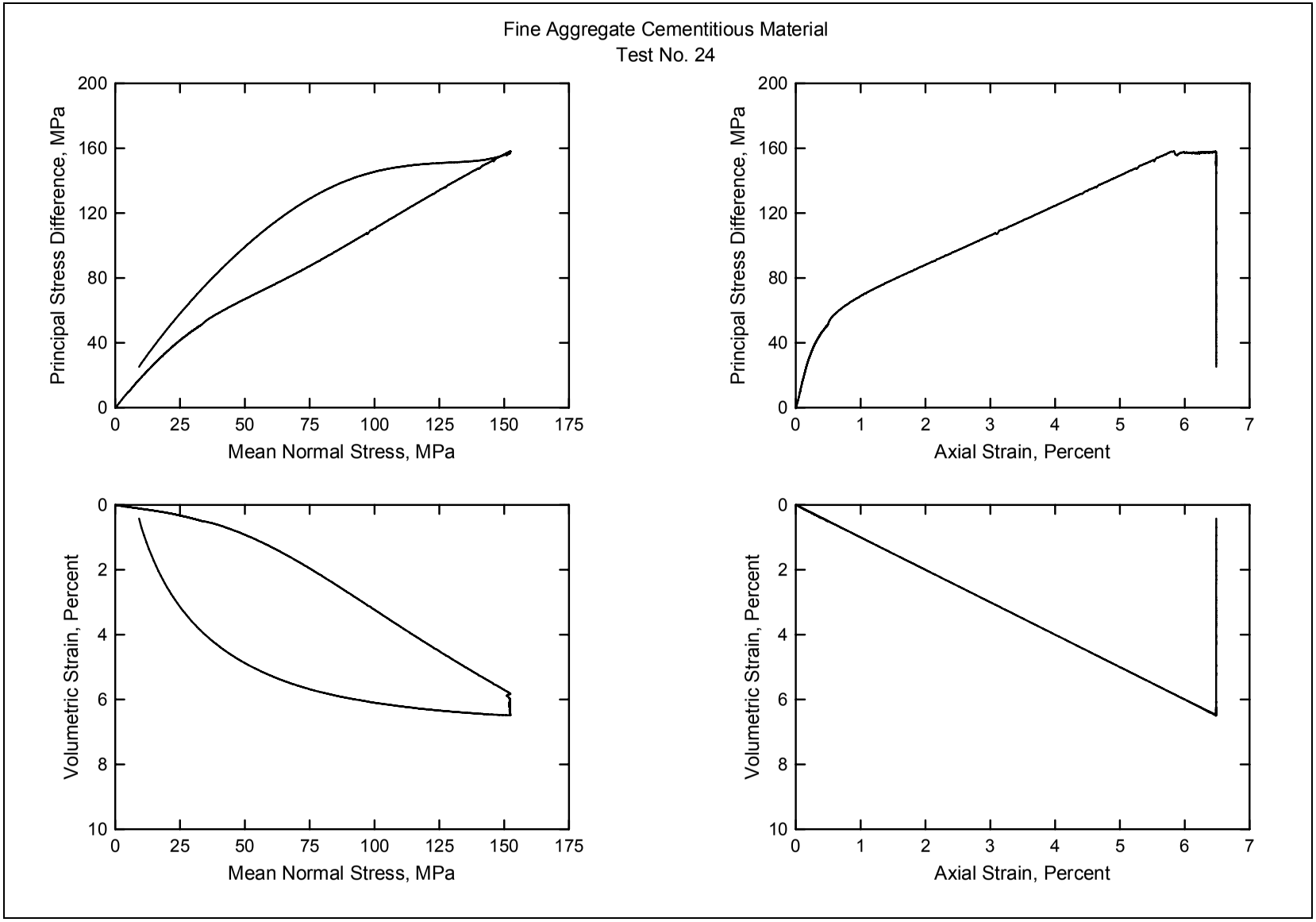
Fine Aggregate Cementitious Material
Test No. 24
Principal Stress Difference, MPa
Mean Normal Stress, MPa
Principal Stress Difference, MPa
Axial Strain, Percent
Volumetric Strain, Percent
Mean Normal Stress, MPa
Volumetric Strain, Percent
Axial Strain, Percent

Plate 31

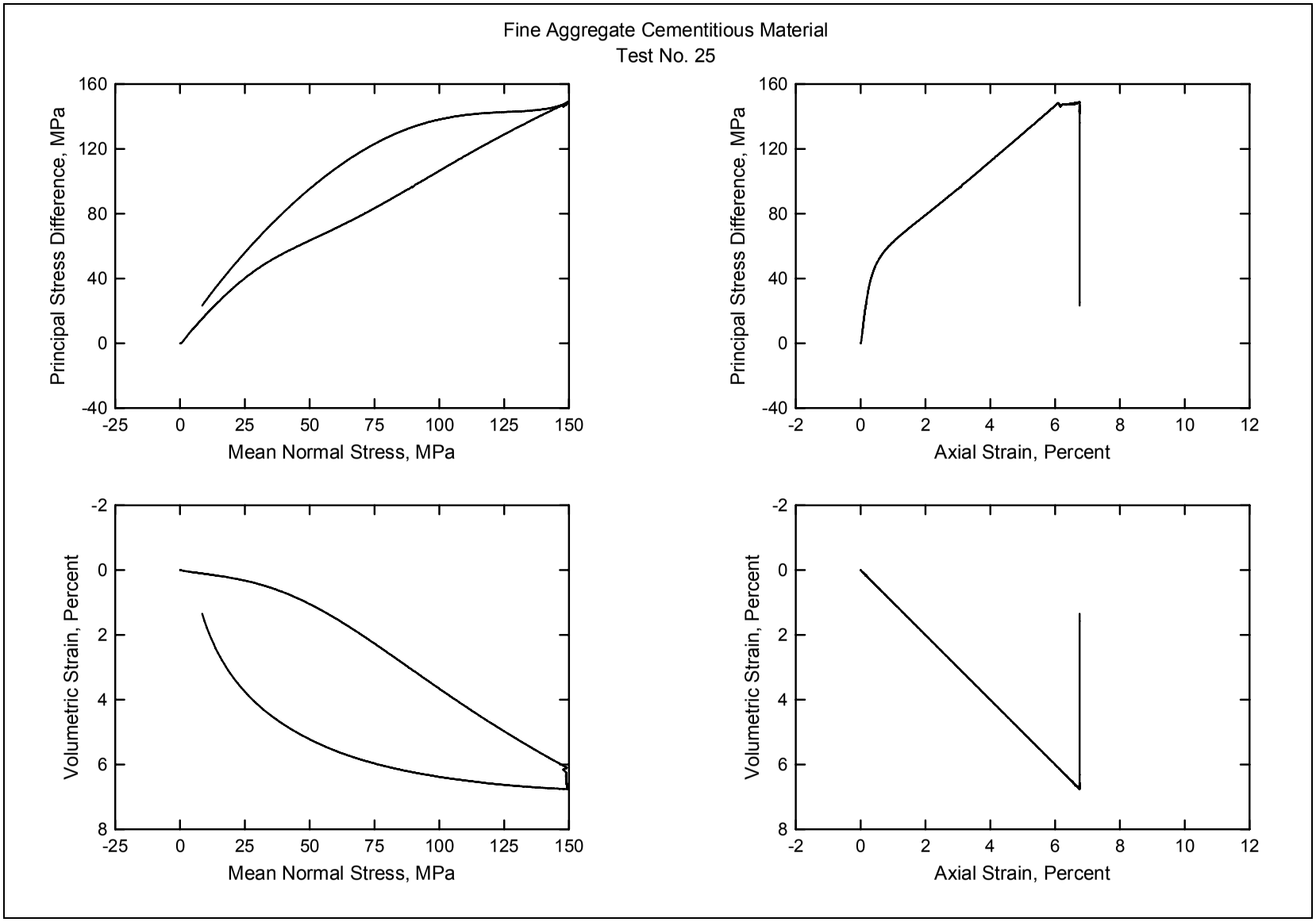
Fine Aggregate Cementitious Material
Test No. 25
Principal Stress Difference, MPa
Mean Normal Stress, MPa
Principal Stress Difference, MPa
Axial Strain, Percent
Volumetric Strain, Percent
Mean Normal Stress, MPa
Volumetric Strain, Percent
Axial Strain, Percent

Plate 32

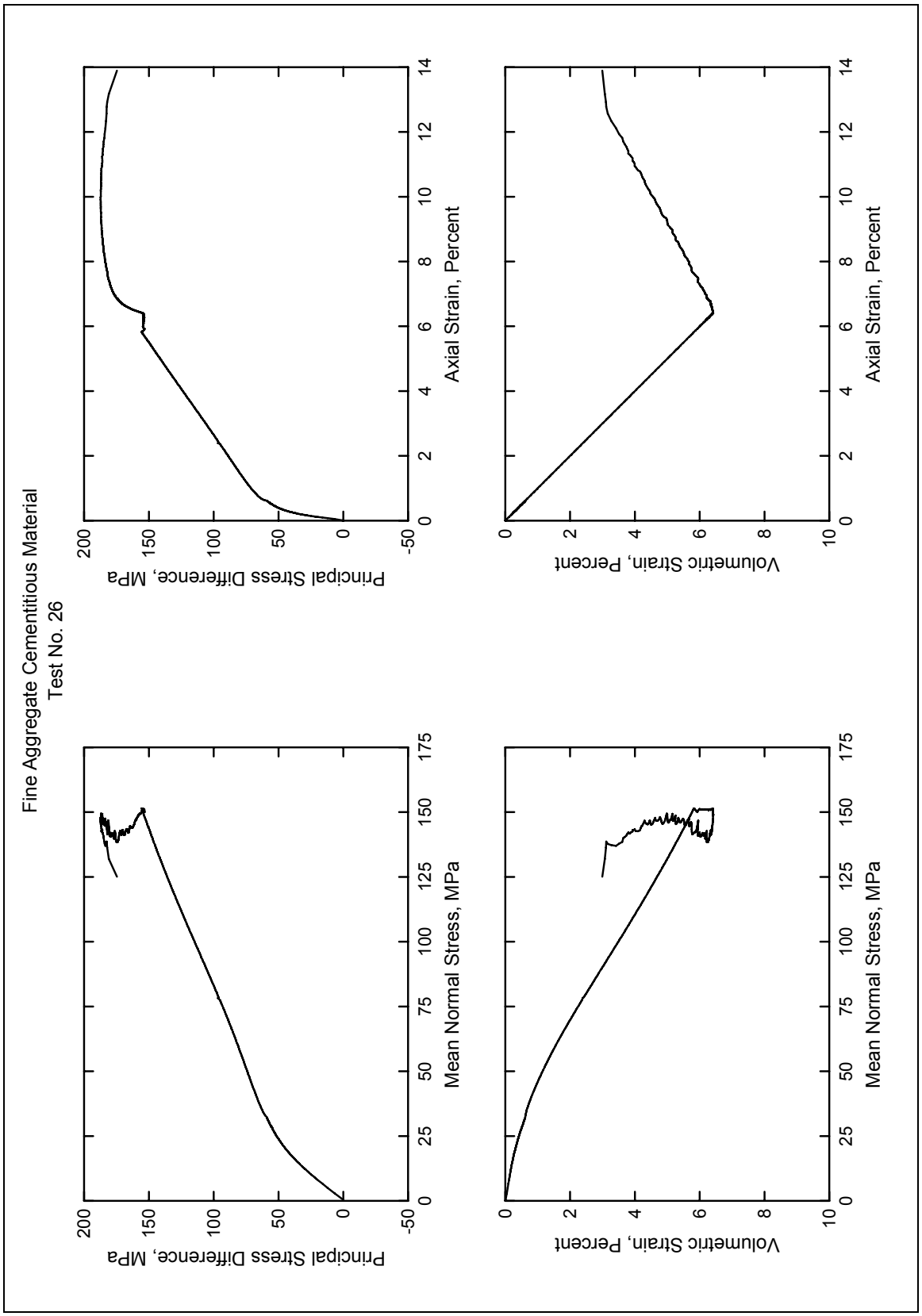
Fine Aggregate Cementitious Material
Test No. 26
Principal Stress Difference, MPa
Mean Normal Stress, MPa
Principal Stress Difference, MPa
Axial Strain, Percent
Volumetric Strain, Percent
Mean Normal Stress, MPa
Volumetric Strain, Percent
Axial Strain, Percent

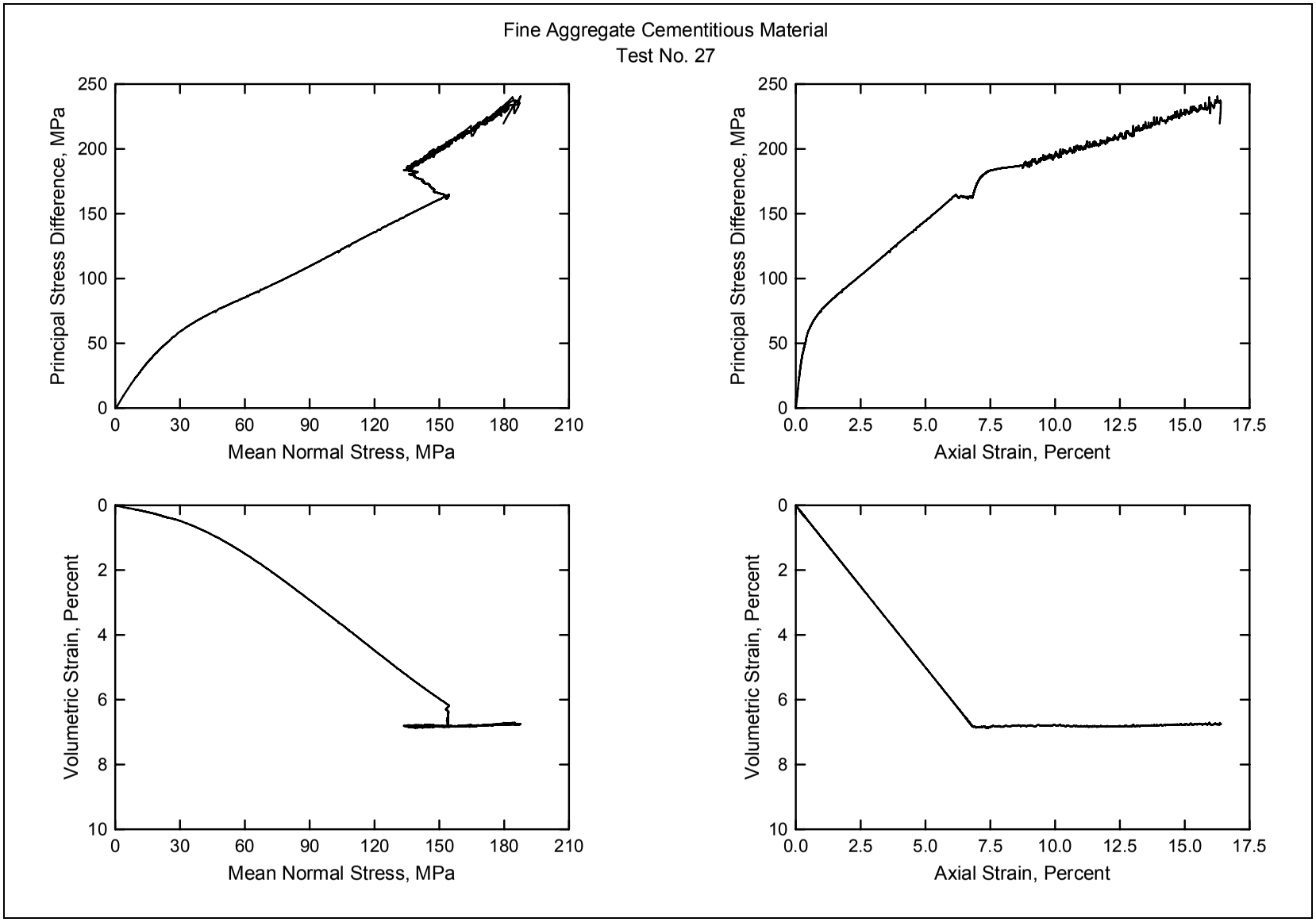
Fine Aggregate Cementitious Material
Test No. 27
Principal Stress Difference, MPa
Mean Normal Stress, MPa
Principal Stress Difference, MPa
Axial Strain, Percent
Volumetric Strain, Percent
Mean Normal Stress, MPa
Volumetric Strain, Percent
Axial Strain, Percent

Plate 34

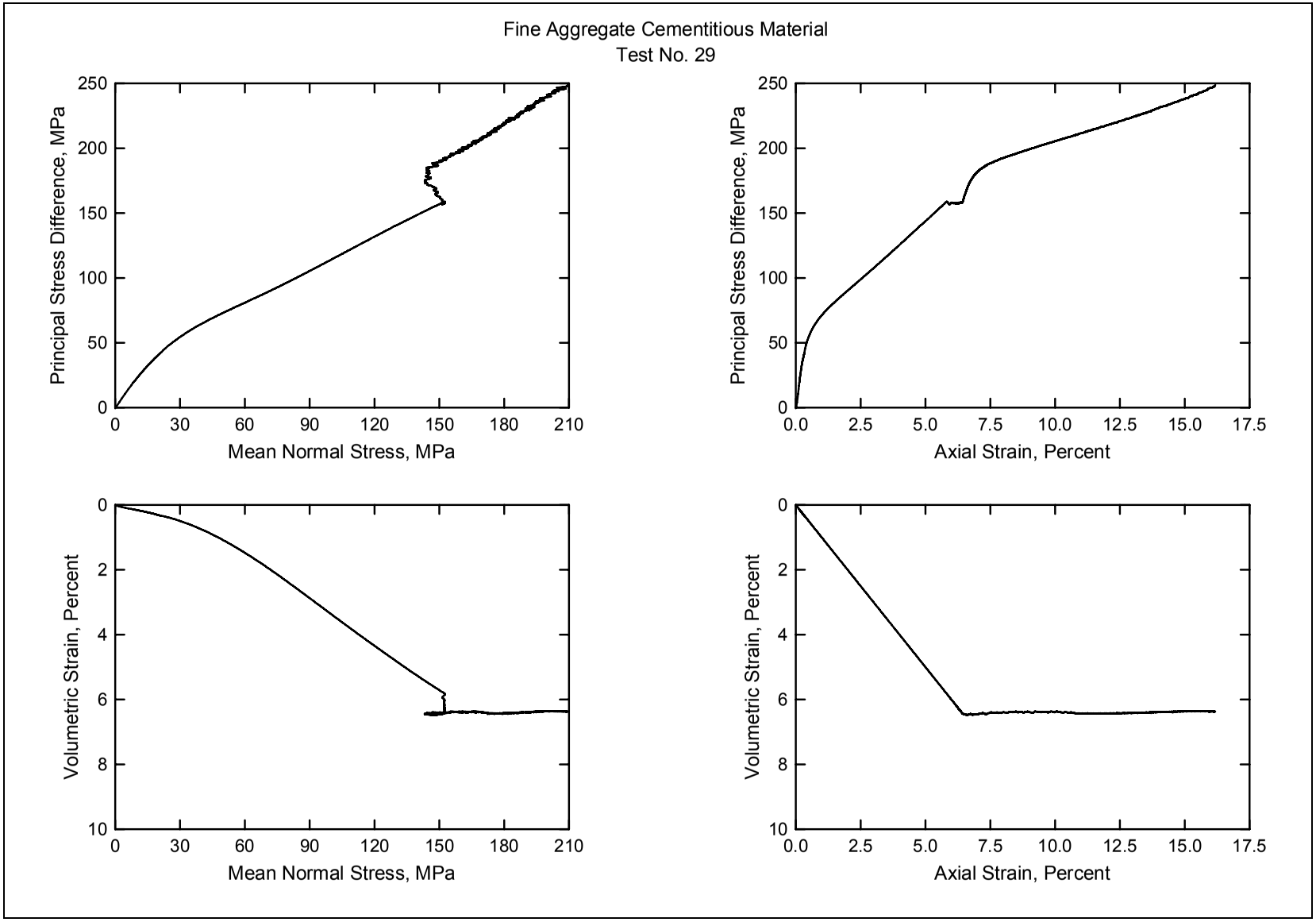
Fine Aggregate Cementitious Material
Test No. 29
Principal Stress Difference, MPa
Mean Normal Stress, MPa
Principal Stress Difference, MPa
Axial Strain, Percent
Volumetric Strain, Percent
Mean Normal Stress, MPa
Volumetric Strain, Percent
Axial Strain, Percent

Plate 35

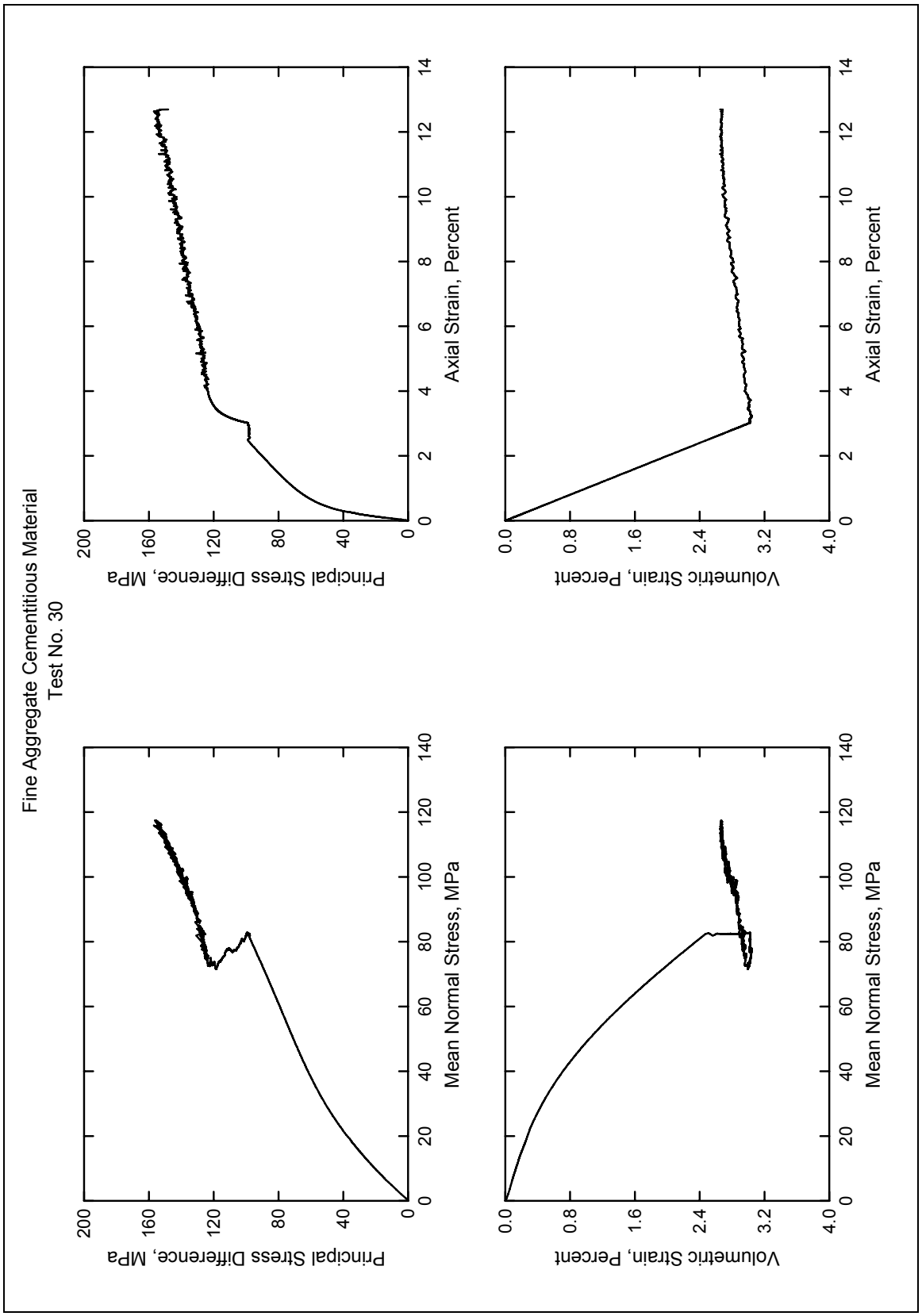
Fine Aggregate Cementitious Material
Test No. 30
Principal Stress Difference, MPa
Axial Strain, Percent
Volumetric Strain, Percent
Axial Strain, Percent
Principal Stress Difference, MPa
Mean Normal Stress, MPa
Volumetric Strain, Percent
Mean Normal Stress, MPa

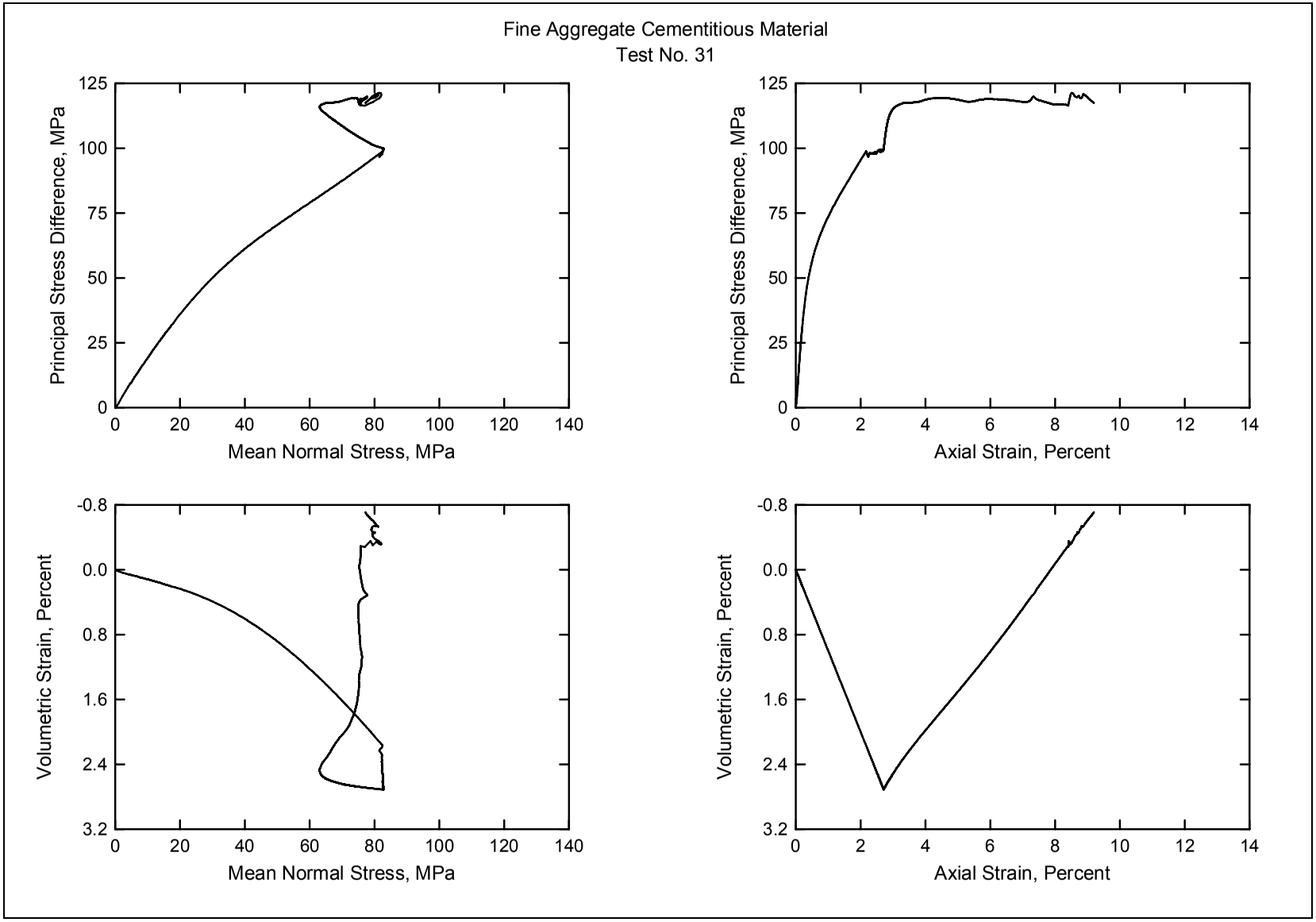
Fine Aggregate Cementitious Material
Test No. 31
Principal Stress Difference, MPa
Mean Normal Stress, MPa
Principal Stress Difference, MPa
Axial Strain, Percent
Volumetric Strain, Percent
Mean Normal Stress, MPa
Volumetric Strain, Percent
Axial Strain, Percent

Plate 37

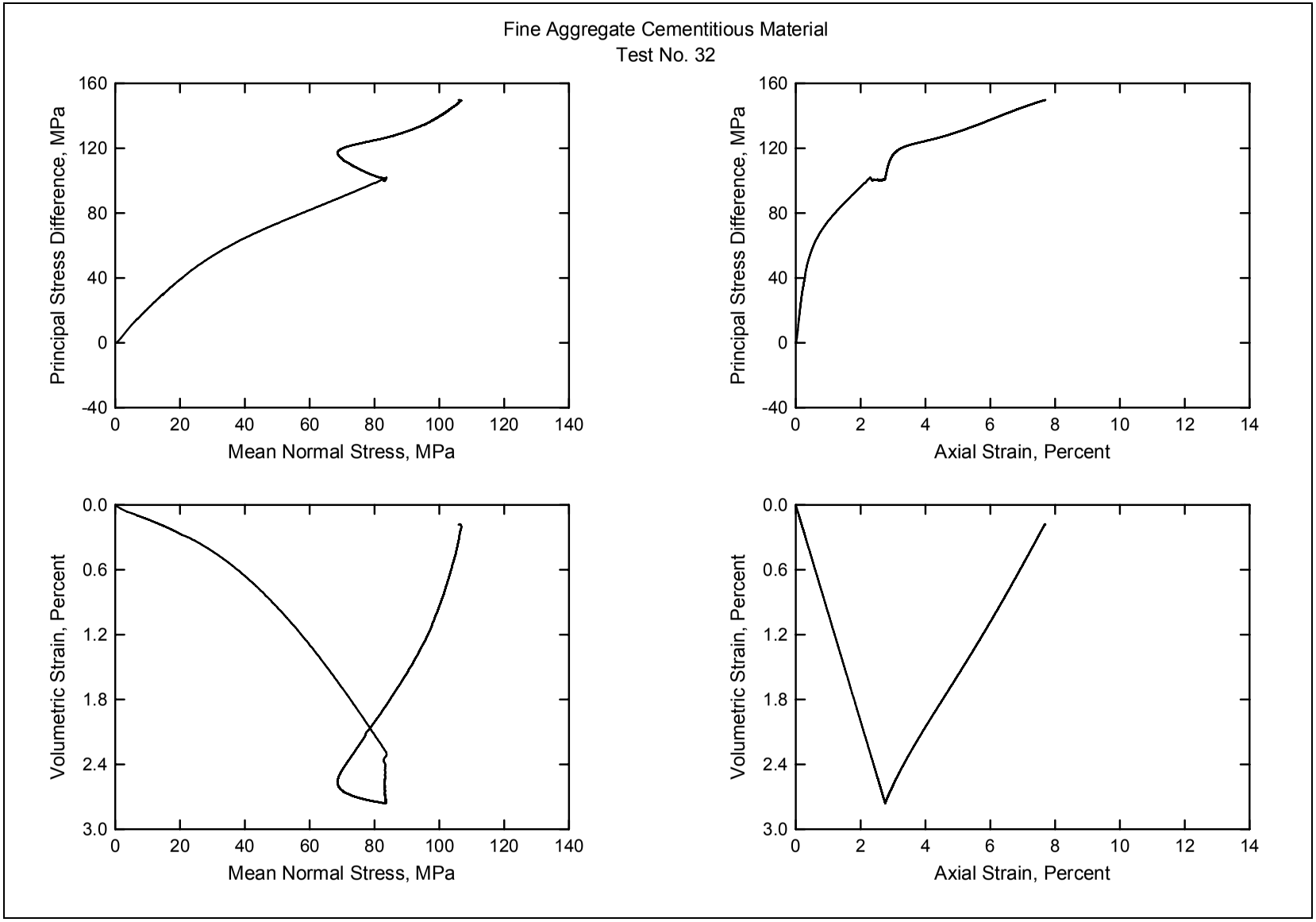
Fine Aggregate Cementitious Material
Test No. 32
Principal Stress Difference, MPa
Mean Normal Stress, MPa
Principal Stress Difference, MPa
Axial Strain, Percent
Volumetric Strain, Percent
Mean Normal Stress, MPa
Volumetric Strain, Percent
Axial Strain, Percent

Plate 38

REPORT DOCUMENTATION PAGE

Form Approved
OMB No. 0704-0188

1. REPORT DATE *(DD-MM-YYYY)*	2. REPORT TYPE	3. DATES COVERED *(From - To)*
July 2005	Final report	

4. TITLE AND SUBTITLE

Laboratory Characterization of Fine Aggregate Cementitious Material

5a. CONTRACT NUMBER

5b. GRANT NUMBER

5c. PROGRAM ELEMENT NUMBER

6. AUTHOR(S)

Erin M. Williams, Stephen A. Akers, and Paul A. Reed

5d. PROJECT NUMBER

5e. TASK NUMBER

5f. WORK UNIT NUMBER
AT22-AR-002

7. PERFORMING ORGANIZATION NAME(S) AND ADDRESS(ES)

Geotechnical and Structures Laboratory, U.S. Army Engineer Research and Development Center, 3909 Halls Ferry Road, Vicksburg, MS 39180-6199

8. PERFORMING ORGANIZATION REPORT NUMBER

ERDC/GSL TR-05-16

9. SPONSORING / MONITORING AGENCY NAME(S) AND ADDRESS(ES)

Headquarters, U.S. Army Corps of Engineers
Washington, DC 20314-1000

10. SPONSOR/MONITOR'S ACRONYM(S)

11. SPONSOR/MONITOR'S REPORT NUMBER(S)

12. DISTRIBUTION / AVAILABILITY STATEMENT

Approved for public release; distribution is unlimited.

13. SUPPLEMENTARY NOTES

14. ABSTRACT

Personnel of the Geotechnical and Structures Laboratory, U.S. Army Engineer Research and Development Center, conducted a laboratory investigation to characterize the strength and constitutive property behavior of a fine aggregate cemented material (FACM). The FACM was designed to have a 34-MPa (5,000-psi) unconfined strength and to contain no coarse aggregate. Forty-three mechanical property tests—two hydrostatic compression tests (HC), four unconfined compression tests (UC), 16 triaxial compression tests (TXC), two uniaxial strain tests (UX), four uniaxial strain load/biaxial strain unloading tests (UX/BX), three uniaxial strain load/constant volume tests (UX/CV), three uniaxial strain load/constant strain path tests (UX/SP), five direct pull tests (DP), one conventional triaxial extension test (CTE), and three reduced triaxial extension tests (RTE)—were successfully completed. In addition to the mechanical property tests, nondestructive pulse-velocity measurements were performed on each specimen. The TXC tests exhibited a continuous increase in principal stress difference with increasing confining stress. A recommended compression failure surface was developed from the TXC and UC test results. Test data from the RTE, CTE, and DP tests were used to develop a recommended extension failure surface for FACM. Results from the stress paths of the strain path tests and the recommended compression failure surface exhibited good agreement.

15. SUBJECT TERMS

Compression tests
Concrete
Extension tests
Material characterization
Material properties

16. SECURITY CLASSIFICATION OF:			17. LIMITATION OF ABSTRACT	18. NUMBER OF PAGES	19a. NAME OF RESPONSIBLE PERSON
a. REPORT	b. ABSTRACT	c. THIS PAGE			19b. TELEPHONE NUMBER *(include area code)*
UNCLASSIFIED	UNCLASSIFIED	UNCLASSIFIED		102	